

NAVAL POSTGRADUATE SCHOOL

Monterey, California

AD-A212 576



THESIS

OPERATION AND CHARACTERISTICS
OF THE
FLASH X-RAY GENERATOR
AT THE NAVAL POSTGRADUATE SCHOOL

by

Renee B. Pietruszka

June 1989

Thesis Advisor

N. K. Maruyama

Approved for public release; distribution is unlimited.

DTIC
ELECTE
SEP 21 1989
S E D

89 9 20 013

Unclassified

security classification of this page

REPORT DOCUMENTATION PAGE

1a Report Security Classification Unclassified			1b Restrictive Markings		
2a Security Classification Authority			3 Distribution Availability of Report Approved for public release; distribution is unlimited		
2b Declassification Denominator Schedule			5 Monitoring Organization Report Number(s)		
4 Performing Organization Report Number(s)			7a Name of Monitoring Organization Naval Postgraduate School		
6a Name of Performing Organization Naval Postgraduate School		6b Office Symbol (if applicable) 33	7b Address (city, state, and ZIP code) Monterey, CA 93943-5000		
6c Address (city, state, and ZIP code) Monterey, CA 93943-5000		7c Procurement Instrument Identification Number			
8a Name of Funding Sponsoring Organization		8b Office Symbol (if applicable)	10 Source of Funding Numbers		
8c Address (city, state, and ZIP code)		Program Element No Project No Task No Work Unit Accession No			
11 Title (include security classification) OPERATION AND CHARACTERISTICS OF THE FLASH X-RAY GENERATOR AT THE NAVAL POSTGRADUATE SCHOOL					
12 Personal Author(s) Renee B. Pietruszka					
13a Type of Report Master's Thesis		13b Time Covered From To		14 Date of Report (year, month, day) June 1989	15 Page Count 153
16 Supplementary Notation The views expressed in this thesis are those of the author and do not reflect the official policy or position of the Department of Defense or the U.S. Government.					
17 Cosati Codes			18 Subject Terms (continue on reverse if necessary and identify by block number)		
Field	Group	Subgroup	flash x-ray, dosimetry, thermoluminescence		
19 Abstract (continue on reverse if necessary and identify by block number) Installation of the Model 112A Pulserad Pulsed X-Ray Generator At the Naval Postgraduate School Flash X-Ray Facility was completed in August of 1988. Characterization of the Pulserad 112A is essential to its effective use in future radiation effects study. This study will describe the basic system components, the principles of beam generation, and the characteristics of the radiation output. Fundamentals of radiation dosimetry and their application to flash X-ray sources will be discussed. Finally, the results of initial mapping of the radiation field generated by the Model 112A Pulserad Pulsed X-Ray Generator will be presented.					
20 Distribution Availability of Abstract <input checked="" type="checkbox"/> unclassified unlimited <input type="checkbox"/> same as report <input type="checkbox"/> DTIC users			21 Abstract Security Classification Unclassified		
22a Name of Responsible Individual N. K. Maruyama			22b Telephone (include Area code) (408) 646-2431	22c Office Symbol 61MX	

DD FORM 1473-4 MAR

83 APR edition may be used until exhausted
All other editions are obsolete

security classification of this page

Unclassified

Approved for public release; distribution is unlimited.

Operation and Characteristics
of the
Flash X-Ray Generator
at the Naval Postgraduate School

by

Renee B. Pietruszka
Lieutenant, United States Navy
B.S., United States Naval Academy, 1981

Submitted in partial fulfillment of the
requirements for the degree of

MASTER OF SCIENCE IN PHYSICS

from the

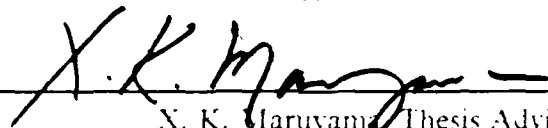
NAVAL POSTGRADUATE SCHOOL
June 1989

Author:

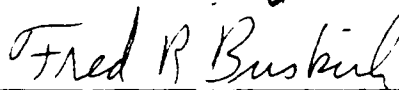


Renee B. Pietruszka

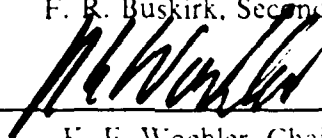
Approved by:



X. K. Maruyama, Thesis Advisor



F. R. Buskirk, Second Reader



K. E. Woehler, Chairman,
Department of Physics



G. E. Schacher,
Dean of Science and Engineering

ABSTRACT

Installation of the Model 112A Pulserad Pulsed X-Ray Generator at the Naval Postgraduate School Flash X-Ray Facility was completed in August of 1988. Characterization of the Pulserad 112A is essential to its effective use in future radiation effects study.

This study will describe the basic system components, the principles of beam generation, and the characteristics of the radiation output. Fundamentals of radiation dosimetry and their application to Flash X-Ray sources will be discussed. Finally, the results of initial mapping of the radiation field generated by the Model 112A Pulserad Pulsed X-Ray Generator will be presented.

Accession For	
NTIS GRA&I	<input checked="checked" type="checkbox"/>
DTIC TAB	<input type="checkbox"/>
Unannounced	<input type="checkbox"/>
Justification	
By	
Distribution/	
Availability Codes	
Dist	Avail and/or Special
A-1	



TABLE OF CONTENTS

I. INTRODUCTION	1
II. MODEL 112A PULSERAD PULSED X-RAY GENERATOR	3
A. SYSTEM DESCRIPTION	3
B. COMPONENTS	5
1. Marx Generator	5
2. Blumlein Pulse Forming Line	8
3. Triggering System	13
4. Electron Accelerator Tube	16
a. Description	16
b. Electron Beam Generation	20
c. Bremsstrahlung	22
III. SYSTEM CHARACTERISTICS	25
A. PREDICTED OUTPUT	25
B. MONITORING DEVICES	29
C. MEASUREMENT OF OUTPUT	32
IV. RADIATION MEASUREMENT AND DOSIMETRY	40
A. TERMINOLOGY	40
B. CHARGED PARTICLE EQUILIBRIUM	45
1. Definition of CPE	45
2. Measurement of Equilibrium Dose	50
C. PHOTON ENERGY SPECTRUM	56
D. DOSIMETRY SYSTEMS	59
1. Calorimeters	59

2.	Photochromic Dosimeters	60
3.	Thermoluminescent Dosimeters	61
a.	Thermoluminescent Process	61
b.	Thermoluminescent Materials	63
c.	TLD Readers	65
d.	Calibration of TLD System	68
e.	Interpretation of Dosimetric Results	70
V.	RADIATION MAPPING OF PULSERAD 112A	71
A.	EQUIPMENT	71
1.	TLD's	72
2.	TLD Readers	73
a.	Victoreen Model 2800 TLD Reader	74
b.	Victoreen Model 2800M TLD Reader	75
B.	EXPERIMENT	77
1.	Radiation Intensity Variation with Marx Charge Voltage	77
2.	Angular Radiation Pattern	79
a.	Procedure	79
b.	75 kV Series	81
c.	100 kV Series	90
d.	Shot - to - Shot Variation	99
3.	Attenuation of Radiation in Air	107
a.	Procedure	108
b.	75 kV	109
c.	100 kV	113
d.	Discussion	116
VI.	CONCLUSIONS AND RECOMMENDATIONS	118
	APPENDIX A - Analysis of Blumlein Resonance Charge Circuit	119

APPENDIX B - Characteristics of Sulfur Hexafluoride and Copper Sulfate . . .	122
APPENDIX C - Radiation Exposure in Air, Data for 75 kV Series	125
APPENDIX D - Radiation Exposure in Air, Data for 100 kV Series	133

I. INTRODUCTION

The development of high voltage pulsed power systems has proceeded rapidly since its conception in the early 60's. These systems, which permit the generation of very high current pulses, have found applications in a variety of fields, ranging from material testing to the control of thermonuclear fusion. [Ref. 1]

In 1962, J.C. Martin of the Atomic Weapons Research Establishment in England first developed techniques to couple existing Marx generator technology to high speed pulse forming lines to produce short duration (10 - 100 nsec) high power pulses. Since then, development of these devices has continued in many major laboratories; Ion Physics Corps., Physics International Co., Maxwell Laboratories, Cornell University, and Sandia National Laboratories to name a few. [Ref. 2] The current pulse powered sources range from small 500 kV, 70 kA generators to larger multi-watt sources, such as the Aurora generator at the Harry Diamond Laboratories (14 MV, 1.6 MA) [Ref. 1].

Although the final system design depends primarily on the intended application of the high power pulse, these systems consist of three basic elements : (1) energy storage device (2) pulse forming network and (3) diode. A block diagram of a typical high power pulse generator is depicted in Figure 1.

The energy storage device, typically a Marx generator, is used to impulse charge the pulse forming line to high voltage. (This charging usually takes place in less than a microsecond.) The pulse forming line is usually chosen to be a Blumlein transmission line (as opposed to a simple co-axial transmission line.) The Blumlein Transmission line permits the full charging voltage to be delivered to a matched load. The vacuum diode is then coupled to the electron generation region through a solid dielectric interface. [Ref. 1]

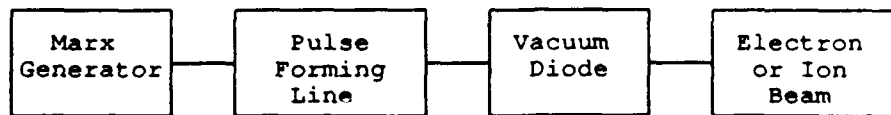


Figure 1: Basic Elements of a Typical High Power Pulse Power Generator.

As a result of the developing interest in high dose rate radiation effects study, Procurement of a Flash X-Ray Generator at NPS was initiated in 1985. The Model 112A Pulserad Pulsed X-Ray Generator installed at the Naval Postgraduate School was built by the Physics International Company. Installation in the new Flash X-Ray Facility was completed in August of 1988. This system, its operation, and characteristics will be discussed in detail in subsequent chapters.

II. MODEL 112A PULSERAD PULSED X-RAY GENERATOR

A. SYSTEM DESCRIPTION

The Model 112A Pulserad Pulsed X-Ray Generator is a high power x-ray source. The basic system is that described in Chapter I with the addition of a bremsstrahlung target for the production of x-rays. A summary of the design specifications as listed in the Operations and Maintenance Manual [Ref. 3] is provided in Table I.

TABLE I: PULSERAD 112A SYSTEM SPECIFICATIONS

X-ray Output	
Dose at 500 mm from anode:	8 Rad (Si)
Pulse Width:	20 ± 2 ns
Pulse Forming Line	
Type:	Coaxial Blumlein
Peak Output Voltage:	1.7 MV
Output Impedance:	43 Ohms
Marx Generator	
Number of stages:	12
Stage Capacitance:	0.05 μ F
Maximum Charge Voltage:	100 kV (\pm 50 kV)

A schematic of the system is shown in Figure 2. The basic theory of operation is relatively simple and will be summarized below. Each component will be described more fully in subsequent sections.

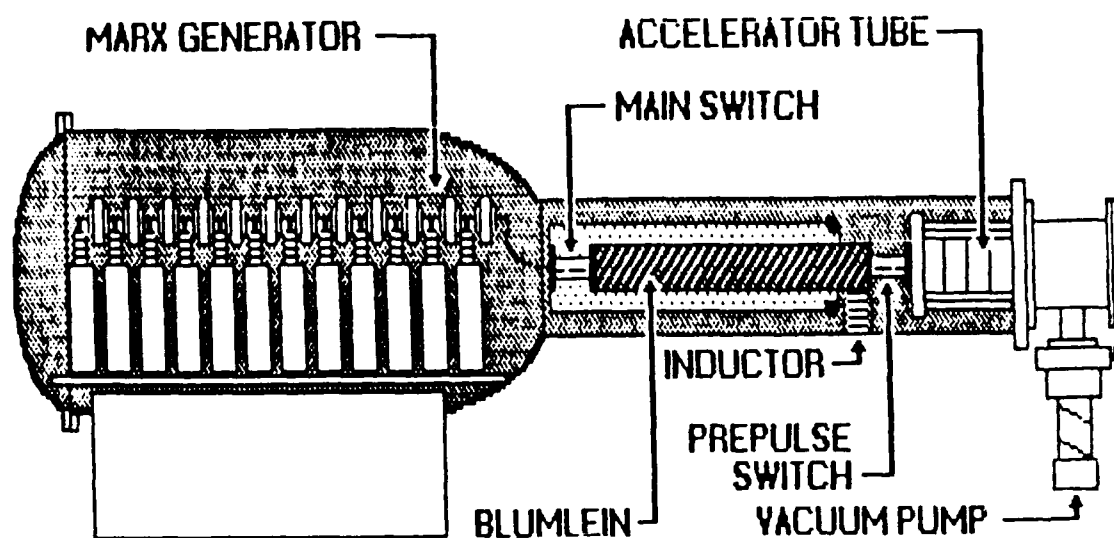


Figure 2: Diagram of Pulserad 112A Components [Ref 4].

The radiation is produced in a relatively simple three step process. The twelve stage Marx Generator is charged via an external power supply to the desired voltage. The Blumlein Pulse Forming Line is then resonance charged from the Marx Generator. When fully charged the Blumlein discharges rapidly into the electron accelerator tube creating a large potential difference across the diode gap. The cathode consists of a stainless steel rod which readily emits electrons when the high voltage is applied. The electrons are accelerated across the anode-cathode spacing until they impact with a tantalum foil target. The resulting bremsstrahlung process produces the desired radiation. The charging and discharging phases of the operation are controlled through a triggering system. This triggering system consists of numerous gas spark gap switches whose closure is a result of the electrical breakdown of the pressurizing gas, sulfur hexafluoride.

B. COMPONENTS

1. Marx Generator

The term "Marx Generator" refers to a system consisting of capacitors which are charged in parallel and discharged in series to produce high output voltages. the discharge of the capacitors is controlled by the use of numerous switches. A simplified four stage Marx generator is depicted in Figure 3 below.

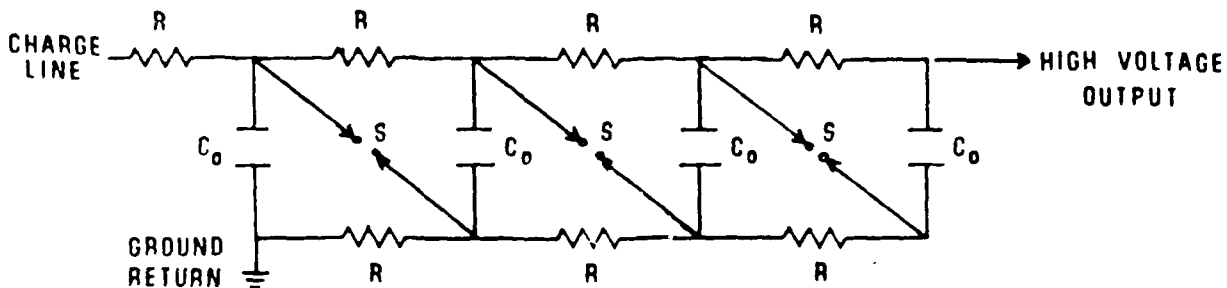


Figure 3: Schematic of Simplified Four Stage Marx Generator [Ref. 2]

Initially, the switches are open. A DC Power Supply is used to charge the system until each capacitor has a net voltage of V_0 across it. Triggering of the switches causes the Marx to "erect"; i.e., connects the capacitors in series. The resulting output voltage is four times the original charging voltage or $4V_0$. [Ref. 2]

The Marx Generator in the Pulserad 112A consists of twelve stages. Each "stage" is made up of two 0.1 micro-Farad capacitors in series, resulting in a total stage capacitance of 0.05 micro-Farads. The midpoint of the two capacitors is permanently connected to the case (Figure 4). This arrangement has the effect of charging the capacitors to opposite polarities with respect to the "center tap", thereby allowing the case to remain at ground potential during the DC charging phase. To

further ensure uniform charging of the stages, the center taps and ground are interconnected via resistors.[Ref. 4]

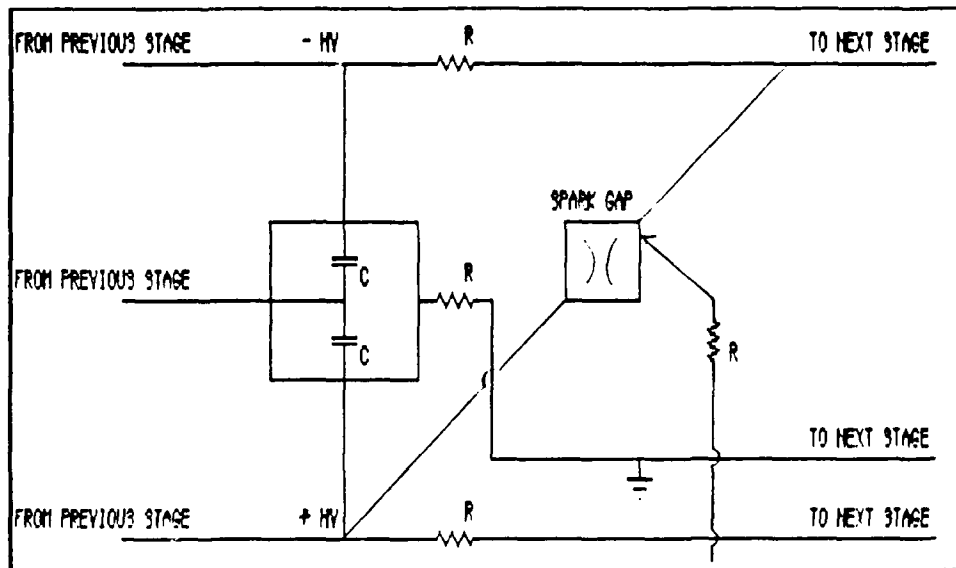


Figure 4: Schematic Diagram of Single Marx Generator Stage. Each Stage Consists of Two Capacitors in Series which are Bi-polarly Charged. Stages are Charged in Parallel (Spark Gaps Open) and Discharged in Series (Spark Gaps Closed). [Ref. 4]

A full schematic of the Pulserad Marx Generator is depicted in Figure 5. The resistors in this diagram are all "liquid resistors" consisting of polyvinylchloride (PVC) tubing filled with a solution of copper sulfate (CuSO_4). [Ref. 4] The advantage of these resistors are two-fold. They are capable of high power dissipation and are flexible enough to be easily contoured to fit the electrical requirements of the generator.

The Spark Gap Switches consist of two main discharge electrodes and a trigger electrode. Operation of the switches is based upon the electrical breakdown of the pressuring gas, sulfur hexafluoride, in the switch. (This mechanism will be discussed more fully in section three.) Each switch connects oppositely polarized ends of adjacent stages. This arrangement increases the potential difference across the switch,

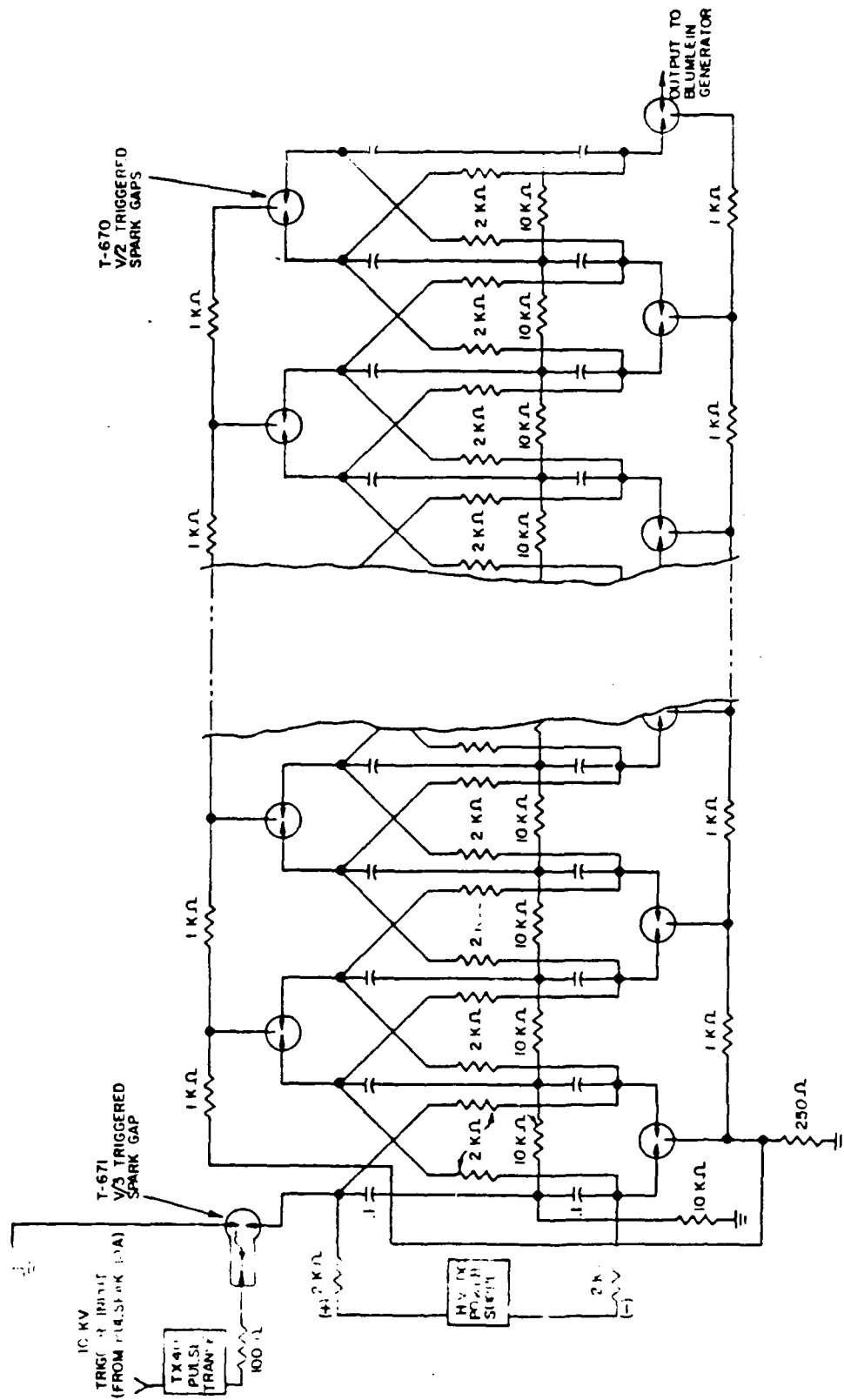


Figure 5: Marx Generator Schematic [Ref. 3]

enhancing the controlled electrical breakdown of the gas. Discharge of the generator is initiated by applying a trigger signal to the first three spark gap switches at the low end (nearest ground) of the Marx. The remaining switches are closed in a complex pattern determined by the propagation of the voltage transient through the capacitances of the various components of the Marx. This "cascading" closure of the Marx Spark Gap Switches, called Marx "erection", takes about 150 ns to occur. The Marx does not discharge until the last switch (Main Output Switch) closes.[Ref. 4]

The fully "erected" Marx has the properties of a capacitor with 1/12 the capacitance and approximately 12 times the charging voltage of a single stage. More specifically, the total capacitance is

$$C = (1/12) \times .05 \mu\text{F}$$

$$C = 4.17 \text{ nF}$$

Although, each capacitor is shunted by isolation resistors the time constants involved are short enough as to make the losses in these isolation resistors as well as the series resistive drop negligible. The output voltage becomes

$$V = 12 \times V_0$$

where V_0 is the DC charging voltage. The erected Marx discharges directly into the Blumlein Pulse Forming Line.

2. Blumlein Pulse Forming Line

In general, Pulse Forming Lines are used to produce short, fast-rising, low impedance beam outputs [Ref. 2]. Although, in some applications the Marx Generator has been directly connected to the diode, the pulse rise time is then limited by the capacitance and inductance of the generator. Additionally, the impedance of the generator is on the order of several tens of ohms. Use of a Pulse Forming Line removes these limitations resulting in a decrease in pulse duration and a corresponding increase in output power. [Ref. 1] The Pulserad 112A uses a Blumlein transmission line

that is resonance charged by the Marx generator. The transmission line is an adaptation of a circuit developed by the English radar expert A. D. Blumlein [Ref. 4]. This circuit acts as a voltage doubler, which when discharged into a matched load returns the original charging voltage.

The Blumlein consists of three co-axial cylinders. (Figure 6.) The intermediate cylinder is charged by the Marx Generator. The center cylinder is connected to the outer grounded cylinder via a few microhenry inductor. Ideally, this inductor acts as a short during the one microsecond charge cycle and as an open during the output pulse. The result is that during the charge cycle the Blumlein conductors forms two co-axial Transmission lines whose voltages essentially cancel resulting in an output voltage of zero (ideally). (Figure 7) Upon closure of the Blumlein switch, the polarity of the forward going voltage wave between the center and intermediate cylinder is reversed. (Figure 8) This pulse sees the inductor as a high impedance load. The result of this "step up" in impedance, is that the output voltage, ($V_{\text{OPEN CIRCUIT}}$), is effectively doubled.(Figure 9)

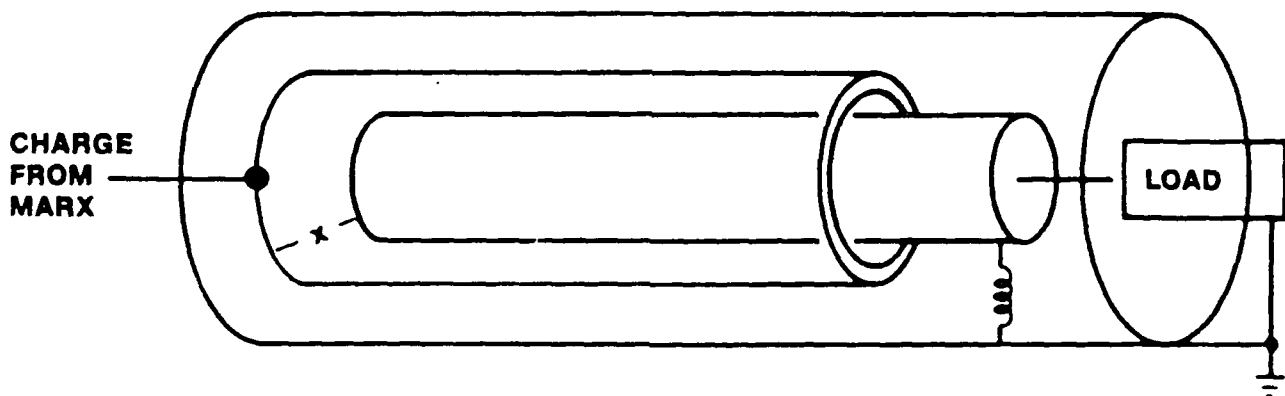


Figure 6: Blumlein Transmission line [Ref. 4]

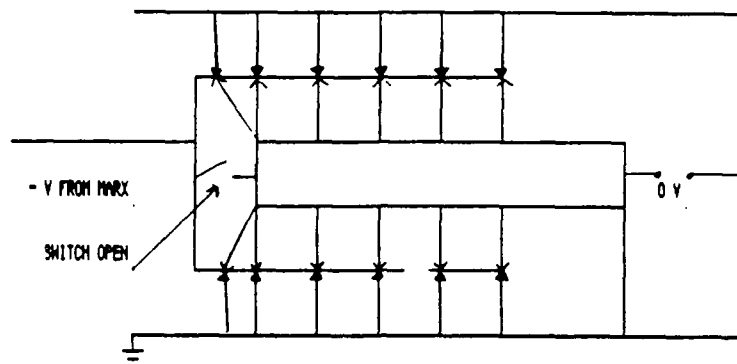


Figure 7: Blumlein During Charge Phase. The Electric Fields of the Co-Axial Transmission Lines Essentially Cancel. [Ref. 4]

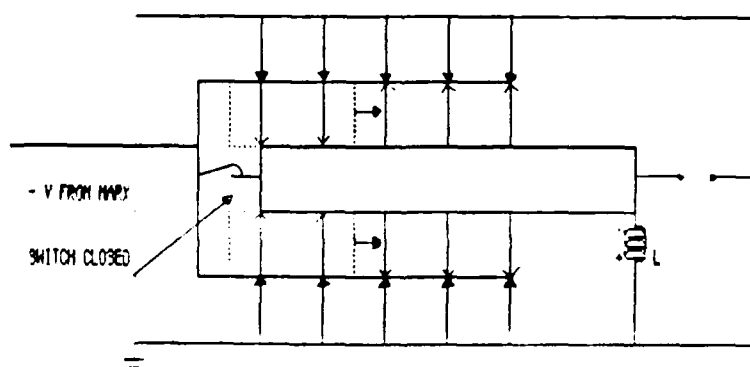


Figure 8: Upon Closure of the Blumlein Switch the Polarity of the Forward Going Waveform Between the Inner and Outer Cylinders is Reversed. [Ref. 2]

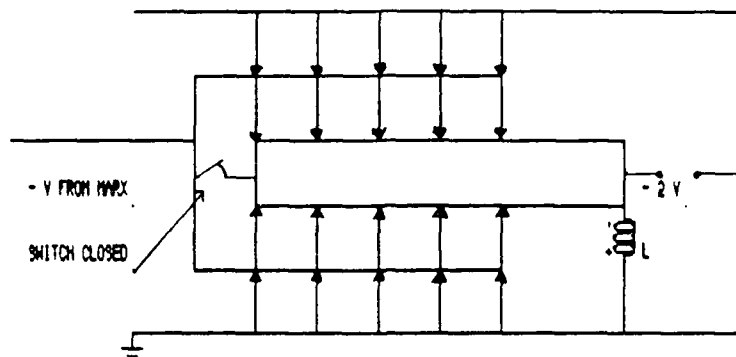


Figure 9: Blumlein During Output Phase. The Output Voltage is Effectively Doubled. [Ref. 4]

The effect is as if the two transmission lines were charged in parallel and discharged in series. When discharged into a load of matched impedance, (i.e. $Z_{\text{Load}} = Z_{\text{Blumlein}}$), the voltage divider relationship becomes

$$(1) \quad V_{\text{LOAD}} = \frac{Z_{\text{LOAD}}}{Z_{\text{LOAD}} + Z_{\text{BLUMLEIN}}} V_{\text{OPEN CIRCUIT}}$$

$$(2) \quad V_{\text{LOAD}} = \frac{1}{2} V_{\text{OPEN CIRCUIT}}$$

In other words, the voltage across the tube is effectively equal to the charging voltage.

The electrical characteristics of the pulse forming line are determined by both its geometry and the choice of insulating dielectric. In general, the relationship

between line impedance and transmission line geometry in a simple coaxial transmission line is given by [Ref. 2]:

$$(3) \quad Z = \frac{60}{\sqrt{\epsilon}} \ln\left(\frac{b}{a}\right)$$

where

Z = line impedance

ϵ = dielectric constant

b = radius of outer conductor

a = radius of inner conductor

The inner and outer radii are determined by the desired line impedance, charge voltage and electrical breakdown limitations.

J. C. Martin has shown the following relation describes the behavior of the liquid dielectric in a uniform field [Ref. 1]:

$$(4) \quad E_{BD} t^{\frac{1}{2}} A^{\frac{1}{10}} = k$$

where

E_{BD} = breakdown electric field of the liquid [V/m]

A = electrode area [m^2]

t = effective time duration of the highvoltage [micro seconds]

k = constant (for oil $k = 2.0 \times 10^3$ in MKS units)

To compensate for rise time effects, the effective time duration is taken to be only that time that the electric field exceeds 63% of the breakdown electric field. Applying this to an electrode area of 0.1 m^2 subjected to a one microsecond charging pulse, leads

to a breakdown strength of approximately 25 MV/m for oil (where $k = 2.0 \times 10^5$). [Ref. 1] These results lead to the primary choice of oil as the insulating dielectric in higher voltage applications where line impedances on the order of 35 Ohms are required. In the Pulserad 112A, both the Blumlein and the Marx Generator bank are completely submerged in transformer oil to prevent electrical breakdown during normal operation.

In actual systems, a diode pre-pulse may be generated as the Pulse Forming line is charged. Depending on actual diode design, this pre-pulse may produce a diode plasma that could negatively affect the main output pulse. This pre-pulse is a result of the unequal charging rates of the two halves of the Blumlein [Ref. 1]. If the inductor were a true short during the charge cycle, there would be no pre-pulse voltage. However, the inductor must be on the order of a few microhenries so as to appear as a large impedance during the rapid discharge of the Pulse Forming Line. As a result, a pre-pulse is developed across the inductor during the Marx charge cycle. To isolate the accelerator tube from this prepulse voltage, a pre-pulse switch is located before the diode. This switch is also a gas pressurized spark gap which is adjusted to withstand the pre-pulse voltage, and then close via self-breakdown when the main pulse arrives.

3. Triggering System

The heart of the Pulserad 112A triggering system are the numerous T-670 Spark Gap switches which control the charging and discharging of the system. The triggering signal to these switches is supplied from the Pulsepak 10A Trigger Generator via a model TX-40 pulse transformer.

The T-670 spark gap switch consists of two main discharge electrodes and a triggering electrode. (Figure 10) [Ref. 4] The switch uses a non-uniform field configuration to initiate the electrical breakdown of the pressurizing gas. The triggering electrode is located along the plane of symmetry between the two main electrodes. It is in the form of a disk with a hole in the center. Upon application of the trigger pulse, the electric field in the spark gap is distorted causing one half of the gap to "fire". As a result, the entire gap voltage is developed across the remaining half of the gap causing it to self fire. [Ref. 2]

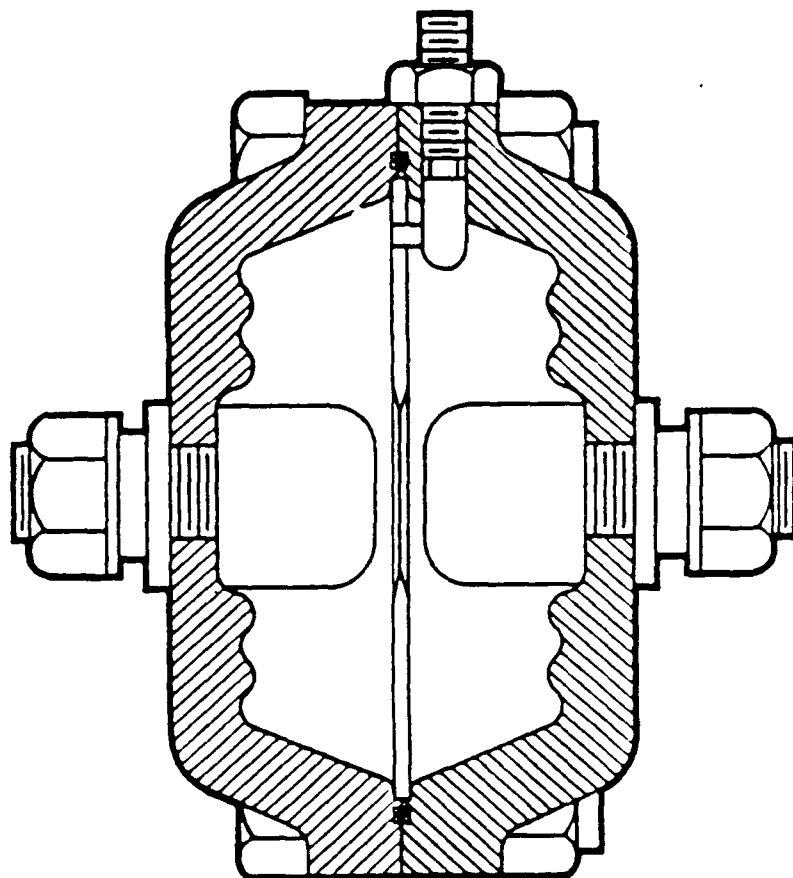


Figure 10: Model T-670 Spark Gap Switch [Ref. 4]

The most commonly used gases in self-break gas switches are air, nitrogen, freon and sulfur hexafluoride. In relatively uniform fields, the breakdown field for air or nitrogen is given by [Ref. 2]:

$$(5) \quad E_{br}(\text{kV/cm}) = \left[24.6p + 6.7 \left(\frac{p}{d_{eff}} \right)^{\frac{1}{2}} \right] F^{-1}$$

where

p = pressure in atmospheres

d_{eff} = effective electrode gap separation

F = field enhancement factor; ratio of the maximum field on the electrodes to the mean field.

The breakdown of SF_6 and freon occur at fields of approximately two and one half times and five times that given for air or nitrogen, respectively. Freon has the disadvantage that carbon is formed during discharge. As a result, SF_6 is the preferred gas for these switches, and the one used in the Pulserad 112A. [Ref. 2]

The actual mechanism by which breakdown occurs is complicated and will not be addressed. As shown in the above equation, the intensity of the field resulting in electrical breakdown of the gas is a function of the gas pressure. Practically speaking, the required pressure settings are verified experimentally for a given switch to obtain the desired output. The operating parameters for the Pulserad 112A were established at the factory and are summarized in the Operations and Maintenance Manual.

There are three settings that must be established in the Pulserad 112A system: (1) the operating pressure of the spark-gaps in the Marx itself; (2) the operating pressure of the pre-pulse switch and (3) the operating pressure of the Main Output Switch. (See Figures 2 and 5 for the location of these switches.) In actual operation of the Pulserad 112A at the Naval Postgraduate School the settings for these switches presented in Figures 20 and 21 of the Operations and Maintenance Manual.

were refined for consistent operation. This was done by carefully tabulating the manufacturer's recommended settings and adjusting the high and low voltage parameters to reflect conditions encountered during operation at these voltages. The revised curves are shown in Figure 11.

The most significant difference between the manufacturer's recommended settings and those shown is at the upper limits of the main output switch settings. It was found that for a Marx charging Voltage of 100 kV the prescribed setting of 92 PSI resulted in a misfire, presumably a result of the failure of the switch to close. As a result the settings for 95 and 100 kV were lowered, as reflected in the upper tapering of the curve. Additionally, the minimum pressure of 5 psig that must be maintained on all spark gaps whenever the system is filled with oil is reflected in these curves.[Ref. 3]

To ensure uniformity in actual machine operation standard pressure settings for various Marx Charging voltages were established. These are summarized in Table II.

4. Electron Accelerator Tube

The electron accelerator tube in the Pulserad 112A is a field emission diode mounted in a vacuum envelope. The high voltage pulse received from the Blumlein accelerates electrons across the anode-cathode gap. X-rays are produced via the Bremsstrahlung process when the electrons strike the tantalum anode .[Ref. 4]

a. Description

The major components of the electron accelerator tube are depicted in Figure 12. The vacuum diode converts the short, high power pulses of the blumlein into a useful beam.[Ref. 2] The vacuum envelope is designed to withstand the high voltage of normal operation. It is made of 6 acrylic insulators separated by aluminum "field grading rings" held together by nylon rods.[Ref. 4] The acrylic insulators are cut at a 45 degree angle with respect to the diode axis. This permits stray electrons to propagate freely without hitting any additional plastic and thereby prevents secondary emission and subsequent breakdown of the insulating material.

FLASH X-RAY GENERATOR

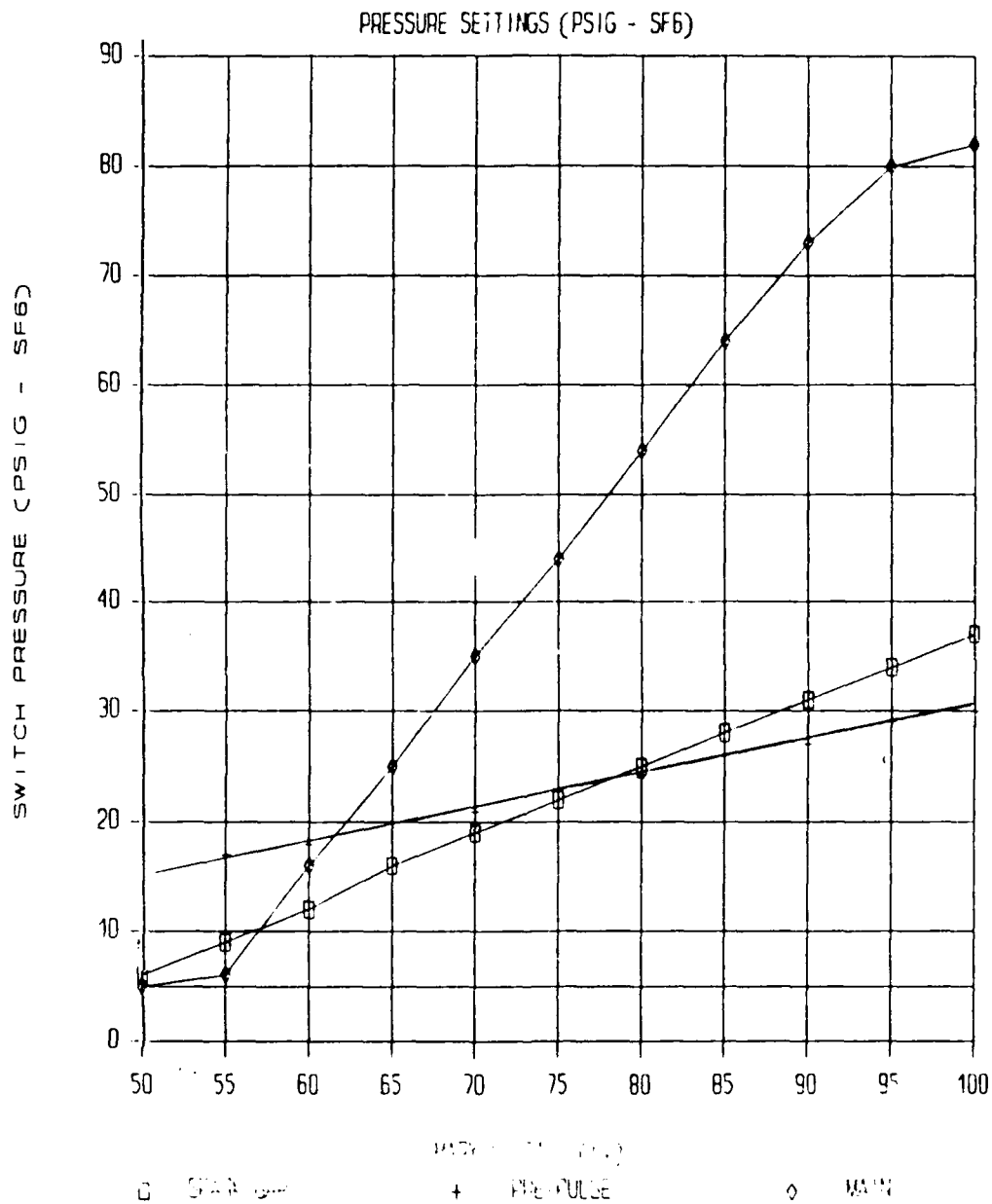


Figure 11: Revised Pulserid 112A Spark Gap Switch Pressure Settings Used at the NPS Facility. Note a Minimum of 5 psig of Pressure Must be Maintained on All Spark Gaps whenever the System is Filled with Oil.

TABLE II: SPARK GAP SWITCH PRESSURE SETTINGS USED IN OPERATION OF THE PULSERAD 112A AT NPS.

PULSERAD 112A SWITCH PRESSURE SETTINGS			
MARX VOLTAGE (kV)	SPARK GAP PRESSURE (PSI)	PRE-PULSE PRESSURE (PSI)	MAIN SWITCH PRESSURE (PSI)
50	6	15	5
55	9	17	6
60	12	18	16
65	16	20	25
70	19	21	35
75	22	23	44
80	25	24	54
85	28	26	64
90	31	27	73
95	34	29	80
100	37	30	82

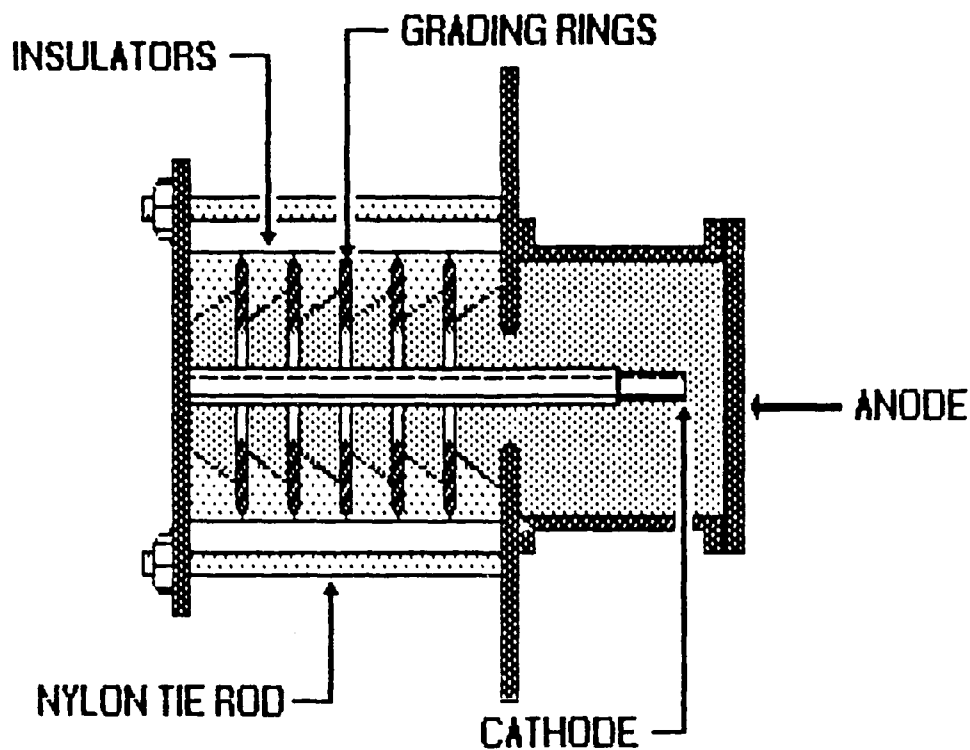


Figure 12: Pulserad 112A Electron Accelerator Tube [Ref. 4]

The aluminum "field grading rings" are designed to 1) distribute the diode voltage more uniformly along the insulator path and 2) prevent "surface flashover cascade". [Ref. 2] In actuality, the ring-to-ring capacitance is reduced by the presence of the oil insulator and the field distribution is therefore less uniform [Ref. 1]. As a result, the rings primarily serve to help control the direction of the electric field, hence reducing surface flashover [Ref. 4].

The cathode is a cylindrical stainless steel rod which tapers from a shank diameter of 3.2 cm (5/4 inch) to a tip diameter of 1.9 cm (3/4 inch). Either end of the cathode may be used for electron beam generation. Initial experiments were

made with the 3.2 cm (5/4 inch) end as the electron emission source. The anode, which acts as the bremsstrahlung target, is made from a sheet of 0.381 mm (0.015 inch) tantalum. The tantalum is protected by a 0.64 cm (1/4 inch) thick aluminum faceplate.

A minimum vacuum of 5×10^{-4} Torr is recommended for proper operation. The vacuum is maintained continuously by an oil diffusion vacuum pump.[Ref. 4]

b. Electron Beam Generation

The mechanism by which the electron accelerator tube generates the electron beam is known as "electron field emission". This mechanism is described by Miller as the "quantum mechanical tunneling of conduction electrons through the potential barrier at the surface of the metal". [Ref. 2]

The surface of almost any material will have microscopic protrusions. These protrusions, known as "whiskers" are on the order of 10^{-4} cm high with a base radius of less than 10^{-5} cm tapering off to a much smaller radius at the tip. (Figure 13) The concentration of whiskers on surfaces has been measured to be between 1 to 10^4 per square centimeter. The intensity of the electric field that results when a high voltage is applied across the diode is greatly enhanced at the tips of whiskers that exist on the cathode surface. This enhancement, on the order of several hundred times the original electric field, results in stable electron field emission.[Ref. 2] The intense electron flow through the whisker causes it to be resistively heated until it eventually vaporizes to form local bursts of "plasma" on the cathode surface. The rapid expansion and merger of these "cathode flares" eventually cover the entire surface of the cathode in a plasma sheath. This greatly increases the effective emission area, and permits extremely large currents to be extracted from the cathode plasma. The plasma gas behaves as a "zero work function" source of electrons, providing essentially an unlimited supply of charge.[Ref. 2]

Once electron emission from the cathode has been initiated and the plasma gas results, the resulting current is a function of the diode impedance and

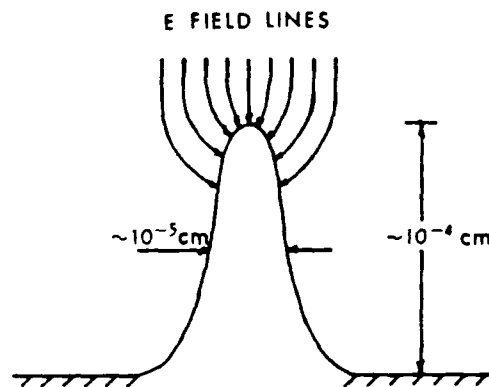


Figure 13: Electric Field Enhancement at the Tip of "Whiskers" on the Surface of the Cathode. [Ref. 2]

magnitude and duration of the applied voltage. There are two principal modes of electron flow in the diode: (1) flow that is parallel to the electrostatic lines of force; and (2) "pinched" or focused flow resulting from the interaction of the beam with the self-magnetic field. Pinched flow results from the $\underline{J} \times \underline{B}$ interaction of the beam and the self-magnetic field. This effect becomes significant when the magnitude of the current flow exceeds the critical value, and the flow becomes non-laminar. The magnitude of the parallel flow is limited by the form of the equipotential surfaces in the diode. The term "space-charge-limited current" refers to this phenomena. [Ref. 2]

c. Bremsstrahlung

X-ray production in the Pulserad 112A is a result of the bremsstrahlung process. The term "bremsstrahlung" comes from the German "brems" meaning "braking" (i.e. decelerating) and "strahlung" meaning radiation. Thus, the term bremsstrahlung refers to the emission of radiation resulting from the deceleration of a charged particle, an electron in this case.[Ref. 5]

When an electron with initial kinetic energy K is incident upon a target material, it will experience deceleration as a result of its interaction with the Coulomb field of the target nucleus. As a result of this interaction, the electron decelerates, losing energy in the form of an x-ray photon emission. (Figure 14)

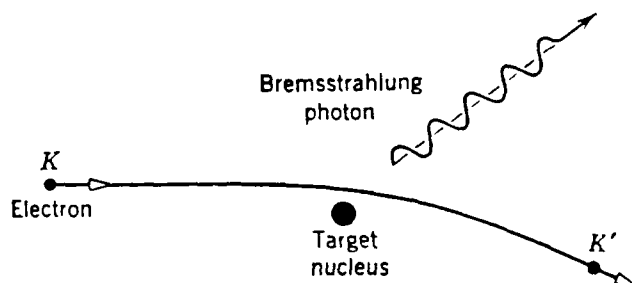


Figure 14: Bremsstrahlung Process [Ref. 5]

Taking the energy transferred to the more massive nucleus to be negligible the emitted photon energy equals the kinetic energy loss by the incident electron; namely,

$$(6) \quad h\nu = K - K'$$

where

K = electron kinetic energy before the
interaction

K' = electron kinetic energy after the
interaction

h = Planck's constant (6.626×10^{-34} J-s)

ν = frequency of the emitted radiation

In terms of wavelength this expression becomes

$$(7) \quad \left(\frac{1}{\lambda} \right) hc = K - K'$$

The electrons in the incident beam can lose different amounts of energy in such interactions. In actuality, while some electrons in the beam may lose all their kinetic energy in a single interaction, others will require several such encounters before coming to rest. The result is a continuous spectrum of emitted radiation spanning from some minimum wavelength (maximum energy). This minimum wavelength may be calculated by taking K' to be zero in the above expressions:

$$(8) \quad \lambda_{\text{MIN}} = \frac{hc}{K}$$

In the electron accelerator tube, the electron is accelerated across the potential difference V . Assuming the electron in the plasma gas to be initially at rest, the energy of the particle when it impacts the target area can be expressed as [Ref. 5]:

$$(9) \quad K = eV$$

Such that

$$(10) \quad \lambda_{\text{MIN}} = \frac{hc}{eV}$$

The differential cross section of the bremsstrahlung process is proportional to the square of the atomic number of the target material.[Ref. 6] As a result, so called "high Z" materials make much more efficient bremsstrahlung targets. In the Pulserad 112A the target anode is made from tantalum. The choice of tantalum, a relatively high Z material, represents a compromise between cost, efficiency and durability. Although, tungsten would be a more "efficient" target, it would be quickly destroyed in the accelerator tube environment.[Ref. 4]

III. SYSTEM CHARACTERISTICS

The intensity and nature of the electron beam generated in the accelerator tube is a function of the potential difference across the tube, as well as the tube design itself. The resulting voltage and current in the diode may be predicted from the characteristics of the machine. In addition, the Pulserad 112A has three monitoring devices that enable one to measure the Marx Generator Output Voltage pulse, Diode Voltage pulse, and Diode Current pulse.

A. PREDICTED OUTPUT

As discussed previously, when erected the Marx Generator acts as a single capacitor with a total voltage of 12 times the original DC charging voltage (V_0), which is used to "resonance charge" the Blumlein. This "resonance-charge" transfer can be depicted by the simplified equivalent circuit shown below. (Figure 15) [Ref. 3]

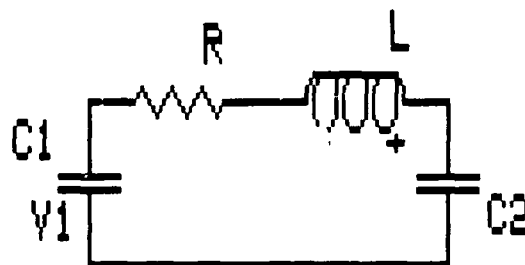


Figure 15: Equivalent Circuit of the Marx Generator and Blumlein during Resonance Charge. (V_1 = Marx Voltage; C_1 = Marx Capacitance; R = Generator; L = Generator Inductance; C_2 = Blumlein Capacitance. [Ref. 4])

Analysis of this circuit for the voltage across the capacitive load yields the following expression (See derivation Appendix A):

$$(11) \quad v_{C_2}(t) = \frac{V_1 C_1}{C_1 + C_2} \left[1 - e^{-\alpha t} \left(\frac{\alpha \sin \beta t + \beta \cos \beta t}{\beta} \right) \right]$$

where

$$\alpha = \frac{R}{2L}$$

and

$$\beta = \sqrt{\frac{C_1 + C_2}{LC_1 C_2} - \left(\frac{R}{2L} \right)^2}$$

which reduces to

$$(12) \quad v_{C_2}(t) \approx \frac{V_1 C_1}{C_1 + C_2} [1 - e^{-\alpha t} \cos \omega t]$$

where

$$\omega = \sqrt{\frac{C_1 + C_2}{LC_1 C_2}}$$

if

$$\left(\frac{R}{2L} \right)^2 \ll \frac{C_1 + C_2}{LC_1 C_2}$$

As indicated by the above equation, if the resistance is low and C_1 is much greater than C_2 , then the voltage across the load approaches twice the initial voltage by the end of the first half cycle. Table III illustrates this for some typical values. In actual operation, voltage multiplication factors on the order of 1.2 to 1.5 are realized. The resulting "ring - up factor" is further reduced by the switching of the Blumlein generator before the end of the first half-cycle. The overall effect is to permit the Blumlein to achieve (at the end of the first half-cycle) a voltage exceeding the output voltage of the Marx. [Ref. 3]

TABLE III: TYPICAL VALUES FOR SCHEMATIC RESONANCE CHARGE CIRCUIT AT MARX VOLTAGE OF 100 kV (See Figure 14). [Ref. 3 & 4]

	VARIABLE	VALUE
Marx Charge Voltage	V_1	100 kV
Marx Capacitance	C_1	4.17 nF
Resistance	R	4 Ohms
Inductance	L	15×10^{-6} H
Blumlein Capacitance	C_2	0.057 nF
Decay Constant	α	$1.3 \times 10^5 \text{ s}^{-1}$
Frequency	β	$3.4 \times 10^7 \text{ s}^{-1}$
	ω	$3.4 \times 10^7 \text{ s}^{-1}$
Period	T	$1.8 \times 10^{-7} \text{ s}$
Output Voltage (at end of first half cycle)	$V_{C2}(T/2)$	$1.96 V_1$

In calculations, a factor of 1.2 is used to account for the ring - up gain of the resonance charge sequence, and a factor of 0.9 is used to represent the loss of gain resulting from the oscillating at other than the peak voltage. The resulting expression for the Blumlein Pulse Charge Voltage (V_2) is [Ref. 3]:

$$V_2 = 12 \times 1.2 \times 0.9 \times V_0$$

The open circuit voltage of the Blumlein (V_{OB}) is twice the pulse charge voltage or

$$V_{OB} = 2 \times V_z .$$

The resulting voltage across the accelerator tube (V_T) follows the voltage divider relationship:

$$(13) \quad V_T = V_{OB} \left[\frac{Z_T}{Z_T + Z_B} \right]$$

where

Z_T = Accelerator tube impedance

Z_B = Blumlein Impedance.

Inserting the output impedance of the Blumlein (approximately 43 Ohms) and a "typical electron-tube impedance" of 50 Ohms yields the following [Ref. 3]:

$$V_T = 0.538 \times V_{OB}.$$

The resulting diode current (I_T) can then be calculated from Ohm's law:

$$I_T = \frac{V_T}{Z_T}$$

Table IV summarizes the results of these calculations for various Marx charging Voltages.

TABLE IV: THEORETICAL VOLTAGE AND CURRENT PARAMETERS FOR PULSERAD 112A.

V (MARX) V_O (kV)	V (BLUMLEIN) V_B (MV)	V (OPEN CIRCUIT) V_{BO} (MV)	V (TUBE) V_T (MV)	I (TUBE) I_T (kA)
50	.65	1.30	.70	13.94
55	.71	1.43	.77	15.33
60	.78	1.56	.84	16.72
65	.84	1.68	.90	18.12
70	.91	1.81	.98	19.51
75	.97	1.94	1.04	20.90
80	1.04	2.07	1.11	22.30
85	1.10	2.20	1.18	23.69
90	1.17	2.33	1.25	25.08
95	1.23	2.46	1.32	26.48
100	1.30	2.59	1.39	27.87

B. MONITORING DEVICES

The two voltage monitors (PIM - 197) are CuSO_4 resistors in a voltage divider arrangement with the main circuit. To calibrate these monitors, a capacitor is charged in air and then discharged into the voltage monitor. The output voltage is then extrapolated back to zero time, to determine the "sensitivity" of the monitor. When used the voltage across the monitor is given by [Ref. 3]:

$$V = V_O \times \text{Sensitivity}$$

where

V_O = the voltage output of the monitor.

Table V lists the calibration information for the voltage monitors in the NPS system.

The current across the diode is monitored with the Model 100 Fluorimeter. It consists of a loop that is mounted in the diode vacuum envelope. The changing magnetic field in the diode vacuum envelope induces a current in the loop. The resulting voltage pulse in the "B-probe" is output from the monitor. The probe is

calibrated in a co-axial line and the field calculated from the Biot-Savart Law [Ref. 3]:

$$(14) \quad B(\text{TESLA}) = \frac{2 \times 10^{-7} i (\text{amps})}{r(\text{meters})}$$

The sensitivity of the probe is then calculated such that when used the measured B field is given by

$$(15) \quad B = \frac{V_o}{\text{Sensitivity}}$$

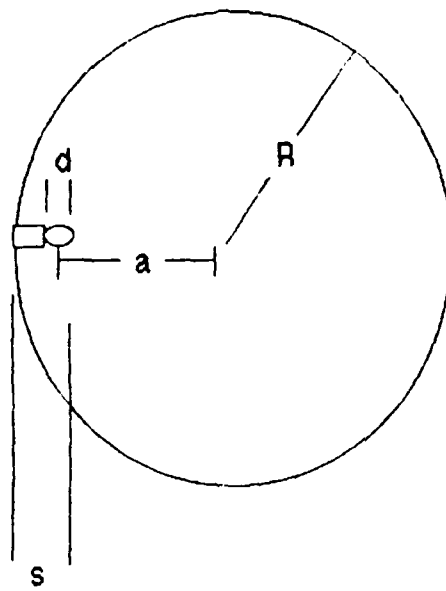
where V_o is again the output voltage of the monitor. (See Table V for calibration values of NPS system.)

TABLE V: VOLTAGE AND CURRENT MONITOR CALIBRATION STATISTICS FOR THE NPS PULSERAD 112A.

MONITOR	MODEL	SERIAL NO.	SENSITIVITY
Pulse Charge Voltage	PIM 197A-53	8401	3.7 kV/V
Diode Voltage	PIM 197A-53	8400	1.6 kV/V
Diode Fluxmeter	PIM 199B		875 V/T

(Accuracy of calibration \pm 5.0 % for all monitors)

The current in the diode can then be calculated from the measured B field, the geometry of the probe in the diode assembly, and the application of the Biot-Savart Law. The geometry of the probe in the diode assembly is depicted in Figure 16.



$$\begin{aligned}
 R &= 14.3 \text{ cm} & s &= 2.64 \text{ cm} \\
 a &= 12.8 \text{ cm} & d &= 2.41 \text{ cm}
 \end{aligned}$$

Figure 16: Schematic Diagram of B-Probe in Pulserad 112A Accelerator Tube Assembly.

The current pulse will produce a magnetic field in the diode assembly. The problem may be approached from the perspective of determining what magnitude current would produce the given magnetic field at the location of the B-probe. The

solution to the problem is simplified to that of an infinite wire, where end effects are neglected. The current at any instant is approximated by the field that would be produced by the flow of current through an infinite wire. For an infinite wire the Biot-Savart Law may be expressed as:

$$(16) \quad B(a) = \frac{\mu_o I}{2a}$$

where

μ_o = permeability constant (1.26×10^{-6} H/m)

a = distance from the wire.

The current is then simply

$$(17) \quad I = 2aB \left(\frac{\pi}{\mu_o} \right) \\ = \frac{Ba}{2 \times 10^{-7}} \text{ Amps}$$

where

B = magnetic field in Tesla

$a = 0.128$ m (from figure 15)

for the Pulserad 112A.

C. MEASUREMENT OF OUTPUT

A Tektronix 7104 Oscilloscope fitted with a Polaroid film holder is used to photograph the output of the various monitors. Additional attenuation must be added in each case to ensure the oscilloscope is not damaged during measuring. The attenuation, in decibels, reduces the voltage "seen" by the oscilloscope according to the relationship

$$(18) \quad \text{Number of decibel} = 20 \log_{10} \left(\frac{V_{out}}{V_{in}} \right)$$

where V_{in} and V_{out} are the voltages into and out of the attenuator respectively. The set-up is schematically shown in Figure 17. The oscilloscope scales must also be

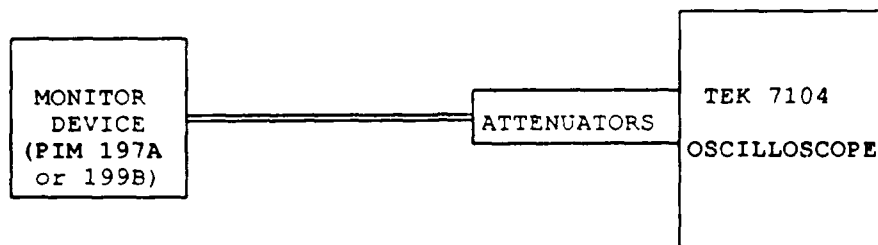


Figure 17: Schematic Diagram of Voltage Read-out of Pulserad 112A Monitoring Devices.

adjusted for each monitor to ensure proper triggering and display of the various output pulses. Table VI summarizes the attenuation required and oscilloscope settings employed for each monitoring device.

TABLE VI: MONITORING DEVICE OSCILLOSCOPE SETTINGS AND ATTENUATION REQUIRED.

MONITOR	ATTENUATION		TEK 7104 SCOPE SCALES	
	dB	Ratio ¹	VOLTAGE	TIME
Marx Output Pulse	34	50	1 V/cm	100 ns/cm
Diode Voltage	46	200	1 V/cm	*
Diode Current	20	10	500 mV/cm	20 ns/cm

¹ Ratio = (V_{in} / V_{out})

* 100 ns/cm, 50 ns/cm, and 20 ns/cm used with acceptable results.

The Marx Output Voltage was monitored during most of the initial shots made on the NPS Pulserad 112A. The form of the pulse is an effective diagnostic tool to ensure proper switching in the system. Since the system is based upon time-dependent electrical breakdown data, oscillation of the Blumlein voltage may result in damage to the various parts of the generator. Figure 18 below illustrates the difference in the Marx waveform between proper and improper switching. It has become standard procedure to monitor the Marx Output Voltage at a lower charge voltage first shot (≤ 75 kV) to ensure the system is operating properly, before proceeding to higher voltages. Figure 19 is a photograph of a typical 75 kV waveform.

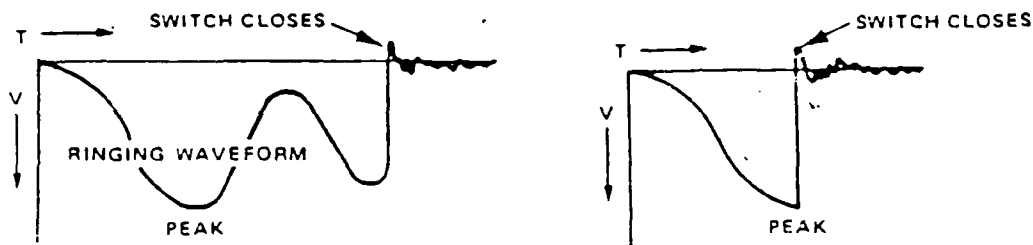


Figure 18: Waveforms Resulting from Proper (Left) and Improper Switching (Right) in the Pulserad 112A. The "Ringing" Waveform may Cause Premature Electrical Breakdown in Generator Components. [Ref. 3]

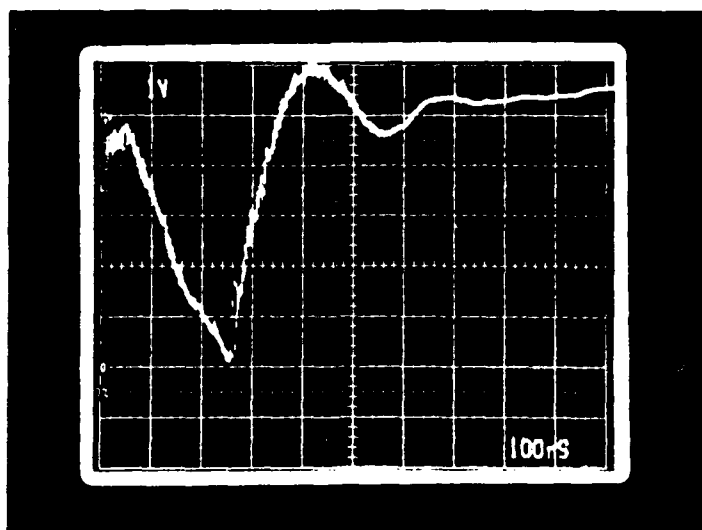


Figure 19: Photograph of a Typical 75 kV Marx Output Pulse of the Pulserad 112A taken April 20, 1989 at NPS. Peak Voltage Measured: 870 kV. (PIM 197A-53 #8401, 34 dB Attenuation.)

Equipment was not available to measure both the Diode current and voltage simultaneously. However, several shots taken in series indicate little variation in the peak pulse height of the waveform between shots taken at identical spark gap settings. Table VII summarizes the results of data taken at Marx charging voltages of 75 kV and 100 kV, and compares it with those theoretical values calculated previously. (Table IV) The uncertainty in the measured values reported is based on the accuracy to which the voltage peaks on the individual photographs may be measured; namely, $\pm .1$ cm. This 0.1 cm uncertainty was then converted to the appropriate units in each case. Figures 20 - 23 show sample photographs of the diode voltage and current waveforms for 75 and 100 kV used in these calculations.

**TABLE VII: MEASURED DIODE CURRENT AND VOLTAGE OUTPUTS
(CALCULATED VALUES ASSUMING $Z_T = 50$ OHMS.)**

Marx Charge (kV)	Diode Voltage		Diode Current	
	Measured (MV)	Calculated (MV)	Measured (kA)	Calculated (kA)
75	$1.34 \pm .03$	1.04	11.0 ± 1	20.9
100	$1.66 \pm .03$	1.39	20.5 ± 1	27.9

(NOTE: Uncertainty determined from units of oscilloscope photographs assuming voltage peaks may be read to an accuracy of ± 0.1 cm)

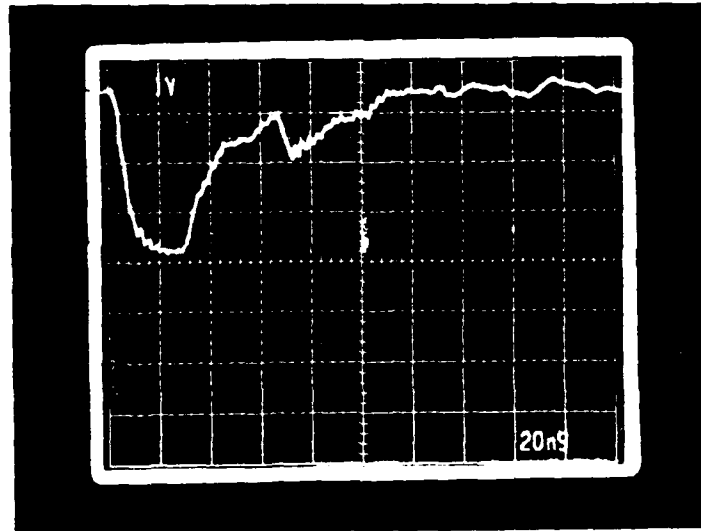


Figure 20: Photograph of typical Pulserad 112A 75 kV Diode Voltage Waveform taken May 2, 1989 at NPS. Peak Voltage Measured: 1.0 MV. (PIM 197A-53 #8400, 46 dB Attenuation.)

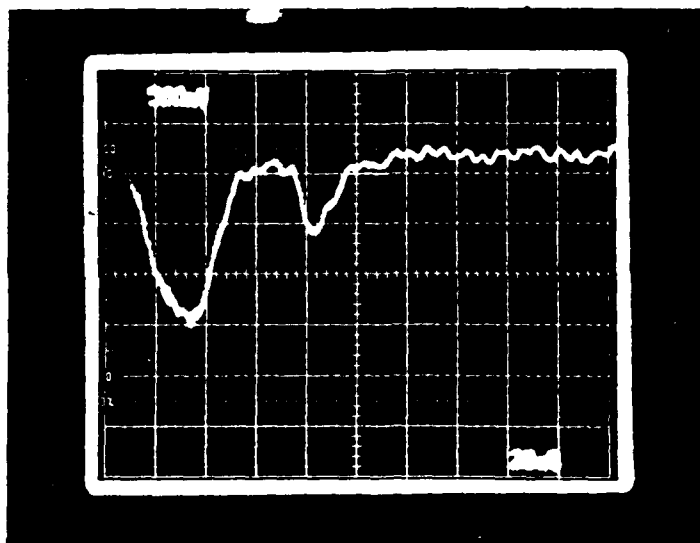


Figure 21: Photograph of Typical Pulserad 112A 75 kV Diode Current Waveform taken April 26, 1989 at NPS> Peak Current Measured: 11.0 kA (PIM 199B, 20 dB Attenuation.)

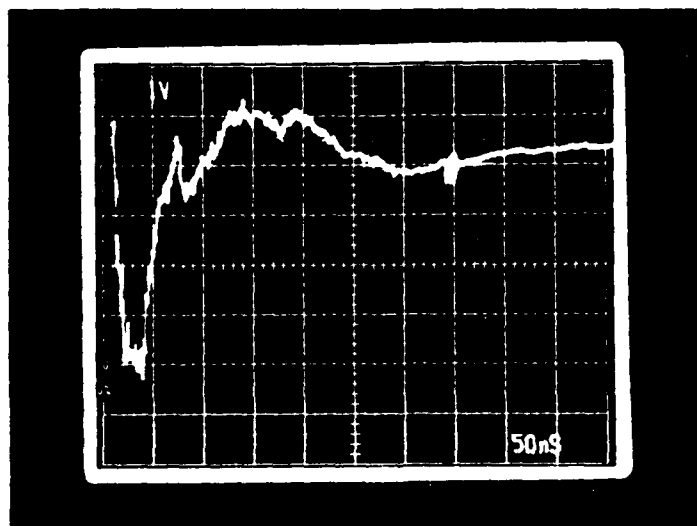


Figure 22: Photograph of typical Pulserad 112A 100 kV Diode Voltage Waveform taken April 26, 1989 at NPS. Peak Voltage Measured: 1.7 MV (PIM 197A-53 #8400, 46 dB Attenuation.)

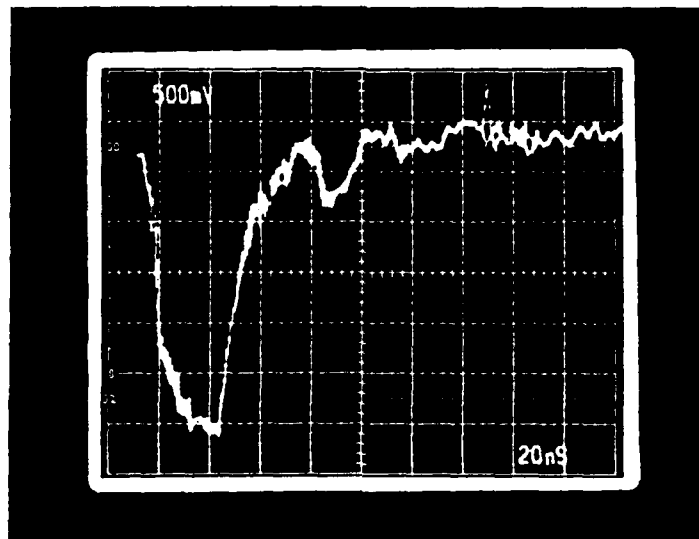


Figure 23: Photograph of Typical Pulserad 112A 100 kV Diode Current Waveform taken April 26, 1989 at NPS. Peak Current Measured: 20.9 kA (PIM 199B, 20 dB Attenuation)

As indicated in Table VII, there is a significant difference between the predicted and measured values. One source of error is the use of the "typical electron tube impedance" value of 50 Ohms in the theoretical calculations. One factor affecting the actual impedance of the accelerator tube is the anode-cathode spacing. The machine was originally installed with the larger end of the cathode as the electron source. When measured the anode-cathode spacing was found to be 175 mm instead of the 254 mm specified in the Pulserad 112A Operations Manual [Ref. 3]. The impedance of the tube was calculated from the peak current and voltage measurements using Ohm's Law:

$$Z_T = \frac{V_T}{I_T}$$

The resulting impedance was found to be 122 ohms at 75 kV and 80 ohms at 100 kV. Using a mean value of 100 ohms in the theoretical calculations of section 1 yielded results much closer to that actually measured, as summarized in Table VIII below.

TABLE VIII: DIODE CURRENT AND VOLTAGE FOR TUBE IMPEDANCES OF 50 OHMS AND 100 OHMS AS COMPARED TO MEASURED VALUES

DIODE VOLTAGE			
Marx Charge	Predicted		Measured
(kV)	50 Ohms (MV)	100 Ohms (MV)	(MV)
75	1.04	1.15	$1.34 \pm .03$
100	1.39	1.80	$1.66 \pm .03$

DIODE CURRENT			
Marx Charge	Predicted		Measured
(kV)	50 Ohms (kA)	100 Ohms (kA)	(kA)
75	20.9	11.5	11.0 ± 1
100	27.9	18.1	20.5 ± 1

The higher impedance of the accelerator tube reduces the voltage output of the system, and hence the intensity of the generated electron beam, and therefore the radiation output. Additional research is required to determine the optimum anode-cathode spacing to achieve the desired "matched impedance" between the Blumlein and the accelerator tube.

The radiation output of the Pulserad 112A system in the current configuration and the measurement techniques involved will be discussed in the following Chapters.

IV. RADIATION MEASUREMENT AND DOSIMETRY

Determination of the output radiation field of the Pulserad 112A Pulsed Flash X-ray Generator requires the application of the basic principles of dosimetry. In the most general sense, the term "dosimetry" refers to the "study of how ionizing radiation imparts energy to matter" [Ref. 7]. Of particular interest in the case of the Pulserad 112A is the manner in which x-rays interact with matter and the measurement of this interaction. This chapter will present a basic overview of the terminology and principles of radiation dosimetry, with specific emphasis on ionization effects resulting from x-ray sources.

A. TERMINOLOGY

Since its establishment in 1925, the International Commission on Radiological Units and Measurements (ICRU) has had as one of its primary responsibilities the development of the basic principles of units, standards, and measurements required in radiation dosimetry. As the field of radiation physics has developed the basic units and standards of measurement have undergone numerous revisions. [Ref. 8] The result has been some confusion in the precise terminology to be used in describing the radiation field in various situations.

There are three basic quantities useful in describing the interaction of the radiation field with matter; namely, the kinetic energy released in matter, or "kerma" (K), the "absorbed dose" (D), and the "exposure" (X). [Ref. 6] The accepted definitions of these three quantities as summarized in ASTM Standard E 170-84b [Ref. 9] are as follows:

- Kerma, K the quotient of dE_{tr} by dm , where dE_{tr} is the sum of the initial kinetic energies of all the charged ionizing particles liberated by uncharged ionizing particles in a material of mass dm (ICRU).

$$K = dE_{tr} / dm$$

The special name of the unit of kerma is the gray (Gy).

$$1 \text{ Gy} = 1 \text{ J/kg}$$

- Absorbed dose, (D) the quotient of $d\varepsilon$ by dm , where $d\varepsilon$ is the mean energy imparted by ionizing radiation to matter of mass dm (ICRU).

$$D = d\varepsilon / dm$$

The special name of the unit for absorbed dose is the gray (Gy). (Note:

Formerly, the special unit for absorbed dose was the rad.

$$1 \text{ rad} = 10^{-2} \text{ J/kg} = 10^{-2} \text{ Gy}$$

- Exposure, X the quotient of dQ by dm , where the value of dQ is the absolute value of the total charge of the ions of one sign produced in air when all the electrons (negatrons and positrons) liberated by photons in air of mass dm are completely stopped in air (ICRU).

$$X = dQ/dm$$

Unit : C/kg

(Note: Formerly, the special unit of exposure was the roentgen (R).)

$$1 \text{ R} = 2.58 \times 10^{-4} \text{ C/kg (exactly)}$$

The term "kerma" as defined above is relevant only to indirectly ionizing fields (photons or neutrons) or for any ionizing source distributed within the absorbing medium. The ionizing field of concern in the Pulserad 112A system is that of a photon field. Here, the kerma for the x-rays consists of the "energy transferred to electrons and positrons per unit mass of medium". The energy transferred to the electrons may be "spent" in either of two ways; collision interactions, or radiative transfer. The collision interactions are the result of the Coulomb force interaction with the atomic electrons resulting in their excitation. The energy is locally dissipated by the ionization of these atomic electrons in or near the electron track. The radiative transfer of energy is the result of the "bremsstrahlung" process in the material. In this case the energy is carried away in the form of x-ray photons. Positrons, on the other hand, lose their energy through "in-flight" annihilation. This energy is removed in the form of extra energy in the resulting photons. This too is a basic radiative process. [Ref. 6]

The result of these energy losses is that the "kerma" of the x-ray source can be divided into two parts; that energy spent in excitation and ionization (K_e) and that carried away by photons (K_r).

$$(19) \quad K = K_e + K_r$$

where the subscripts c and r refers to "collision" and "radiative" respectively. Hence, "kerma" includes the radiative-loss energy, but excludes energy that is passed from one charged particle to another. It is simply the expectation value of the energy transferred to the material divided by the mass. [Ref. 6]

The kerma at a particle point in a photon field is closely related to the energy fluence at that point. In general, the kerma is related to the energy fluence by the "mass energy -transfer coefficient" (μ_{tr}/ρ), which is a characteristic of both the photon energy and the atomic number of the material at the point of interest. The basic equation for monoenergetic photons is

$$(20) \quad K = \left(\frac{\mu_{tr}}{\rho} \right) \Psi$$

where

Ψ = energy fluence (J/cm²)

μ_{tr} = linear energy transfer coefficient (cm⁻¹)

ρ = density (g/cm³)

If a spectrum of photon energies is present, then the kerma is determined by expressing the above equation in terms of a energy fluence distribution and integrating over the limits of the energy spectrum:

$$(21) \quad K = \int_{E=0}^{E_{MAX}} \Psi'(E) \left(\frac{\mu_{tr}}{\rho} \right)_{E,Z} dE$$

where $\Psi'(E)$ is the energy fluence distribution. Note that mass energy-transfer coefficients do not have a differential form. Rather they are tabulated for various energies and materials. (See Appendix D.3 of [Ref. 6].) As a result this integral must be evaluated numerically. Analogous equations defining the "collision kerma" may

also be written where the mass energy-transfer coefficients are replaced by the "mass energy-absorption coefficients" (μ_{en}/ρ), where the subscript "en" refers to energy absorbed. Specifically, for monoenergetic photons

$$(22) \quad K_C = \left[\frac{\mu_{en}}{\rho} \right]_{E,Z} \Psi$$

and for an energy spectrum of photons

$$(23) \quad K_C = \int_{E=0}^{E_{MAX}} \Psi'(E) \left[\frac{\mu_{en}}{\rho} \right]_{E,Z} dE$$

As before, the integral must be solved numerically using tabulated values for the mass energy-absorption coefficients. Note the collision kerma is the expectation value of the energy transferred to charged particles per unit mass. It does not include either the radiative losses or energy passed from one particle to another. [Ref. 6]

The radiative kerma requires no explicit definition. It is simply the difference between K and K_C . [Ref. 6]

Closely related to "kerma" is the quantity "exposure". By convention, this term is only defined for x-ray and γ -ray photons. More specifically, "the exposure X is the ionization equivalent of the collision kerma, K_C , in air, for x- and γ -rays." [Ref. 6] The conversion from kerma to exposure requires the introduction of a factor defining the mean energy expended per ion pair formed. This factor, symbolized by W is defined as

$$(24) \quad W = \frac{\sum N_i T_i (1 - g_i)}{\sum N_i (1 - g_i)}$$

where

N_i = total number of ion pairs formed by the i th electron or positron

T_i = Kinetic energy of the i th electron or positron

g_i = fraction of T_i spent in radiative interaction

g_i' = fraction of ion pairs generated by photons resulting from radiative processes.

As is the case for "exposure", this definition of W does not include radiative energy losses nor ionization produced by the resulting photons. The units of W are that of eV per ion pair. Dividing this by the charge of an electron in Coulombs and converting eV to Joules results in the expression of this factor as J/C, or energy per unit charge. Thus, the "ionization equivalent" of the collision kerma is simply expressed

$$(25) \quad X = (K_c)_{\text{air}} \left(\frac{e}{W} \right)_{\text{air}}$$

where

X = exposure in C/kg

K_c = collision kerma in J/kg

W = mean energy expended per ion pair

$(e/W)_{\text{air}} = (1/33.97) \text{ C/J}$

Although the SI units for exposure is the C/kg, the Roentgen is frequently encountered in radiation measuring equipment. The Roentgen is defined as "that exposure that produces, in air, one esu of charge of either sign per 0.001293 g of air (i.e., the mass contained in 1 cm³ at 760 Torr, 0° C) irradiated by photons. Thus $1 \text{ R} = 2.580 \times 10^{-4} \text{ C/kg}$. [Ref. 6]

The final quantity, "absorbed dose", describes the effects of any form of radiation, ionizing or non-ionizing. It represents the energy per unit mass that remains in the material to produce any effects that may be attributable to the radiation. As such it is the most universal means of defining radiation effects, and the desired end to most practical dosimetry problem.

Table IX summarizes the basic dosimetry terms and units described above.

B. CHARGED PARTICLE EQUILIBRIUM

The determination of the absorbed dose in a test material is a two step process. First is the measurement of the energy deposited in a reference material at some point of interest, and second is the conversion of this to that energy absorbed in the test material at some point of interest. As discussed in section A, the interaction of radiation with matter manifests itself in both radiative and collision processes. Additionally, the nature of these interactions are affected by a variety of factors, photon energy fluence, and atomic number of the material for example. However, the establishment of "charged particle equilibrium" greatly simplifies the problem, by relating "exposure" to "absorbed dose", and by relating the effect in various materials to the mass-absorption coefficients of those materials.

1. Definition of CPE

The formal definition of Charge Particle Equilibrium (CPE) found in ASTM E 170 - 84b [Ref. 9] is quoted below:

Charged particle equilibrium - a condition that exists in a material under irradiation if the energies, number, and direction of charged particles induced by the radiation are constant throughout the volume of interest. Therefore, within such a volume, the sum of the energies of all charged particles entering it is equal to the corresponding sum for all particles leaving it.

To understand this definition of CPE, consider a small volume of material, m exposed to a beam of ionizing radiation. The absorbed dose in the material is by definition

$$(26) \quad \Delta D = \frac{\Delta E_D}{\Delta m}$$

where

$$(27) \quad \Delta E_D = \Delta E_E - \Delta E_L$$

TABLE IX: BASIC DOSIMETRY TERMS AND UNITS.

SYMBOL	EXPLANATION OF TERM	UNIT
K	Kerma - kinetic energy released in matter per unit mass.	Gy (J/kg)
D	absorbed dose - mean energy deposited per unit mass	Gy (J/kg) (Rad)
X	Exposure	R (C/kg)
$\psi(E)$	Photon energy fluence	J/cm ²
$\psi'(E)$	Distribution in photon energy fluence.	J/(cm ² -keV)
μ_{tr}	linear energy transfer coefficient	cm ⁻¹
μ_{en}	linear energy absorption coefficient	cm ⁻¹
μ_{tr}/ρ	mass-energy transfer coefficient	cm ² /g
μ_{en}/ρ	mass-energy absorption coefficient	cm ² /g
W	mean energy expended per ion pair	eV per ion pair (J/C)
E_e	energy entering volume of mass	J
E_l	energy leaving volume of mass	J
$E_e(\gamma)$	photon energy entering volume of mass	J
$E_e(e)$	electron energy entering volume of mass	J
$E_l(\gamma)$	photon energy leaving volume of mass	J
$E_l(e)$	electron energy leaving volume of mass	J

is the energy deposited in the material. (the subscripts E and L refer to the energies entering and leaving the volume of mass.) In the case of incident photon radiation only the energy transfer to matter is a two step process. The photons impart energy to electrons via the photoelectric effect, Compton scattering, and pair production. These electrons then impart energy to matter via excitation, ionization and elastic scattering. Considering these energy depositions to consist of only photons and electrons the energy deposited can be defined as

$$(28) \quad \Delta E_D = \Delta E_E(\gamma, e) - \Delta E_L(\gamma, e)$$

or

$$\Delta E_D = [\Delta E_E(\gamma) + \Delta E_E(e)] - [\Delta E_L(\gamma) + \Delta E_L(e)]$$

where γ and e refer to photons and electrons respectively. However, by definition, CPE exists when the energy carried into the mass by electrons equals the energy carried out of the mass by electrons. (Figure 24) Hence,

$$(29) \quad \Delta E_D = \Delta E_E(\gamma) - \Delta E_L(\gamma) \quad (\text{for CPE})$$

The so-called equilibrium dose is then the ionization energy deposited in the material per unit mass. [Ref. 7]

$$(30) \quad D_{eq} = \frac{\Delta E_E(\gamma) - \Delta E_L(\gamma)}{\Delta m} \quad (\text{for CPE})$$

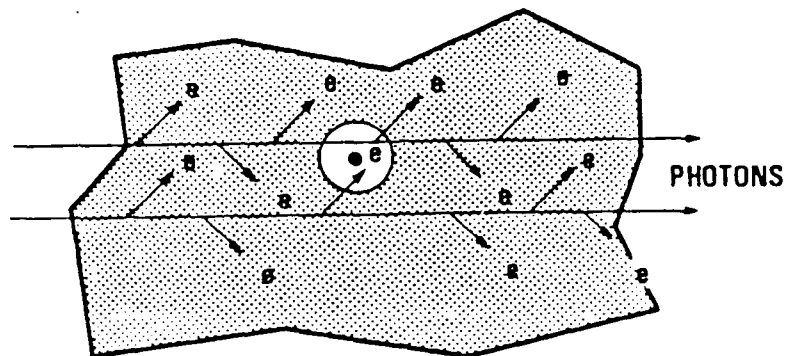


Figure 24: CPE. The Energy Deposited in a Material is the Result of the Incident Photons and Secondary Electrons. CPE Exist when the Number of Secondary Electrons Entering a Given Mass Volume is Equal to the Number Exiting. [Ref. 7] [Ref. Kerris]

This expression for the "equilibrium dose" is the equivalent to the definition of "collision kerma". Specifically,

$$(31) \quad D = K_c \text{ (for CPE)}$$

Therefore, measurement of the collision kerma under conditions of CPE enables one to determine the absorbed dose directly. Additionally, since (From Equation 25)

$$(K_c)_{air} = X \left(\frac{W}{e} \right)_{air}$$

measurement of an exposure X in air under conditions of CPE permit the calculation of how much absorbed dose would be deposited at that point in air. [Ref. 6]

To relate the absorbed dose in some reference material to the absorbed dose in the test material requires the use of the photon absorption equation [Ref. 7]:

$$(32) \quad E_L(\gamma) = E_E(\gamma) e^{-\left(\frac{\mu_{en}}{\rho}\right) \rho \Delta x}$$

where

μ_{en}/ρ = mass energy absorption coefficient of the material

ρ = density of the absorbing material

Δx = thickness of the absorbing material

Since the argument of the exponential is generally small a Taylor series approximation may be applied. The resulting form of the photon absorption equation is then:

$$(33) \quad E_L(\gamma) = E_E(\gamma) - E_E(\gamma) \left(\frac{\mu_{en}}{\rho}\right) \rho \Delta x$$

Substituting in the definition of density

$$(34) \quad \rho = \frac{\Delta m}{\Delta A \Delta x}$$

where

ΔA = area of the mass volume

and the definition of photon energy fluence (MeV/cm^2):

$$(35) \quad \Psi = \frac{\Delta E_F(\gamma)}{\Delta A}$$

yields the following

$$(36) \quad D_{eq} = \left(\frac{\mu_{en}}{\rho} \right) \Psi \quad (\text{for CPE}).$$

[Ref. 7] This is the same result presented in section A (Equation 22) for the collision kerma dependence on photon energy fluence.

The significance of this relationship is that the dose absorbed in any two materials subjected to the same photon fluence differs by the ratio of their mass energy absorption coefficients. Specifically, for two materials 1 and 2, [Ref. 7]

$$(37) \quad \frac{D_{eq}(1)}{D_{eq}(2)} = \frac{(\mu_{en}/\rho)_1}{(\mu_{en}/\rho)_2} \quad (\text{for CPE})$$

2. Measurement of Equilibrium Dose

As discussed above, CPE exists when the energy carried into a volume of material by secondary electrons exactly equals the energy carried out. It is apparent from Figure 25 that a volume of mass near the front face of a homogeneous slab of material will have more electrons scattered out of it than are scattered into it. However, as one moves deeper into the slab, a point is reached where CPE is established. [Ref. 7] This depth is approximately equal to the range of the maximum energy secondary electrons generated by the primary photons. [Ref. 10] The minimum thickness of material required to establish CPE is referred to as the "equilibrium thickness" of the

material. (Figure 26) Table X lists some typical values of equilibrium thicknesses for X-Rays. [Ref. 11]

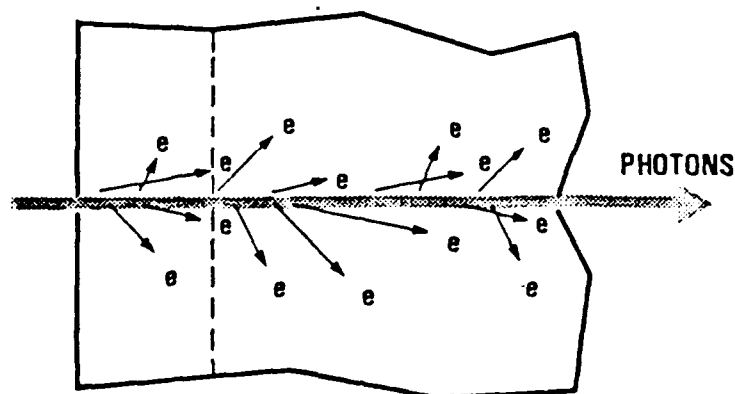


Figure 25: CPE is Established at a Depth approximately Equal to the Range of the Most Energetic Secondary Electrons. [Ref. 7]

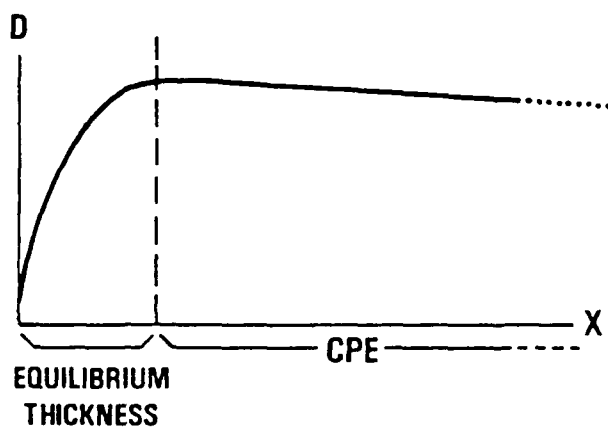


Figure 26: Dose vs. Material Thickness. CPE is Established when Energy Carried out of the Material by Secondary Electrons No Longer Exceeds the Energy Scattered Into the Material by Secondary Electrons. [Ref. 7]

Ideally then, to measure equilibrium dose in a particular material one merely needs to surround the sample with an equilibrium thickness of the same material.

TABLE X: TYPICAL VALUES OF EQUILIBRIUM THICKNESSES FOR X-RAYS [Ref. 11]

Photon Energy (MeV)	Equilibrium Thickness (g/cm ²)
0.2	< 0.05
1.0	0.2
2.0	0.4
5.0	1.0
10.0	2.0
20.0	4.0
50.0	7.0
100.0	11.0
Co ⁶⁰ (1.25)	0.4

(Figure 27) However, this becomes difficult to do in practice. Therefore, what is commonly done is that a passive dosimeter (such as a TLD) is surrounded with an equilibrium shield of some material. The choice of the materials used for both the dosimeter and the shield depend on the nature of the material and the energy spectrum of the photon fluence. An example of this is depicted in Figure 28, where a CaF₂:Mn TLD is surrounded by an Aluminum shield. [Ref. 7]

The determination of dose in the TLD shown in Figure 28 requires the application of "Bragg-Gray" cavity theory. According to this theory the dose in the encapsulated material can be related to the dose in the "wall" (Al) in two limiting cases. If the cavity is much thinner than the range of the secondary electrons produced in the "wall" then the following relation holds:

$$(38) \quad D_{\text{wall}} = \left(\frac{S_{\text{wall}}}{S_{\text{det}}} \right) D_{\text{det}}$$

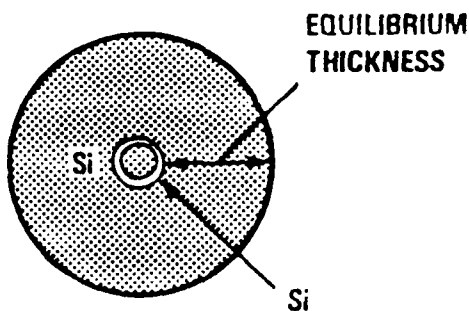


Figure 27: Charged Particle Equilibrium. Idealized Dosimeter Consists of Encapsulation of the Detector in an Equilibrium Thickness of the Same Material. [Ref. 7]

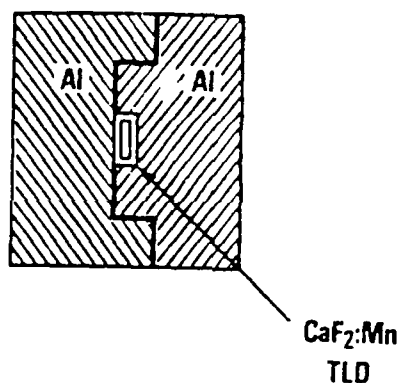


Figure 28: Charged Particle Equilibrium. Practical Implementation of Idealized Dosimeter. The Detector is Encapsulated in an Equilibrium Thickness of an Appropriately chosen Shielding Material. [Ref. 7]

where the subscripts "wall" and "det" refer to the shielding material and detector (TLD) respectively, and S is the electron mass stopping power. The second limiting case occurs when the cavity is much thicker than the range of the most energetic secondary electrons produced in the wall; i.e., CPE is reestablished in the cavity material. In this case the applicable relationship is:

$$(39) \quad D_{\text{wall}} = \frac{(\mu_{\text{en}}/\rho)_{\text{wall}}}{(\mu_{\text{en}}/\rho)_{\text{det}}} D_{\text{det}}.$$

In practice, the cavity dimension is somewhere in between these two limiting cases, such that there is no simple relationship between D_{wall} and D_{det} . Additionally, the dose measured in the reference material (e.g., TLD) must still be related to the dose in the original test material as discussed in section 1.[Ref. 7]

In any case, the determination of absorbed dose requires the determination of the photon source spectrum. The spectrum must be known well enough so that all the required stopping ratios and mass absorption coefficients may be determined for the above relations. Additionally, one of the three following conditions must apply if the dosimeter type depicted in Figure 28 is used [Ref. 7]:

- One of the Bragg-Gray cavity theory limits apply, or
- The spectrum is such that all the required mass absorptions coefficient ratios and stopping power ratios are on the order of unity, or
- Dose is calculated using a complete electron-photon transport theory calculation.

The second condition listed above is applicable in many situations. For the practical dosimeter above (Figure 28) the ratio of the mass energy absorption coefficients of CaF_2 and Aluminum is on the order of unity (minimum value of approximately 1/2) at all energies.(See Figure 29) Similarly, the ratio of the mass stopping power ratios is also on the order of one for these materials. (See Figure 30) As a result, this configuration approximates CPE and permits the calculation of dose using the equations of section 1 (Equations 26 - 35).

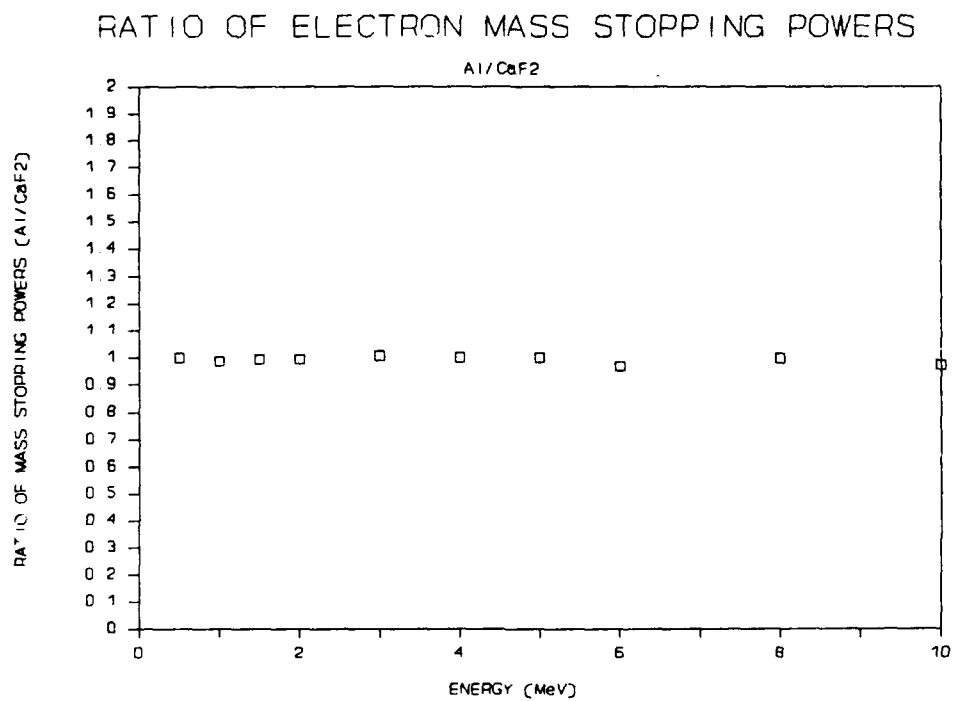


Figure 29: Ratio of Mass Absorption Coefficients of CaF₂:Mn and Aluminum. The Ratio is on the Order of Unity for These Two Materials. [Ref. 6]

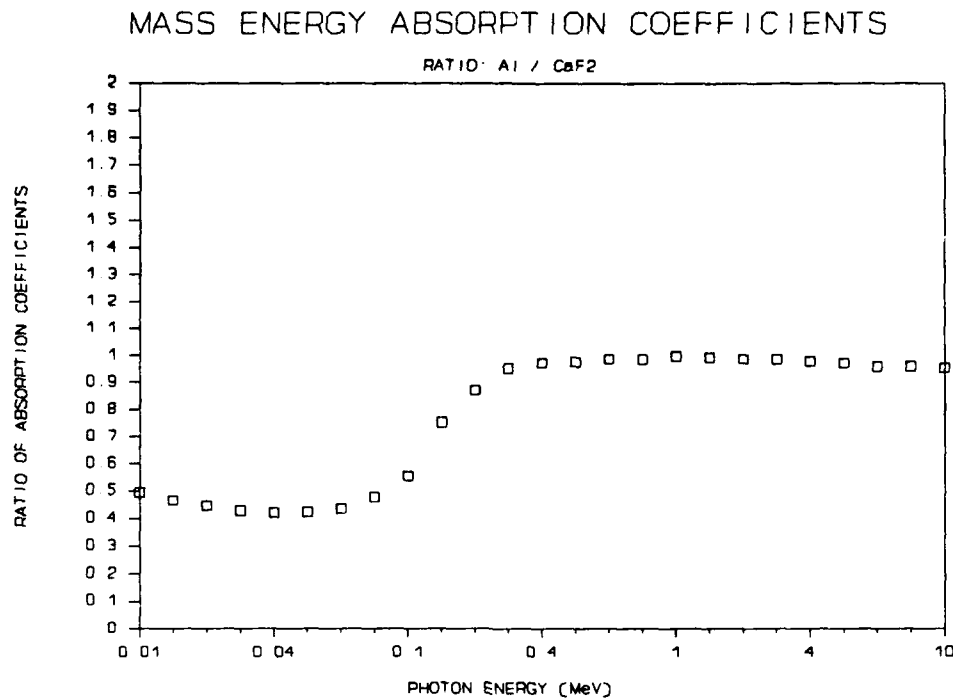


Figure 30: Ratio of Electron Mass Stopping Power for CaF₂ and Al. The Ratio is on the Order of Unity for These Two Materials. [Ref. 6]

C. PHOTON ENERGY SPECTRUM

As discussed in the previous section, knowledge of the energy spectrum of the photon source is required to calculate the absorbed dose in a test material. In fact, the accuracy within which the absorbed dose may be determined is limited to the accuracy within which the incident energy spectrum of the photon source is known. [Ref. 12]

The production of x-rays in the Pulserad 112A is discussed in detail in Ch 2. In general, the distribution of unfiltered x-rays resulting from a bremsstrahlung source have a spectral distribution characterized by that shown in Figure 31.

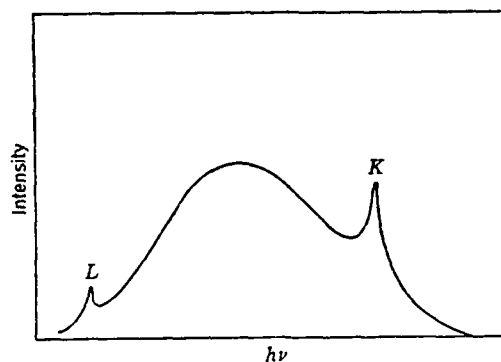


Figure 31: Typical Unfiltered X-ray Distribution. The Spectrum Rises to a Maximum Well Below that of the Photons Producing It and Falls Off to Zero. The Location of the Characteristic L- and K-lines is a Function of the Target Material. [Ref. 11]

Increasing the energy of the incident electrons on the target shifts both the upper limit of the spectrum and the location of the maximum towards higher energies. The x-rays generated by the Pulserad 112A are filtered through the 0.64 cm (1/4 in) thick aluminum anode faceplate. This filter acts as an absorbing filter and as such reduces the intensity at all photon energies, but not uniformly. In general, the reduction in energy is greater at lower energies and the resulting mean energy of the filtered spectrum is higher than that of the unfiltered spectrum. [Ref. 11]

In the case of a flash x-ray source, the photon energy distribution will also vary over the duration of the pulse. Determination of the energy spectrum by crystal scintillation or theoretical calculations based on the physical characteristics of the source become very difficult. However, determination of the integrated energy spectrum over the duration of the pulse is possible by dosimetry. This method, as applied to a 500 kV field emission flash x-ray tube, is described in detail by Cracknell. [Ref. 13] It consists of measuring the attenuation of the beam through plane copper attenuators by measuring the absorbed dose for the duration of a pulse in thermoluminescent dosimeters. Since the attenuation coefficients of x-radiation of energies between 100 to

3000 keV decreases monotonically with increases in energy, a knowledge of the attenuation coefficient of the attenuating material (copper) allows calculation of the incident spectrum from the absorbed doses measured through various thicknesses of the attenuating material. [Ref. 13] This experiment was conducted for a 500 kV Fexitron field emission flash X-ray tube by Cracknell, Hall, Twidell and Whitrow. The spectrum depicted in Figure 32 was obtained by applying a histogram fit to the data.

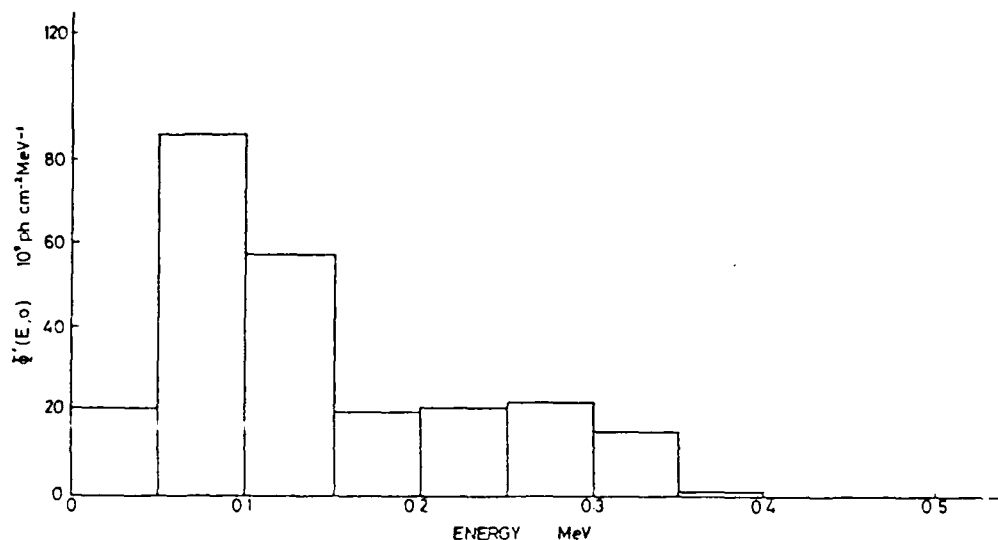


Figure 32: 500 kV Fexitron Field Emission Flash X-ray Spectrum of the Distribution in Photon Fluence for the Complete Duration of One Pulse. Curve is the Result of a Application of a Histogram Fit of Data. [Ref. 13]

Of importance in this figure, is the significant low energy component of the resulting integrated spectrum. Although, the incident pulse had a peak energy of 0.5 MeV, it produces a majority of photons with energies less than 0.2 MeV.

D. DOSIMETRY SYSTEMS

There are two basic categories of dosimetry systems. They are, as defined in ASTM E 170 -84b. [Ref. 9]

- Primary-standard dosimetry system - a system that measures energy deposition directly without the need of conversion factors for interpretation of the radiation absorption process. Examples of such systems are calorimeters and Fricke dosimeters.
- Secondary-standard dosimetry system - a system that measures energy deposition indirectly; it requires conversion factors to account for such considerations as geometry, dose rate, relative stopping power, incident energy spectrum, or other effects, in order to interpret the response of the system. Therefore, it requires calibration against a primary dosimetry system or by means of a standard radiation source.

The three most commonly used dosimeters for absorbed dose (total dose) measurements at flash x-ray facilities are the calorimeter, radiachromic dye film dosimeter, and the thermoluminescent dosimeter (TLD). [Ref. 7] Each of these will be described below.

1. Calorimeters

As mentioned above, calorimetry is a primary-standard dosimetric method. It is based on the fact that the amount of heat (energy) absorbed by a material is proportional to the resulting temperature rise in that material. The basic relationship

$$(40) \quad \Delta T = \left(\frac{1}{C_p} \right) \left(\frac{\Delta E}{\Delta m} \right)$$

where

C_p = the specific heat at constant pressure

E = energy deposited in the material

ΔT = the temperature rise in the material

Δm = mass of material

becomes

$$(41) \quad D = C_p \Delta T$$

upon substitution of the basic definition of dose. (Equation 26) Therefore, assuming that all the energy deposited by ionization in the material goes into heat, and the specific heat of the material is known, the dose can be calculated directly from the rise in temperature. [Ref. 7]

Specific advantages of this system are that they offer a wide choice of materials in which to measure absorbed dose, their response is not dependent on the dose rate, and the conversion from absorbed energy to heat takes places almost instantaneously (on the order of 10 μ s). [Ref. 7]

There are several disadvantages in the practical use of calorimeter dosimeters. They are not commercially available, and in fact must be carefully designed for each particular application, to insure the thermal properties of the materials used are appropriate for the dose range to be measured. Additionally, the dose range in which a particular calorimeter is useful is more restricted than other types of dosimeters. Another disadvantage, is that since they are not "passive detectors", they require instrumentation capable of measuring signals in the microvolt region in an environment of high electromagnetic interference. This is a significant problem in the use of a flash x-ray source, with it's accompanying high EMP. [Ref. 7]

As a result, calorimeters are primarily used in large flash x-ray facilities with fairly low-energy photon spectra (accelerating voltages less than 1.5 MeV) where appropriate instrumentation channels are available. [Ref. 7]

2. Photochromic Dosimeters

Photochromic dosimeters are based on the optical sensitivity of organic dyes to ionizing radiation. The type most commonly used in radiation hardening dosimetry is radiachromic dye film dosimeter. These dosimeters consist of aminotriphenylmethane

dye derivatives which have been stabilized and sensitized in solid solution in nylon, and formed into film. [Ref. 7]

In actual use, the optical density of the unirradiated film is measured. After exposure in a suitable equilibrium shield, the optical density is again measured. The change in optical density is proportional to the dose absorbed by the film. [Ref. 7]

These dosimeters are perfect for use in passive high dose measurements. They have a useful range of about 10^4 to 10^7 rad and their optical response to ionizing radiation is stable for extended periods of time after exposure. When used in sheets a detailed determination of the incident dose pattern is possible. [Ref. 7]

However, there are some significant disadvantages that preclude the use of these dosimeters in many situations. First, although they are readily available from commercial sources, these film dosimeters are relatively expensive and can only be used once. Secondly, and perhaps the biggest disadvantage is their lack of sensitivity at doses below about 10^4 rads. This limits their use to high energy sources making them impractical for use with many flash x-ray sources.

3. Thermoluminescent Dosimeters

Thermoluminescent Dosimeters (TLD's) are extremely popular passive dosimeters, and the dosimeters in use at the Naval Postgraduate School Flash X-ray Facility. They are readily available, relatively inexpensive and useful over a wide range of doses. However, care must be exercised in the proper use of these dosimeters and the interpretation of the results obtained. This section will discuss in detail the thermoluminescent process, various thermoluminescent materials and their uses, the "reading" of TLD's and the interpretation of the output.

a. Thermoluminescent Process

Thermoluminescent materials consist of a small mass of crystalline dielectric material with added dopants, or activators, that give it its thermoluminescent nature. These activators provide two types of crystal lattice imperfections, or centers, in the materials. The two centers are "traps" and "luminescence centers". The traps for the electrons or "holes" function to capture and hold the charge carriers in an electrical potential well for long periods of time. The luminescent centers are located at either

the electron or hole traps and emit light when an electron and hole are allowed to recombine.[Ref. 6]

The thermoluminescent process is illustrated in Figure 33. Ionizing radiation elevates an electron to the conduction band where it migrates to an electron trap (i.e., a place in the crystal lattice where a negative ion is missing). The hole left behind similarly migrates to a hole trap. The "depth" of these traps, i.e., the energy required for the particle to overcome the potential well of the hole, is sufficient to prevent escape of the hole or electron at room temperature. Continued exposure of the material to ionizing radiation, increases the number of electrons (and holes) trapped in the material. Determination of exposure simply becomes a matter of counting the number of trapped holes and electrons. [Ref. 6]

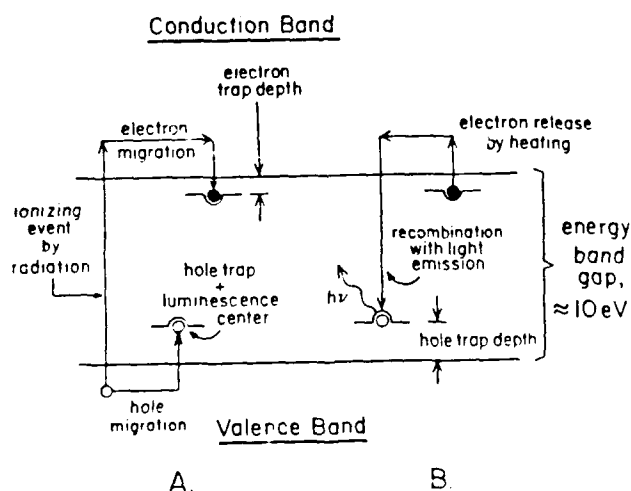


Figure 33: Energy Level Diagram of the Thermoluminescence Process. (A) Ionization by Radiation, and Trapping of Electrons and Holes; (B) Heating to Release Electrons, Allows Luminescence Production. [Ref. 6]

b. Thermoluminescent Materials

The choice of the specific TLD material depends on the specific application. The two primary considerations in choice of TLD material are trap depth and atomic number. Materials with shallow traps; i.e., where the trap energy levels are very near the edge of the band gaps; are very sensitive to low exposure. The number of trapped carriers per unit exposure is very large permitting measurement of exposures as low as 2×10^{-5} rads. However, this same characteristic makes the material somewhat unstable in that sufficient thermal energy may exist at room temperature to "free" the trapped electrons/holes. The term "fading" is used to describe this phenomena. On the other hand, materials with deeper traps which are relatively insensitive to fading at room temperature, are much less sensitive. They are better suited to longer term exposure and higher doses. A typical "fading" curve is shown in Figure 34. [Ref. 14]

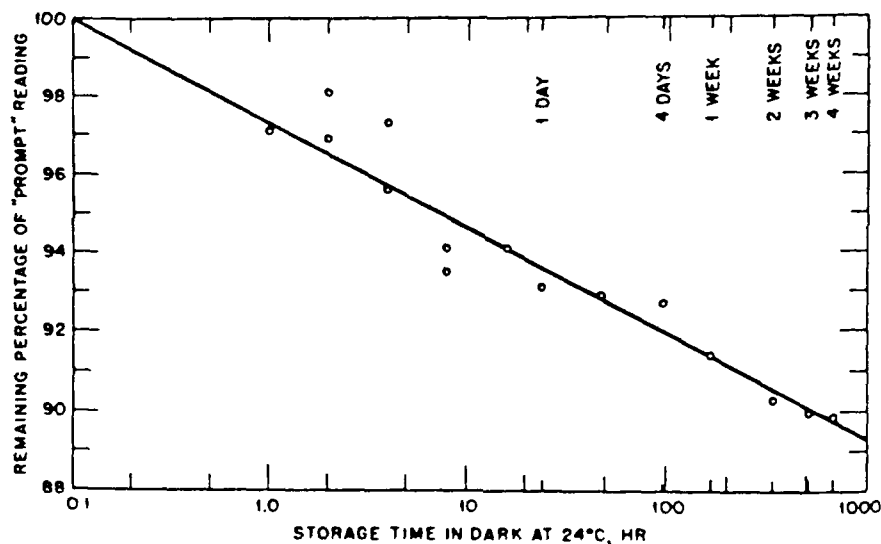


Figure 34: Loss of Signal in $\text{CaF}_2\text{:Mn}$ as a Function of Time. [Ref. 14]

The atomic number of the TLD material is significant particularly in the measurement of response to low energy radiation sources. The enhanced photoelectric interaction probabilities of high Z-material, exaggerates the response of the material to low energy X - or gamma rays. [Ref. 15] While higher Z material, such

as CaF_2 , may more closely resemble the response of the material under study (silicon for example). Table XI summarizes the characteristics of the more popular TLD's.

The relatively low atomic number of LiF, coupled with its almost negligible fading at room temperature, makes it a popular choice for relatively low dose measurements. However, LiF becomes supralinear at doses in excess of 400 rads. (See Figure 35) Its sensitivity is highly dependent on its previous thermal history and requires special annealing techniques to regain this sensitivity following exposures in excess of 400 rads. [Ref. 16] This makes it unsuitable for many measurements of the Flash X-ray output.

TABLE XI: PROPERTIES OF THERMOLUMINESCENT MATERIALS

	LiF	$\text{CaSO}_4:\text{Mn}$	$\text{CaF}_2:\text{Mn}$
Minimum dose (rad)	10^{-2}	20×10^{-6}	10^{-3}
Maximum linear dose (rad)	400	10^4	10^5
Maximum dose (rad)	10^5	10^5	3×10^5
Glow peak ($^{\circ}\text{C}$)	210	80 to 100	260
Peak Wavelength (Angstroms)	4000	5000	5000
Fading (25°C)	5%/year	50%/10hr	10% first 16hr; then 1%/day
Thermoluminescence efficiency	0.039	1.2%	0.44%
Density (g/cm^3)	2.64	2.61	3.18
Average Z	8.14	15.3	16.5

For higher dose measurements, $\text{CaF}_2:\text{Mn}$ is among the most popular choices. Its response is linear over a wide range of absorbed dose, and once exposed retains its information for a long time with a small and well known fading correction. [Ref. 7] Although, it displays exaggerated response at low energies, proper shielding removes this effect. (Figure 36) Additionally, since its atomic number (16.3) is approximately the same as that of silicon (14), unshielded dosimeters may be used to measure the absorbed dose in this material. This is particularly useful in the study of radiation effects in semiconductors. [Ref. 16]

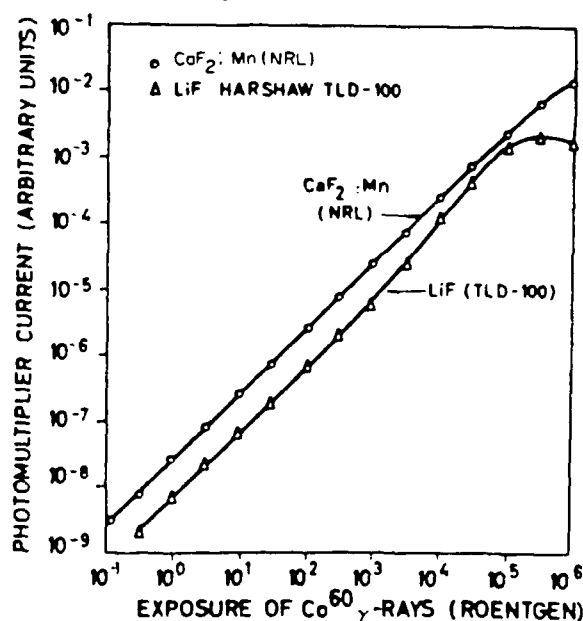


Figure 35: Response Curves for $\text{CaF}_2:\text{Mn}$ and LiF. Note the Supralinearity of LiF at Higher Doses. [Ref. 14]

c. TLD Readers

Care must be exercised in the proper reading of TLD's to obtain good results. Only a small fraction of the absorbed dose in a TLD phosphor is emitted as light upon heating of the phosphor. This fraction (TL light emitted per unit mass / absorbed dose) is called the "intrinsic thermoluminescence efficiency" of the phosphor. This has been measured to be 0.039% in LiF, and 0.44% in $\text{CaF}_2:\text{Mn}$. Since such a small fraction of the absorbed dose is relied upon to determine the entire dose, it is essential that measurements are made under reproducible conditions. [Ref. 6]

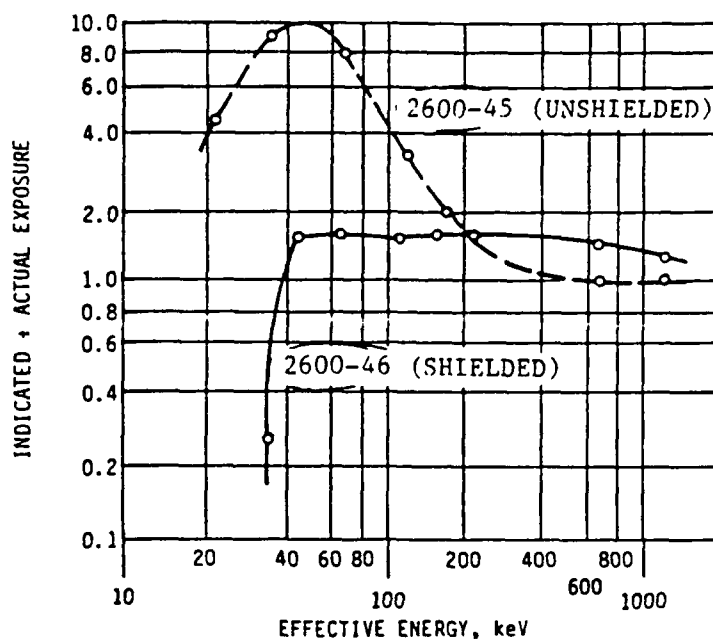


Figure 36: Energy Response of Victoreen 2600-45 Hot Pressed Chip $\text{CaF}_2\text{:Mn}$ TLD's With and Without Shielding. Note the Exaggerated Response of Unshielded TLD's to the Low Energy Component of the Photon Field. [Ref. 16]

A schematic diagram of a typical TLD reader is depicted in Figure 37. The instrument heats the sample at a rate compatible with the energy required to release the trapped electrons and holes. The light emitted upon the recombination of the electrons and holes in the luminescence centers is measured by use of a photomultiplier tube.

The heating cycle used in a typical TLD reader is often more complicated than simply linear heating as a function of time. Commercial TLD readers often use a heating cycle where the sample is rapidly heated through the "unstable-trap region", ignoring the light emission until some predetermined temperature is reached. The sample may be either heated linearly or abruptly raised to a temperature sufficient to excite the glow peak of interest, while measuring the emitted light. The amount of light emitted is displayed as a charge or exposure reading. Finally, the heating cycle may continue to a higher temperature to anneal the sample, removing any remaining charges from deeper traps, or may simply proceed to the cooling phase. The light output during the annealing and cooling phases are ignored. [Ref. 6] Figure 38 shows a typical TLD read cycle. [Ref. 16]

The primary requirement of any TLD reader is strict control and reproducibility of the heating cycle. Additionally, the light sensitivity of the reader must be consistent from one use to another. TLD readers are available from a variety of commercial sources. Those in use at the NPS Flash X-ray Facility are Victoreen Models 2800 and 2800M. Their use will be described in detail in Chapter V.

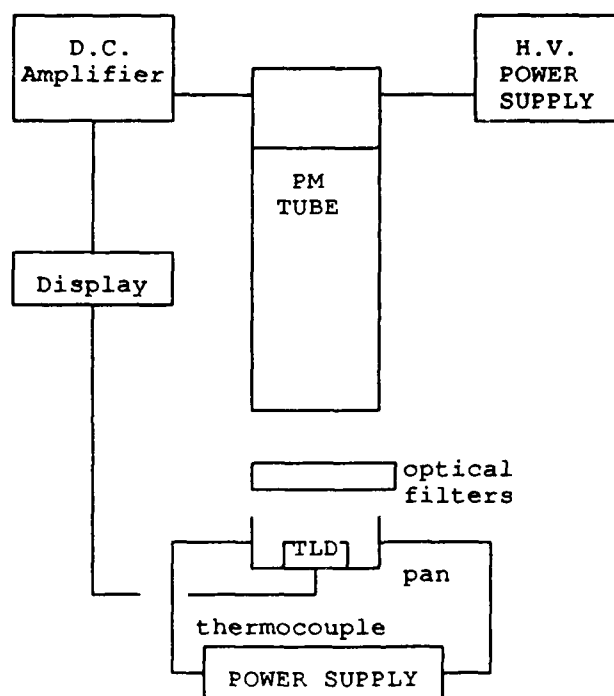


Figure 37: Schematic Diagram of Typical TLD Reader.
[Ref. 6]

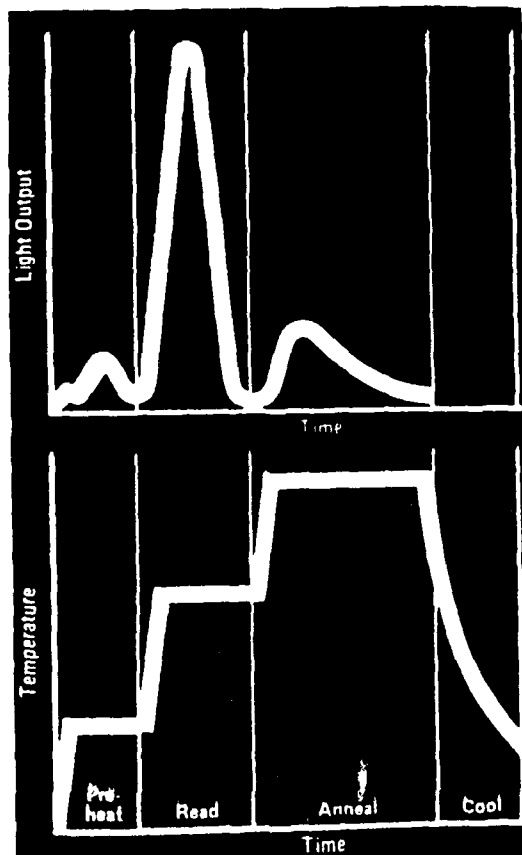


Figure 38: Typical Programmed Readout Cycle in Victoreen TLD Reader. [Ref. 6]

d. Calibration of TLD System

The proper calibration of the TLD system to be used is necessary to ensure reproducibility in the results of radiation hardening experiments. The term "TLD system" in this context refers to both the TLD's and the TLD reader used.

The calibration of the TLD system is basically a two step process; (1) the calibration of the dosimeters themselves, and (2) the calibration of the reader. The

following list summarizes those tests required to completely test the performance of a TLD system:

1. Uniformity of TLD response within a batch of TLD's.
2. Dependence of TLD response on absorbed-dose rate.
3. Dependence of TLD response on energy.
4. Dependence of TLD response on direction of incident radiation.
5. Reproducibility of TLD response of individual reusable dosimeters.
6. Dependence of TLD response on time between preparation and irradiation.
7. Dependence of TLD response on time between irradiation and readout.
8. Dependence of TLD response on temperature during storage or irradiation.
9. Dependence of TLD response on humidity.

Each of these tests and the proper procedures for conducting them is found in ASTM E 668 -78 [Ref.10]. It is not necessary to conduct these tests on every batch of TLD's. In fact, once a particular phosphor type has met these performance requirements outlined in Reference 10 , new batches of the same TLD's need only be tested for Batch Uniformity, (#1 above). For example, $\text{CaF}_2\text{:Mn}$ TLD chips commercially available from Victoreen are characterized by the energy response curve shown in Figure 36. It would therefore not be necessary to conduct this performance test unless additional specific information is required.

The Batch Uniformity test consists of selecting a sample of 30 TLD's that have been irradiated at a calibration facility under identical conditions. The sample size, 30, is chosen as that required to give a 95% confidence level in measurements. The TLD's are then read out in the TLD reader to be used in the experiment to determine the reproducibility of the TLD reader measurements. The standard deviation of the readings should not exceed 8% of the mean value of the sample readings. Uniformity of the TLD Batch should be verified periodically when the TLD's have

been subjected to several irradiation / anneal cycles and/or when they have been irradiated to high dose levels (in excess of 10^4 rads). [Ref. 10]

e. Interpretation of Dosimetric Results

Care must be taken in the reporting of dosimetric results obtained. The output of the TLD readers, as mentioned above, is in terms of charge or exposure. Conversion of this to absorbed dose is dependent on the proper establishment of charged particle equilibrium, a thorough understand of the source energy spectrum, and proper calibration of the TLD system. In all cases, the measurements made should be explicitly defined in terms of quantity measured (absorbed dose, kerma, exposure), methods of measurements, calibration techniques applied, and the type of dosimeter used. Chapter V will discuss the methods employed and the results obtained in the initial radiation mapping of the output of the Pulserad 112A at the Naval Postgraduate School.

V. RADIATION MAPPING OF PULSERAD 112A

The use of the Model 112A Pulserad pulsed X-ray generator in radiation experiments requires some knowledge of the characteristics of the output radiation. The initial "radiation mapping" of the Pulserad 112A installed at NPS was divided into three principle areas:

1. Determination of the dependence of radiation intensity on charging voltage.
2. Determination of the angular radiation pattern at the surface of the anode faceplate.
3. Determination of the intensity of the radiation as one moves axially away from the anode.

The characteristics described in this chapter should only be used as a guide in designing radiation effects experiments. As stressed in section 2d, each experiment conducted in the radiation field must include a *means of measuring* the field at the time of exposure of the test material.

A. EQUIPMENT

The dosimetry system in use at the Naval Postgraduate School Flash X-ray Facility consists of thermoluminescent dosimeters and associated TLD readers. Victoreen Model 2800 and Model 2800M Thermoluminescence Dosimeter Readers were both used during the initial radiation mapping of the Pulserad 112A. For the reasons discussed in Chapter IV, $\text{CaF}_2:\text{Mn}$ chip dosimeters were the primary TLD's used.

1. TLD's

CaF₂:Mn chip TLD's were used for the initial radiation mapping experiments. Prior to each use they were annealed in accordance with the dedosing schedule listed in Table XII below, and allowed to cool. The effectiveness of the dedosing of the batch was verified by readout of a representative sample of TLD's prior to experimental use. The average post anneal dose read was 0.5 R.

TABLE XII: Schedule for Annealing of Victoreen CaF₂:Mn Chip TLD's Used during Radiation Mapping of Pulserad 112A. [Ref. 16]

Exposure Since Last Dedosing	Minimum Times at 350 - 400°C
0 - 500 mR	5 min
500 mR - 5 R	10 min
5 - 50 R	15 min
50 - 500 R	45 min
500 - 5000 R	2 hrs
over 5000 R	5 hrs

Since the sensitivity and stability of CaF₂:Mn TLD's are not dependent upon prior dose or thermal history [Ref. 16], no attempt was made to keep track of individual chips between experiments. Rather, they were randomly placed in the radiation field, and after read-out, annealed as a batch for the time required for proper dedosing of the TLD receiving the maximum exposure.

Signal fading in CaF₂:Mn is small and predictable. The corrections listed in Table XIII are those recommended by the manufacturer [Ref. 16] All TLD's used in these experiments were read-out between 1 and 24 hours after they were exposed. As a result, application of the appropriate fading correction factor had little effect on the resulting radiation patterns. Therefore, all reported results are uncorrected for fading.

TABLE XIII: Recommended Correction for Fading in $\text{CaF}_2\text{:Mn}$ Chip TLD's [Ref. 16]

Time Since Last Exposure	Multiply Reading By
5 minutes	0.89
15 minutes	0.91
30 minutes	0.92
1 hour	0.94
5 hours	0.97
10 hours	0.98
1 day	1.00
3 days	1.02
1 week	1.04
4 weeks	1.07
12 weeks	1.09

Energy compensating shields were not used, and charged particle equilibrium was not established during exposure of the TLD's in the radiation field. As illustrated in Figure 36, the response of the unshielded dosimeters may be exaggerated by factors ranging from 2 to 10 times the actual exposure for effective photon energies less than .2 Mev. Therefore, the quantity measured and reported is exposure, in Roentgens. The orientation of the TLD's in each experiment will be addressed individually.

2. TLD Readers

The Victoreen Model 2800 TLD Reader was used for the first series of experiments to determine the magnitude of the radiation intensity expected for various charging voltages. The Model 2800M, procured specifically for use at the Flash X-ray Facility, was used for all subsequent radiation pattern measurements. A description of each reader, and the procedures followed in their use is outlined below.

a. Victoreen Model 2800 TLD Reader

The Victoreen Model 2800 TLD Reader is "a semi-automatic system for evaluating radiation dose received by a wide variety of thermoluminescence materials". [Ref. 16] It is typical of the basic commercially available TLD reader, and follows the fundamental principles of operation outlined in Chapter IV. The TLD is inserted into the heating pan which slides into proximity of the photomultiplier tube. The instrument then heats the material according to one of the four precisely controlled heating cycles. The total light output is integrated and automatically displayed. Extensive use of solid state integrated circuitry provides reproducibility in heating cycles and accurate read out of the light.

The output measured by the Model 2800 is displayed in units of exposure, specifically, Roentgens or milli-Roentgens. The maximum exposure measurable under normal operating conditions with $\text{CaF}_2\text{:Mn}$ chip TLD's is approximately 6000 R. Although higher exposures may be measured by readjusting the HV and recalibrating the instrument in the range of interest [Ref. 16]. For low exposure measurements, LiF is recommended because of its much higher sensitivity as compared to $\text{CaF}_2\text{:Mn}$. In any case, special measurement techniques are required for accurate measurement of exposures less than about 400 mR. (The 2800 TLD Reader Instruction Manual [Ref. 16] should be consulted for specific procedures.) This was not necessary for the radiation experiments presented here since our lowest measurements were on the order of 30 R.

The Model 2800 TLD Reader has four factory preset heating cycles, which may be adjusted by the user for non-routine work. The standard cycles were used for TLD's read out with this instrument. The heating cycle for $\text{CaF}_2\text{:Mn}$ chip TLD's is as follows [Ref. 16]:

- a. Rapid climb to 120°C (about 1 second)
- b. Ramp at 10°C/second to 355°C (35 seconds)
- c. Cool.

Initial calibration of the 2800 was conducted at the factory for use with LiF and $\text{CaF}_2\text{:Mn}$ chip, rod, and bulb TLD's. The calibration light source settings for operation in both the low (mR) and high (R) exposure range are stamped on the inside cover of the control panel. Prior to use, the instrument must be allowed to warm up for at least 30 minutes to permit stabilization of the photomultiplier tube. Additionally, it must be standardized for use with the desired TLD's in the appropriate exposure range using the calibration light source settings. The procedures outlined in the 2800 Instruction Manual should be followed to ensure the instrument is properly set-up. Verification of this initial factory calibration by use of a TLD exposed to a known dose is essential to ensure accurate readings.

The calibration of the 2800 Reader in use at the Flash X-ray Facility was verified for high exposure measurements by read-out of a $\text{CaF}_2\text{:Mn}$ TLD which was exposed to 1000 R by a standard source by the manufacturer. No other calibration of this instrument was conducted.

b. Victoreen Model 2800. 1 TLD Reader

The Victoreen Model 2800M Thermoluminescence Dosimeter Reader is a relatively new, easy-to-operate, microprocessor based system designed for use with a variety of TLD phosphors [Ref. 17]. The reader uses the same heating pan / photomultiplier tube set-up for read-out of the TLD's as the 2800, but offers a much wider range of operation.

The front panel consists of a CRT display, five soft-keys, a fifteen button keypad, and a power switch. Set-up of the instrument for operation is menu-driven via the installed user-friendly software. The Preliminary Instruction Manual [Ref. 17] gives step by step instruction for "programming" of the unit for use via the various menus. However, it provides no warm-up instructions, nor calibration procedures. The accompanying calibration certificate indicates the setting for LiF chips only.

The Model 2800M Reader offers a wide variety of heating cycles. These heating cycles are divided into two categories: temperature step cycles, and temperature ramp cycles. Each category offers a selection of standard cycles for use

with LiF and $\text{CaF}_2\text{:Mn}$ TLD's, as well as the option to enter other cycles. The heating cycle used for all $\text{CaF}_2\text{:Mn}$ TLD's read-out with this instrument was the standard ramp temperature cycle described below:

- a. Preheat temperature: 200°C
- b. Temperature Rate: 10°C/second
- c. Maximum Temperature: 400°C
- d. Cycle Time: 30 seconds

The display of the reader gives both the exposure and the "glow curve", a graph of intensity vs time. The units of exposure may be user defined as Coulombs, Roentgens, or Grays. Initial use of this instrument resulted in "saturation" at exposures in excess of 1000 R. (This was indicated by a "flat top" on the glow curve.) As a result, a filter was added and the instrumented calibrated to agree with the Model 2800 Reader. This calibration was done by exposing two $\text{CaF}_2\text{:Mn}$ TLD's simultaneously in the x-ray field (centered on the anode faceplate) and reading them out in both readers. The correction factor was found to be 2.877 pC/mR. Table XIV summarizes the results of simultaneously exposed TLD's read out on the two readers.

TABLE XIV: COMPARISON OF EXPOSURE OF SIMULTANEOUSLY RADIATED $\text{CaF}_2\text{:Mn}$ CHIP TLD'S READ-OUT IN THE MODEL 2800 AND MODEL 2800M TLD READERS. (MODEL 2800M CALIBRATION FACTOR IS 2.877 pC/mR)

Marx Charge Voltage	Exposure	
	2800	2800M
75 kV	237 R	236 R
75 kV	334 R	390 R
85 kV	1282 R	1310 R
100 kV	3630 R	3880 R

The addition of the filter makes this instrument unreliable for low dose measurements. This unit, with the correction factor of 2.877 pC/mR was used in all radiation "mapping" measurements. Again, the quantity reported is exposure, in Roentgens.

B. EXPERIMENT

1. Radiation Intensity Variation with Marx Charge Voltage

The first step in the characterization of the radiation output of the Pulserad 112A was to determine the magnitude of the radiation field as a function of the system parameters. Since the Marx charge Voltage is the primary variable controlled by the operator, this experiment was designed to measure exposure at various Marx charge Voltages.

Exposure measurements were taken by placing a $\text{CaF}_2\text{:Mn}$ chip TLD in a small plastic baggie and taping the baggie tightly against the face of the generator so that the chip was flat and centered at the geometric center of the aluminum faceplate. this position was chosen for two reasons:

1. reproducibility of location of the individual TLD's from shot to shot;
2. expectation that this position represented a maximum in the radiation field.

Measurements were taken over the entire operating range of the Pulserad 112A (50 - 100 kV) in increments of 5 kV. The TLD's were read out using the Model 2800 TLD Reader, with results summarized in Table XV.

This experiment provides valuable insight into the variation of the intensity of the radiation field with Marx Charging Voltage. A definite trend is reflected in the data. (Figure 39) The exposure varies from tens of roentgens to kilo-roentgens as the charging voltage is increased. However, the actual exposure measured for any given shot at a particular charge voltage may vary considerably. Additional experimentation at a Marx charge Voltage of 75 kV resulted in exposure measurements ranging from 350 - 800 R. The magnitude, effect and possible causes of "shot-to-shot" variation are discussed in Section 2d.

TABLE XV: CENTER EXPOSURE AS A FUNCTION OF MARX CHARGE VOLTAGE FOR THE PULSERAD 112A BASED ON EXPOSURE MEASURED WITH $\text{CaF}_2\text{:Mn}$ CHIP TLD'S.

Marx Voltage (kV)	Charge Exposure (R)
50	44
60	109
75	487
85	1590
90	1870
100	3090

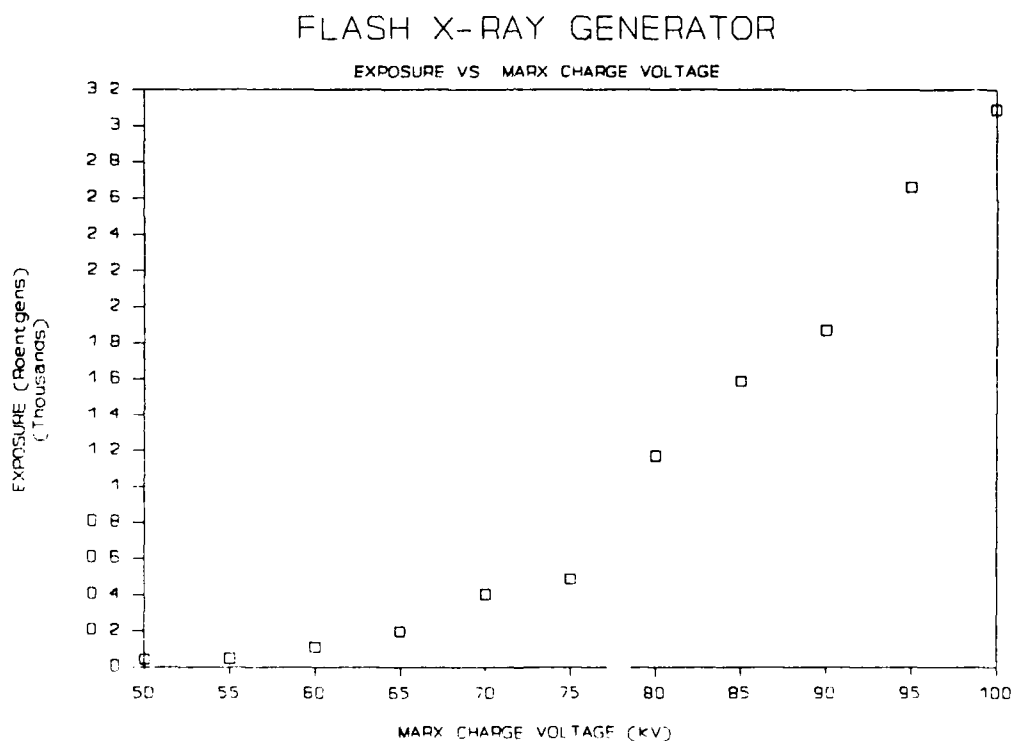


Figure 39: Central Exposure as a Function of Marx Charge Voltage over the Operating Range of the Pulserad 112A. Measurements Made at the Geometric Center of the Anode Face Plate.

2. Angular Radiation Pattern

The purpose of this series of experiments was two-fold; namely,

1. To determine if the radiation field is symmetric about the geometric center of the anode assembly.
2. To determine how the intensity of the field varies as one move radially outward along the faceplate.

Initial "mapping" of the radiation field indicate the following:

- a. The radiation field is not symmetric about the geometric center of the anode assembly. The radiation "pattern" varies with orientation.
- b. Peak exposure is not measured at the geometric center of the anode faceplate.
- c. Changes in the relative orientation of the cathode and anode are reflected on changes in the radiation patterns.
- d. The condition of the cathode greatly affects the intensity of the resulting radiation.

As a result of the factors above, the variation in exposure measured between shots made at equivalent voltages varied between 13% and 25%.(See Tables XVII and XVIII) However, sequential shots made under identical conditions were found to be almost identical.

a. Procedure

CaF₂:Mn chip TLD's orientated along the diameter of the anode faceplate were used to "map" the radiation field. The "TLD Holder" shown in Figure 40 was constructed to properly position the TLD's during exposure. The TLD Holder is constructed of 0.95 cm (3/8 inch) plexiglas cut to fit on the face of the generator. A slot , 0.32 cm (1/8 inch) high and 0.089 cm (0.035 in) deep, was machined across the diameter of the disk for placement of the TLD's. Additionally, a circular groove

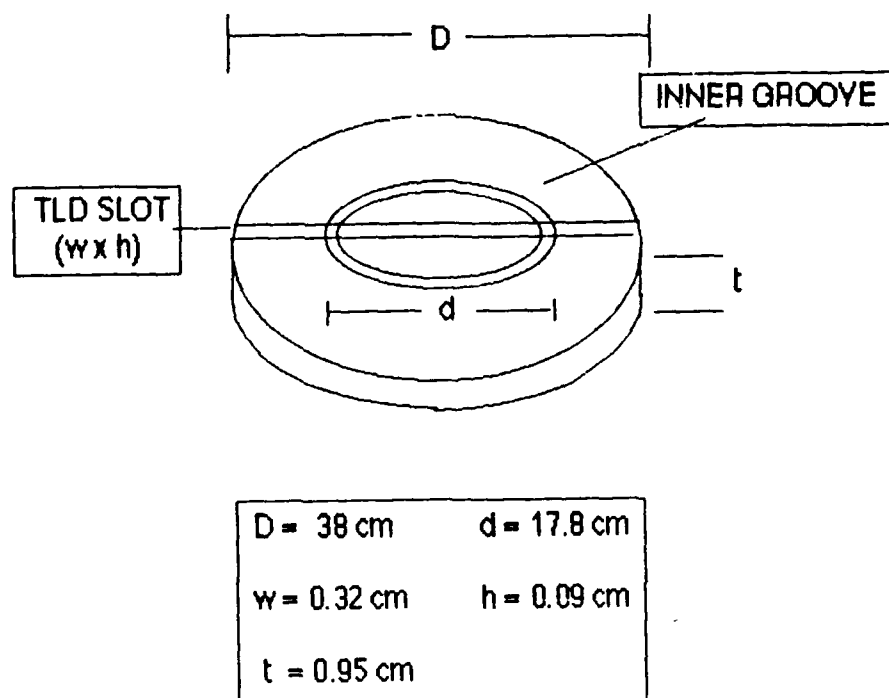


Figure 40: TLD Holder Used to Position $\text{CaF}_2:\text{Mn}$ Chip TLD's During Exposure.

was machined at a radius of 8.89 cm (3.5 in) from the center to allow the disk to fit over the protruding screws of the anode assembly and permit the TLD's to be flush against the faceplate. Once positioned in the TLD Holder, the chips were held in place by a thin piece of plastic. C-clamps were used to fasten the holder firmly against the faceplate of the anode assembly.

A series of four shots was taken for each Marx charge Voltage setting investigated. The holder was rotated between shots such that the four shots dissected the faceplate of the anode assembly into eight equal wedges. The orientation of the four shots, (090-270, 000-180, 045-225, and 135-315) is illustrated in Figure 41.

This experiment was conducted for two Marx Charge Voltages, 75 kV and 100 kV. The results of these experiments follow.

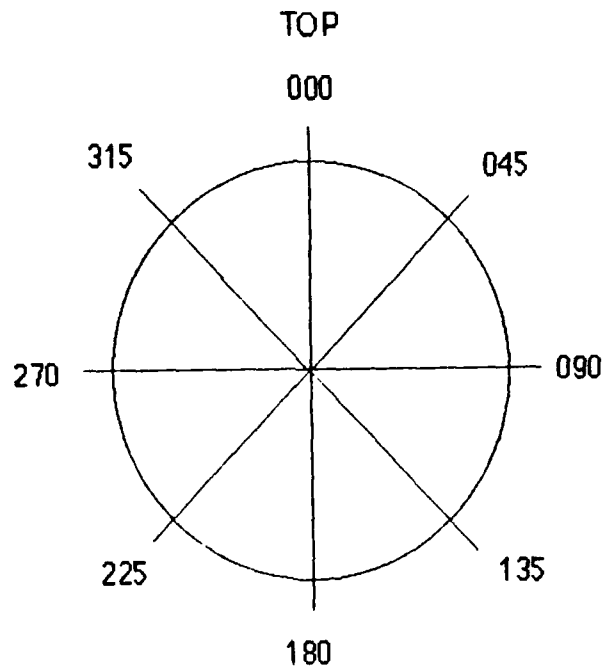


Figure 41: Orientation of $\text{CaF}_2\text{:Mn}$ TLD's during Angular Radiation Pattern Experiments.

b. 75 kV Series

The results of the 75 kV series, shown in Figures 42 - 45, indicate that the radiation field is not symmetrical. In fact, relative maxima were found to occur at either side of the geometric center in all shots. This effect is most apparent in the 045-225 orientation shot. (Figure 44).

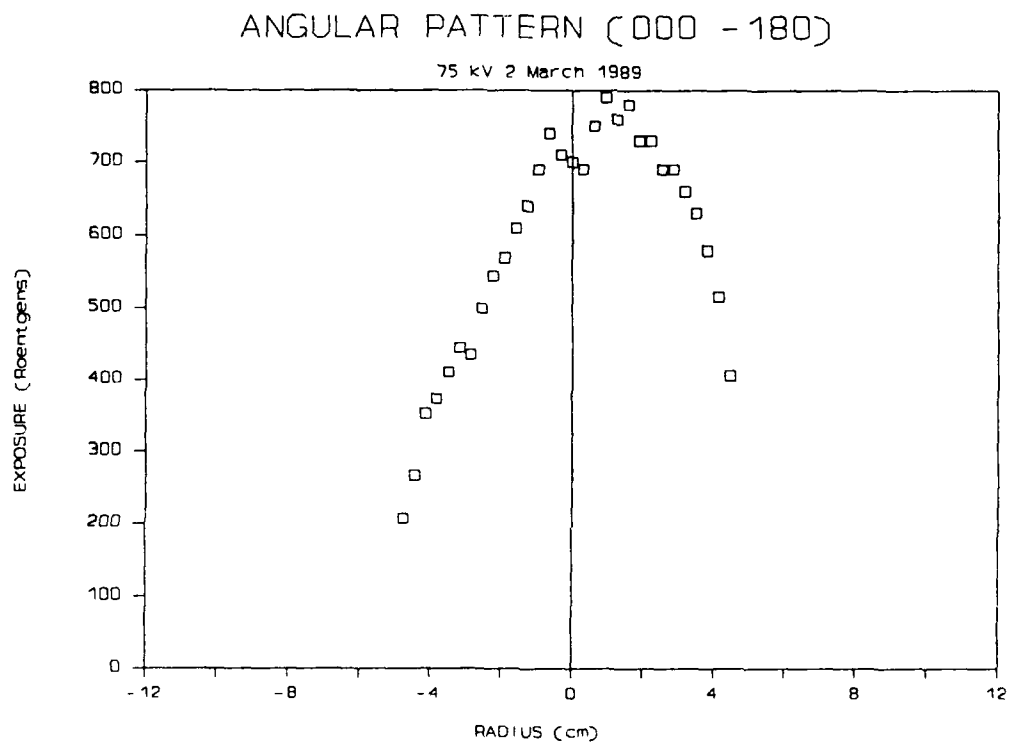


Figure 42: Pulserad 112A 75 kV Radiation Exposure Pattern Measured with $\text{CaF}_2:\text{Mn}$ TLD's Orientated at $000^\circ - 180^\circ$ with respect to the Vertical (See Fig 41)

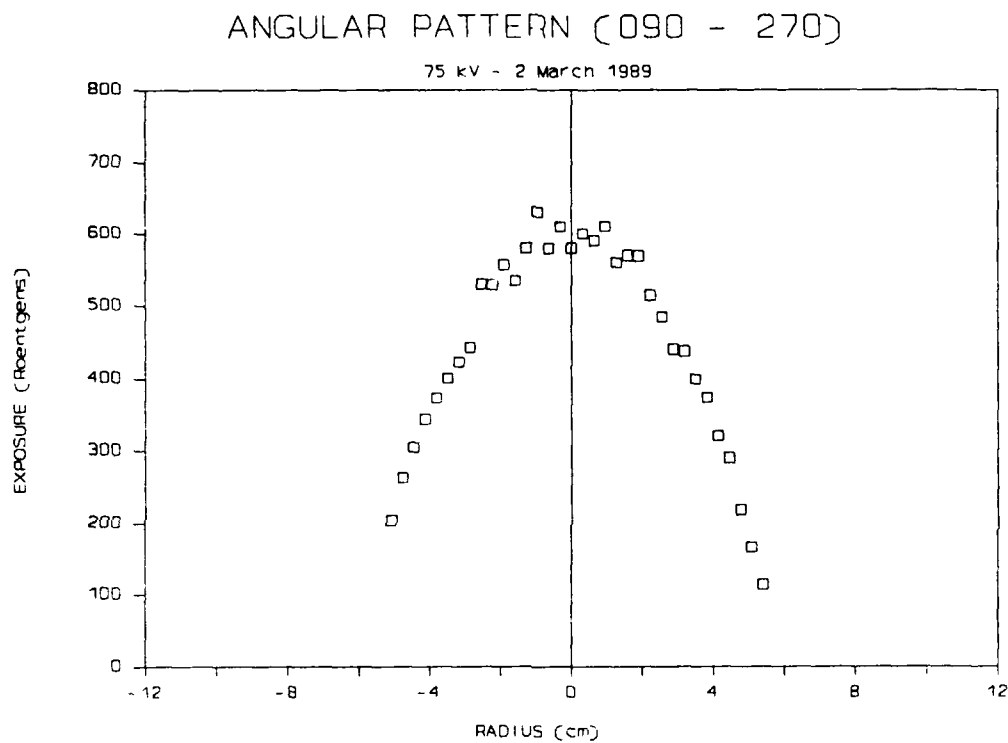


Figure 43: Pulserad 112A 75 kV Radiation Dose Pattern Measured with $\text{CaF}_2:\text{Mn}$ TLD's Orientated at 090° - 270° with Respect to the Vertical. (See Fig 41)

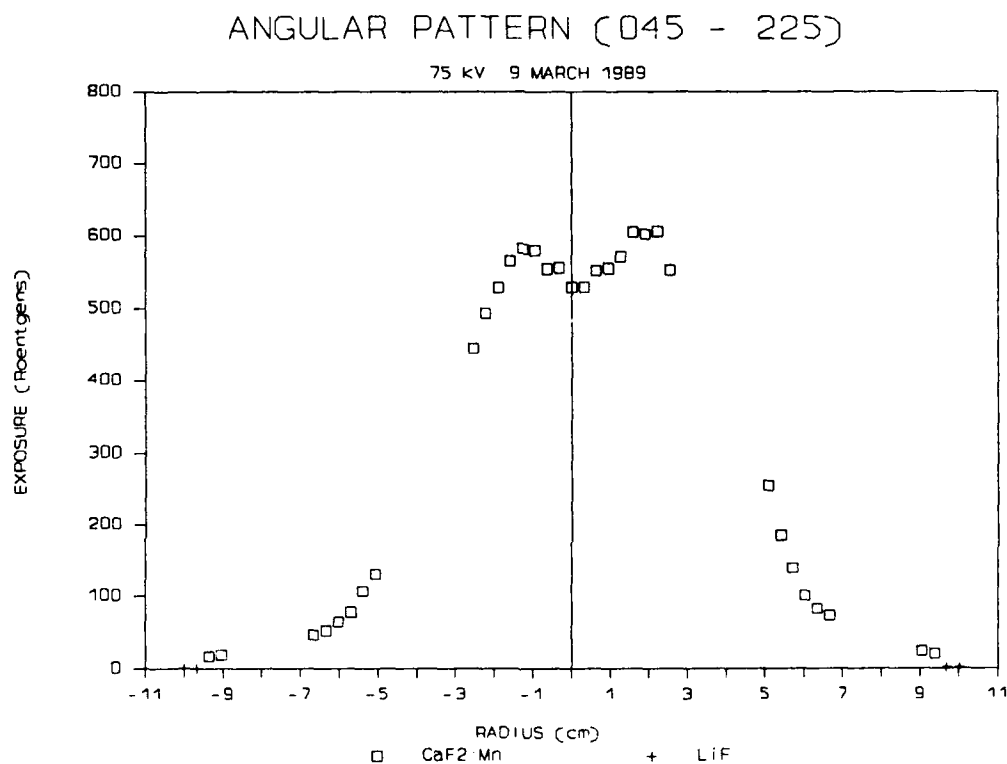


Figure 44: Pulserad 112A 75 kV Radiation Exposure Pattern Measured with $\text{CaF}_2\text{:Mn}$ TLD's Orientated at $045^\circ - 225^\circ$ with respect to the Vertical (See Fig 41) (Note: No Data Recorded for Blank Areas Between 2.54 and 5.08 cm (1-2 in)).

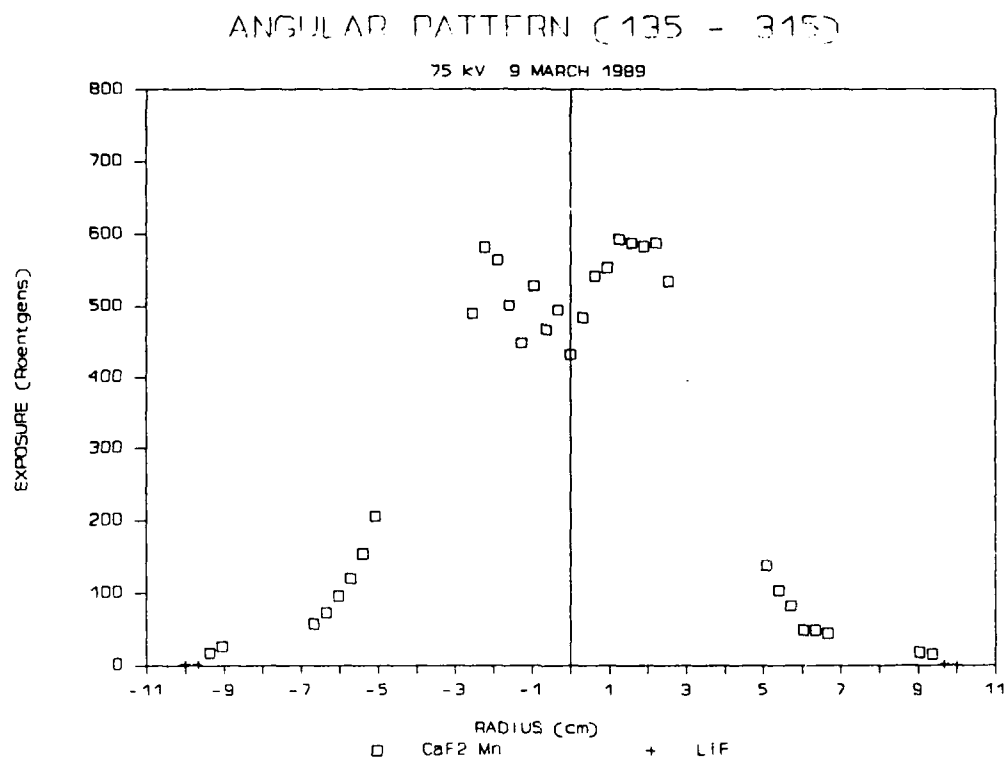


Figure 45: Pulserad 112A 75 kV Radiation Exposure Pattern Measured with CaF₂:Mn TLD's Orientated at 135° - 315° with respect to the Vertical (See Fig 41) Note: No Data Recorded for Blank Areas Between 2.54 and 5.08 cm (1 - 2 in).

The exposure recorded at the geometric center for each shot varied between 432 - 700 R. The maximum exposure recorded for each shot varied between 593 - 790 R. To remove the effect of this shot-to-shot variation, the normalized pattern was produced at each angle. This normalization was performed by dividing each recorded exposure by the maximum exposure for that particular shot. The results of this are depicted graphically below. (Figures 46 - 49) Note the variation in intensity and position of the relative minimum. In the 090-270 orientation (Figure 47) the "dip" is almost indiscernible, while in the 135-315 orientation (Fig 49) the center "intensity" reduces to almost 75% of the maximum.

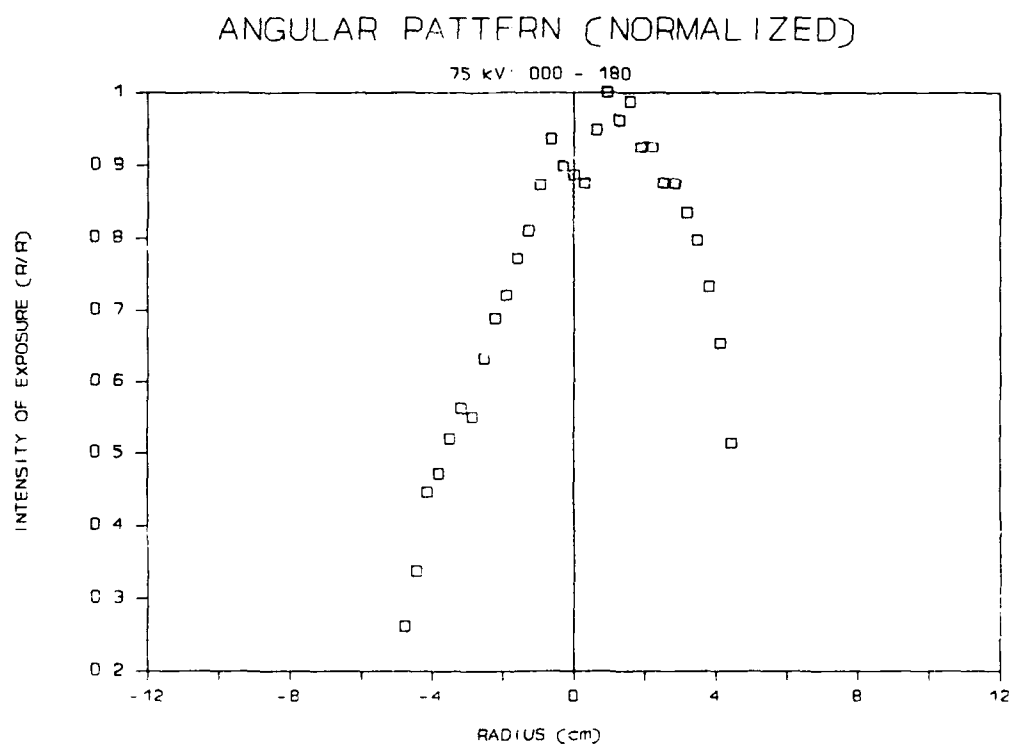


Figure 46: Normalized 75 kV Exposure Pattern of 000° - 180° Orientation . (See Fig 42)

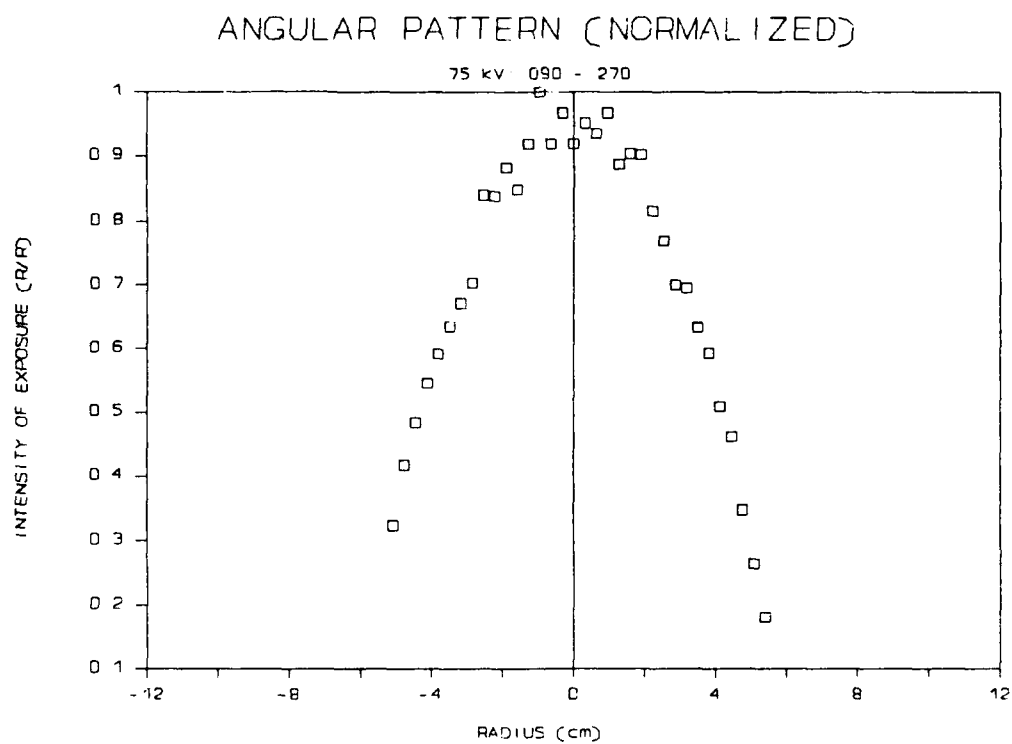


Figure 47: Normalized 75 kV Exposure Pattern of 090° - 270° Orientation. (See Fig 43) The Center "dip" is Almost Indiscernible at this Orientation.

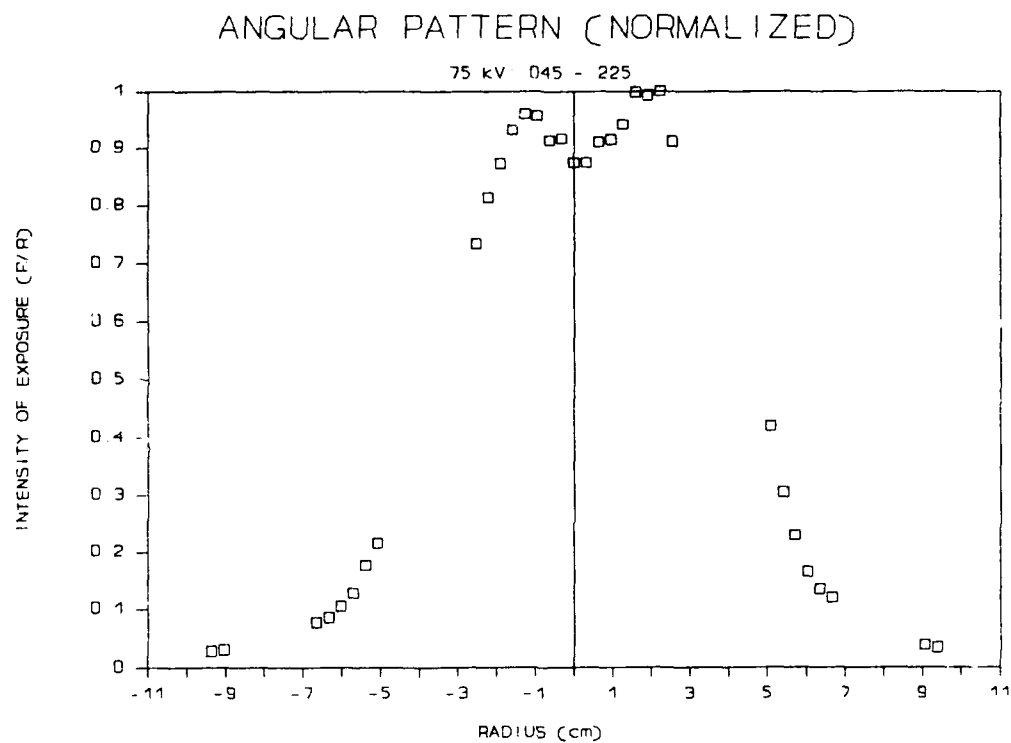


Figure 48: Normalized Exposure Pattern of 045° - 225° Orientation. (See Fig 44) The "dip" at the Center is most Clearly Shown here.

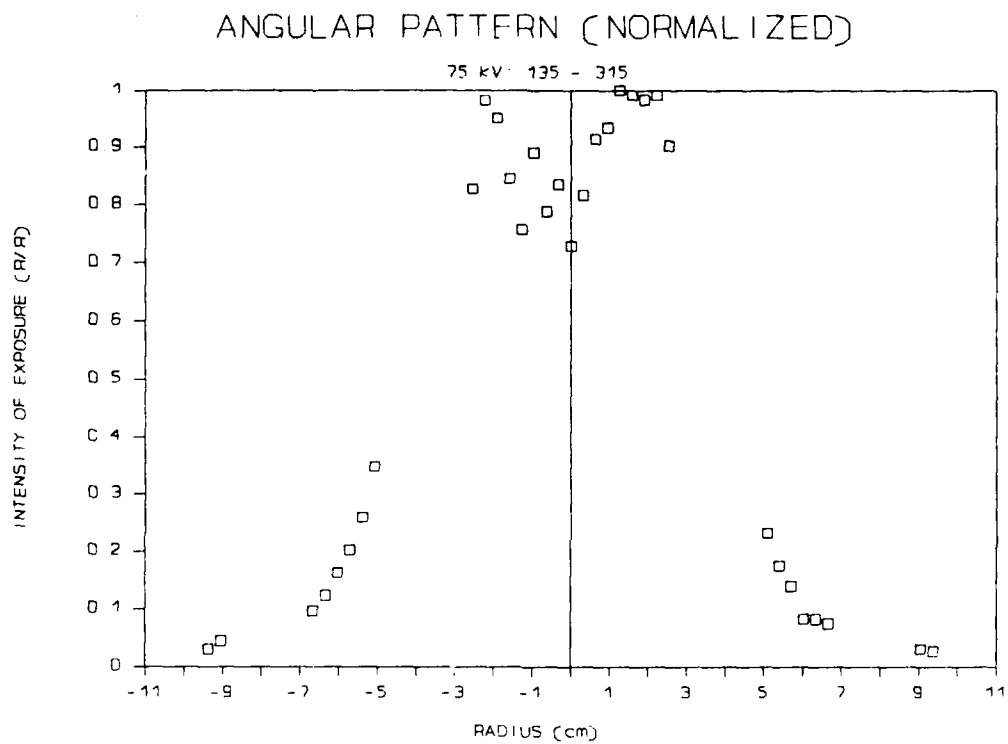


Figure 49: Normalized 75 kV Exposure Pattern of 135° - 315° Orientation. (See Fig 45) The Relative Minimum at the Center is approximately 75% of the Maximum Intensity.

Table XVI lists the position of the relative maxima for each orientation. They all occur between 0.635 cm (2/8 in) and 2.25 cm (7/8 in) from the geometric center.

TABLE XVI: LOCATION OF RELATIVE MAXIMA IN 75 kV ANGULAR PATTERN EXPERIMENTS.

Angle (degrees)	Radius (cm)	Exposure (R)
000	0.95	790
045	2.22	606
090	0.95	630
135	1.27	593
180	0.64	740
225	1.27	582
270	0.95	610
315	2.22	582

The average radius of the relative maxima is $1.3 \pm .6$ cm. The cathode tip in use had a radius of 1.58 cm (5/8 in), indicating a "maxima ring" is formed approximately .32 cm (1/8 in) inside the outer edge of the cathode tip. (Figure 50)

c. 100 kV Series

Figures 51 - 54 summarize the results of the 100 kV Series. As before, the patterns are not symmetrical about the geometric center of the anode assembly. The exposures at the center varied between 2040 R and 2820 R, while the maximum recorded exposures varied between 2720 R and 3330 R in this series.

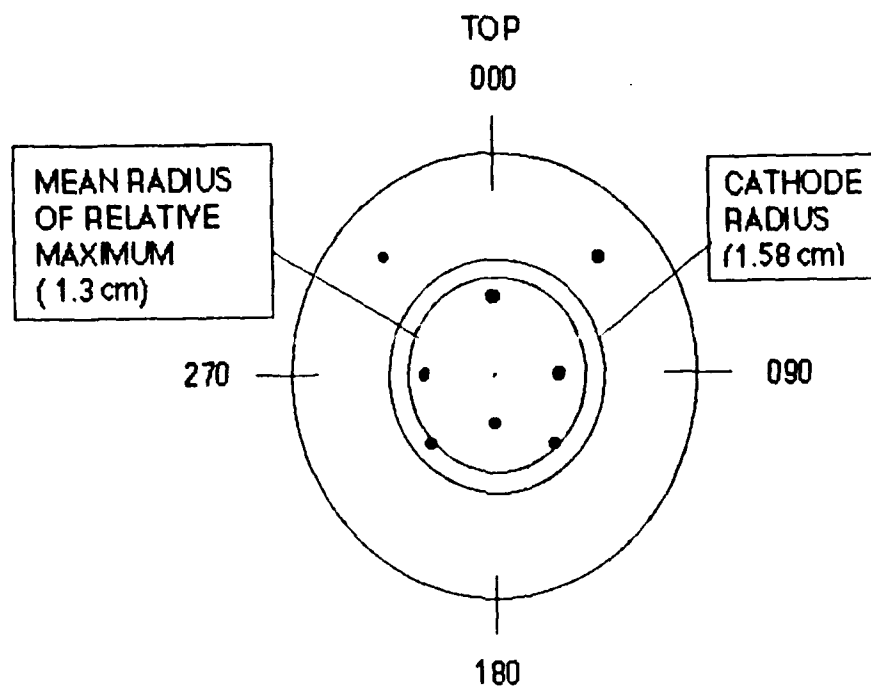


Figure 50: Location of Measured Relative Maxima with respect to Cathode Geometry during 75 kV Angular Pattern Experiments.

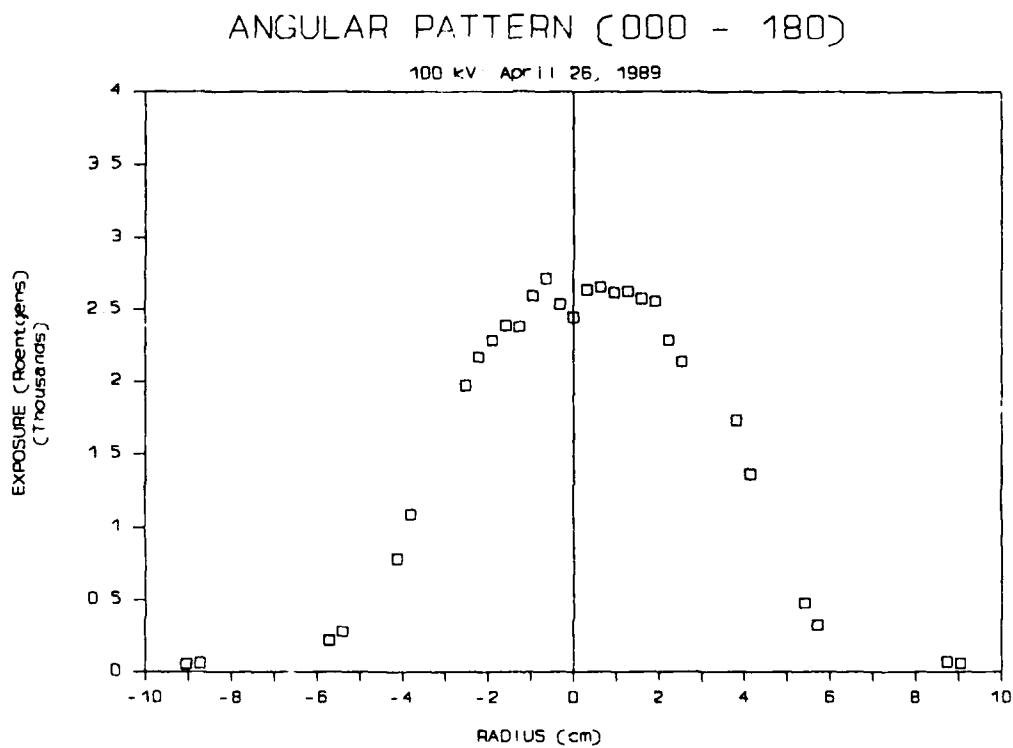


Figure 51: Pulserad 112A 100 kV Radiation Exposure Pattern Measured with $\text{CaF}_2:\text{Mn}$ TLD's Orientated at $000^\circ - 180^\circ$ With Respect to Vertical . (See Fig 41)

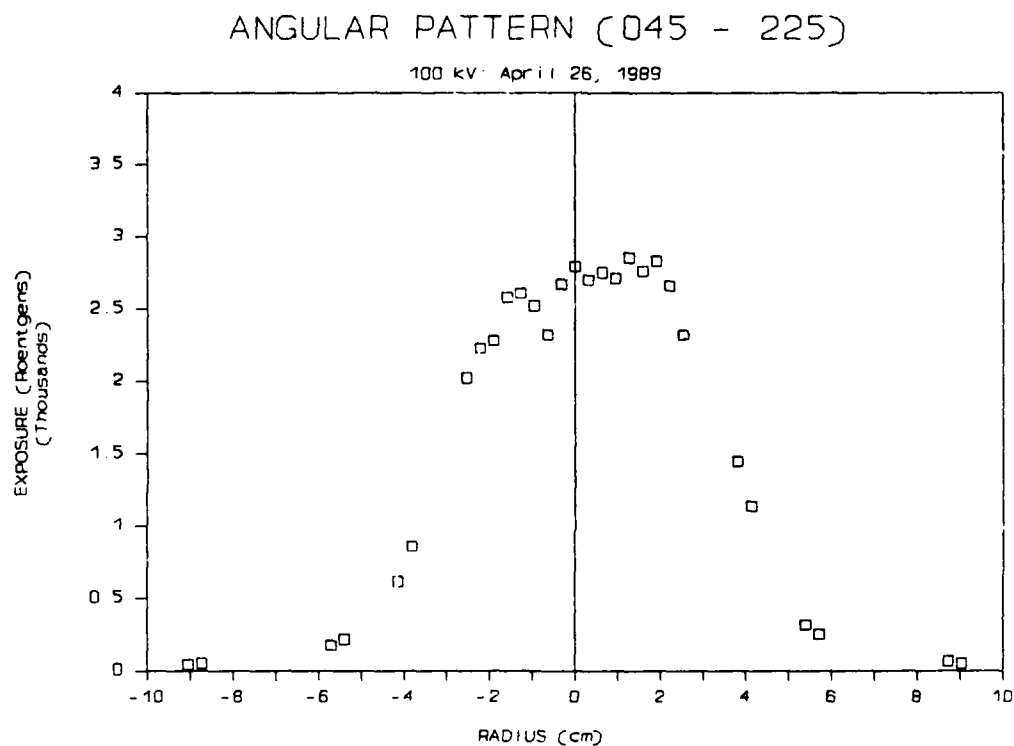


Figure 52: Pulserad 112A 100 kV Radiation Exposure Pattern Measured with $\text{CaF}_2\text{:Mn}$ TLD's Orientated at 045° - 225° with Respect to Vertical (See Fig. 41)

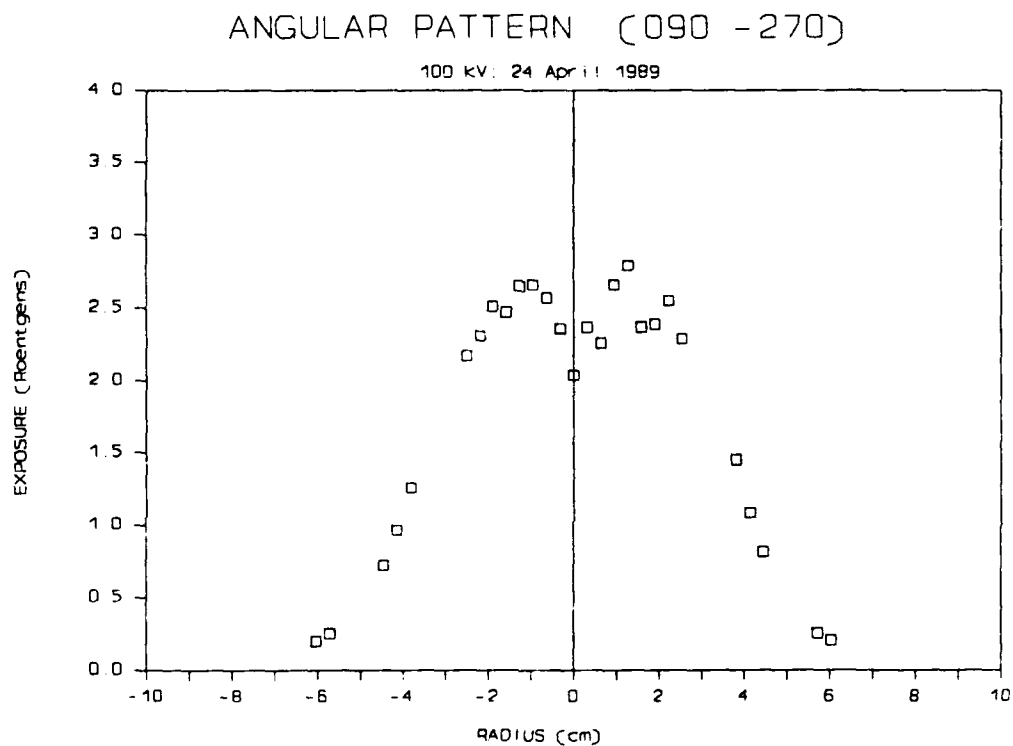


Figure 53: Pulserad 112A 100 kV Radiation Exposure Pattern Measured with $\text{CaF}_2\text{:Mn}$ TLD's Orientated at 090° - 270° with respect to Vertical. (See Fig 41)

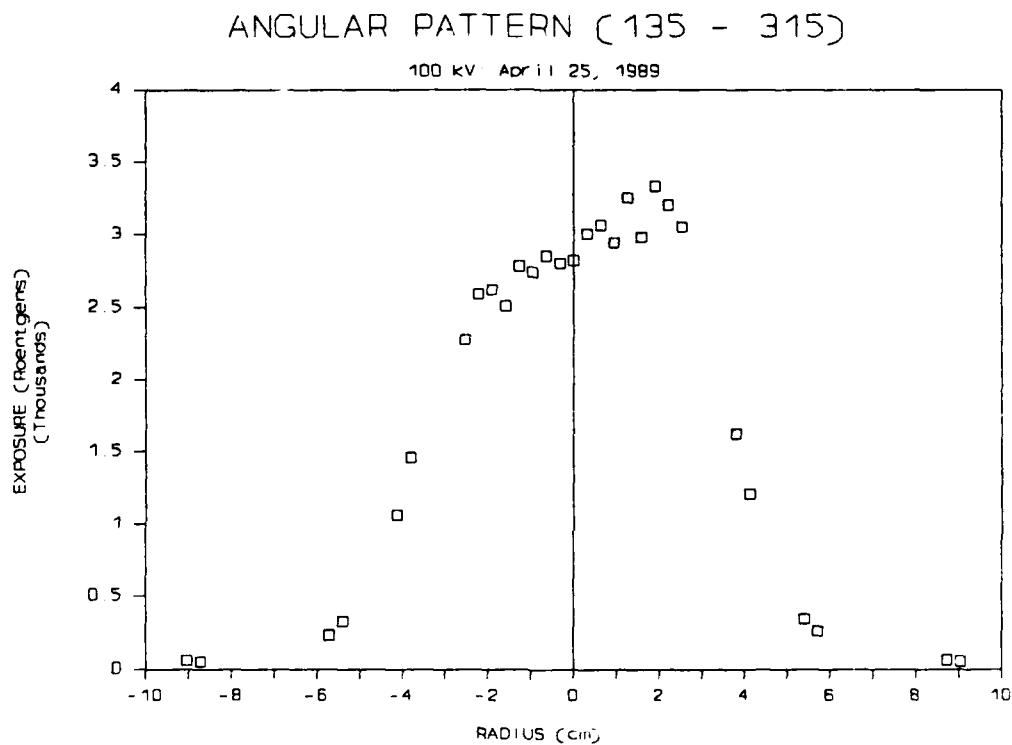


Figure 54: Pulserad 112A 100 kV Radiation Exposure Pattern Measured with $\text{CaF}_2:\text{Mn}$ TLD's Orientated at $135^\circ - 315^\circ$ with respect to Vertical. (See Fig 41)

The normalized pattern for each orientation is shown in Figures 55 - 58. Note that the center "dip", characteristic of the 75 kV series, is significant only in the 090 - 270 orientation (Figure 56) In fact, the 135 - 315 orientation (Fig 58) shows a skewed peak at 135° with respect to the vertical.

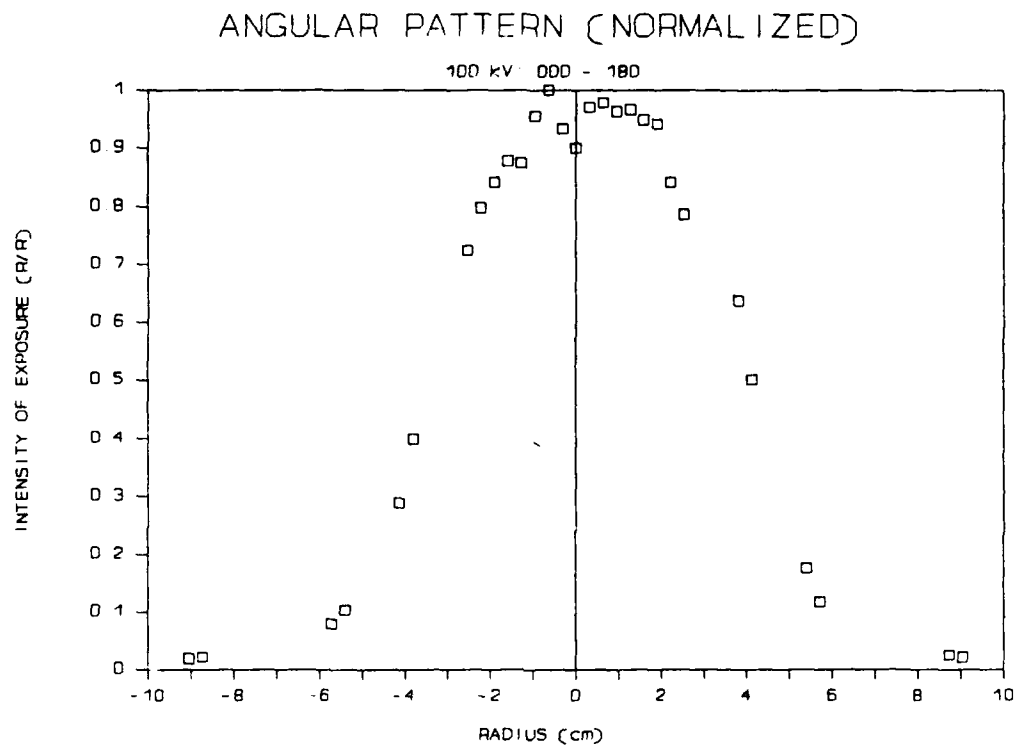


Figure 55: Normalized 100 kV Exposure Pattern of 000° - 180° Orientation. (See Fig 51) The "dip" at the Center is on the Order of 10% of the Maximum Exposure.

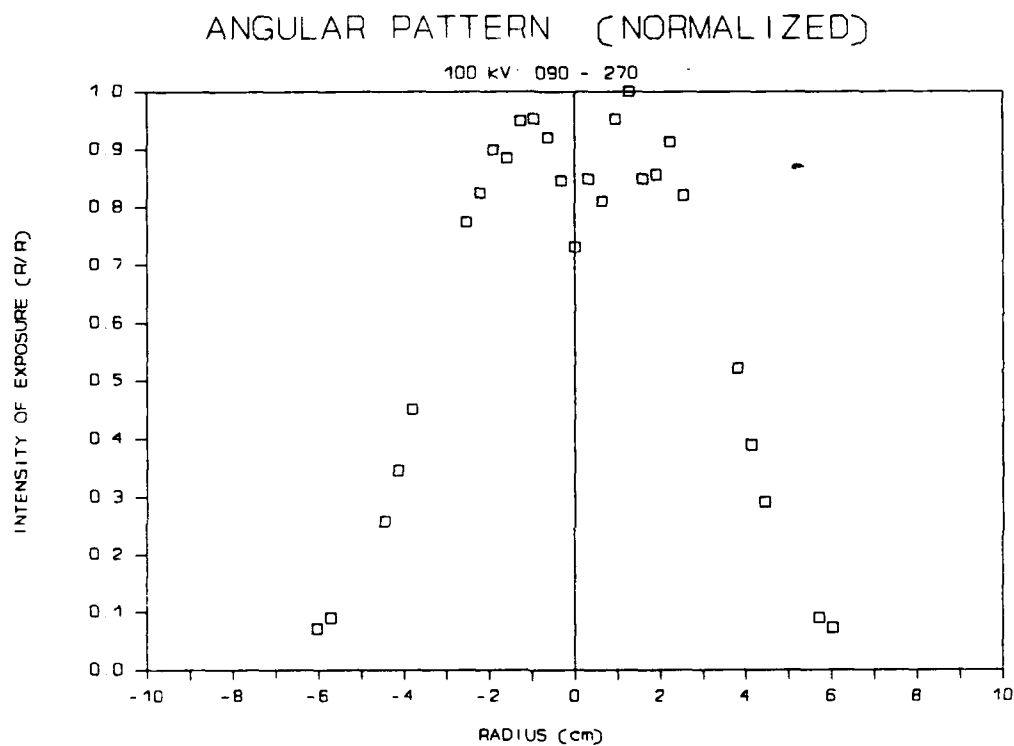


Figure 56: Normalized 100 kV Exposure Pattern of 090° - 270° Orientation. (See Fig 53) The Center "dip" is Most Prominent on this 100 kV Shot.

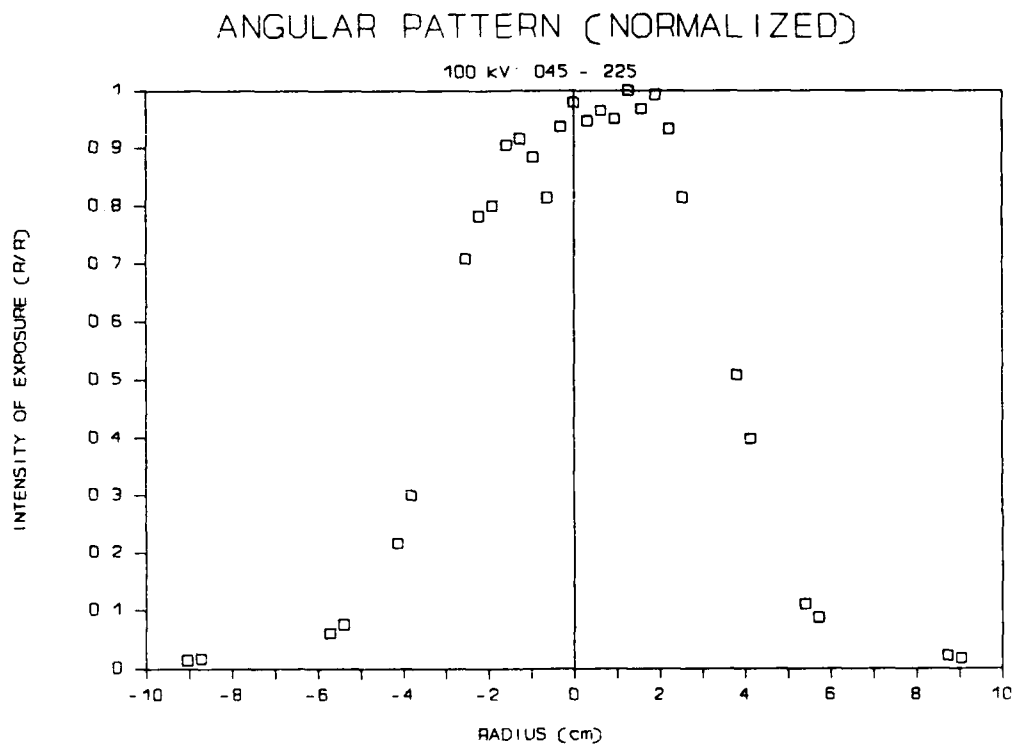


Figure 57: Normalized 100 kV Exposure Pattern of 045° - 225° Orientation. (See Fig 52)

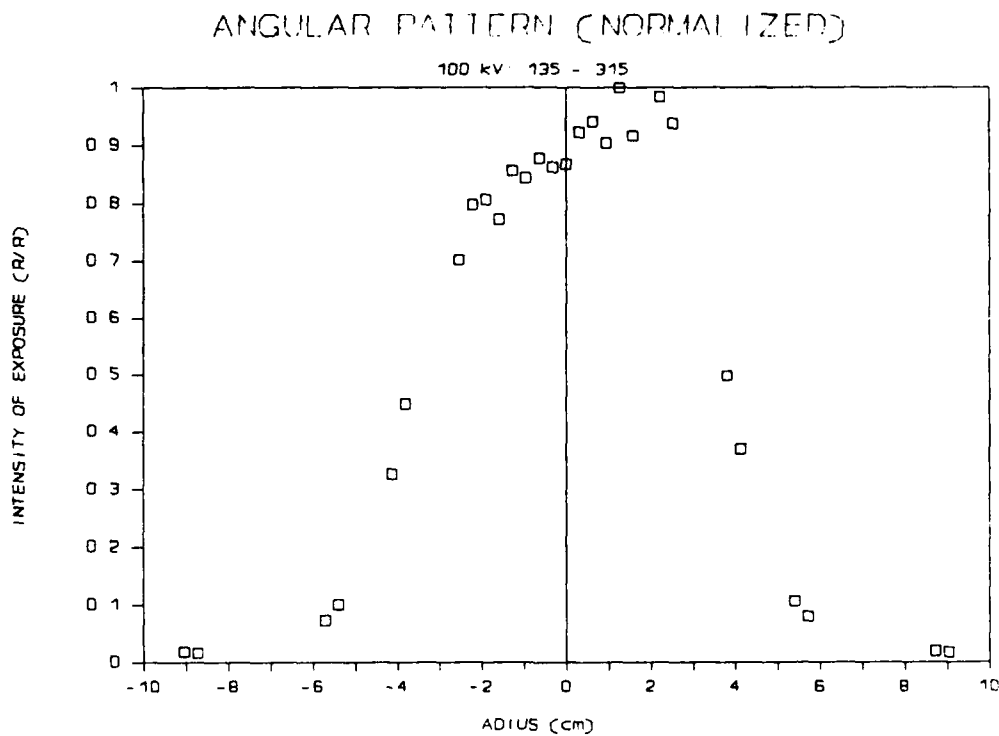


Figure 58: Normalized 100 kV Exposure Pattern of 135° - 315° Orientation (See Fig 54).

d. Shot - to - Shot Variation

As mentioned in Section 1, variations in the exposures recorded were noted between shots made at the same Marx Charge Voltage. To quantify the amount of variation, analysis of the maximum recorded exposure for angular pattern shots and analysis of recorded geometric center exposures for all shots taken was made for voltages of 75 and 100 kV. The results are summarized in Tables XVII and XVIII below.

TABLE XVII: VARIATION OF EXPOSURE MEASURED WITH $\text{CaF}_2\text{:Mn}$ TLD'S AT GEOMETRIC CENTER OF ANODE ASSEMBLY.

Voltage	75 kV	100 kV
Minimum Exposure	432 R	2040 R
Maximum Exposure	895 R	3090 R
Number of Data Sets	10	7
Mean Exposure	600 ± 150 R	2600 ± 340 R

TABLE XVIII: VARIATION OF MAXIMUM EXPOSURE MEASURED WITH $\text{CaF}_2\text{:Mn}$ TLD's DURING ANGULAR PATTERN EXPERIMENTS.

Voltage	75 kV	100 kV
Minimum Exposure	606 R	2330 R
Maximum Exposure	790 R	3850 R
Number of Data Sets	4	6
Mean Exposure	660 ± 90 R	3000 ± 500 R

Additionally, in Section 2, it was noted that the radiation pattern varied as a function of orientation. In fact, comparison of similar orientations between the 75 kV and 100 kV Angular Patterns series shows considerable differences. However, between these two series, the cathode was removed several times to permit "firing" of "new" cathodes. Although the original cathode was replaced for these "mapping" experiments, the orientation of the cathode and anode were probably changed upon reassembly. (The original orientation had not been marked.) Figures 59, 60 and 61 show the various radiation pattern recorded at 100 kV for the 090 - 270 orientation on various days.

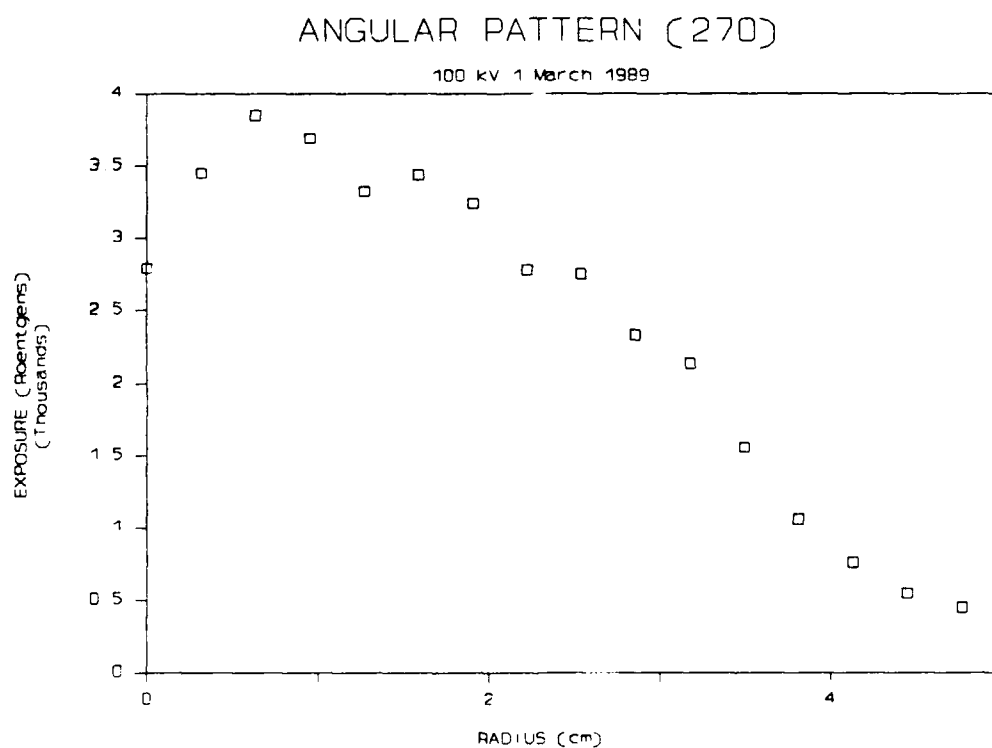


Figure 59: Pulserad 112A 100 kV Exposure Pattern Measured with $\text{CaF}_2:\text{Mn}$ TLD's Orientated 270° with Respect to Vertical. (See Fig 41).

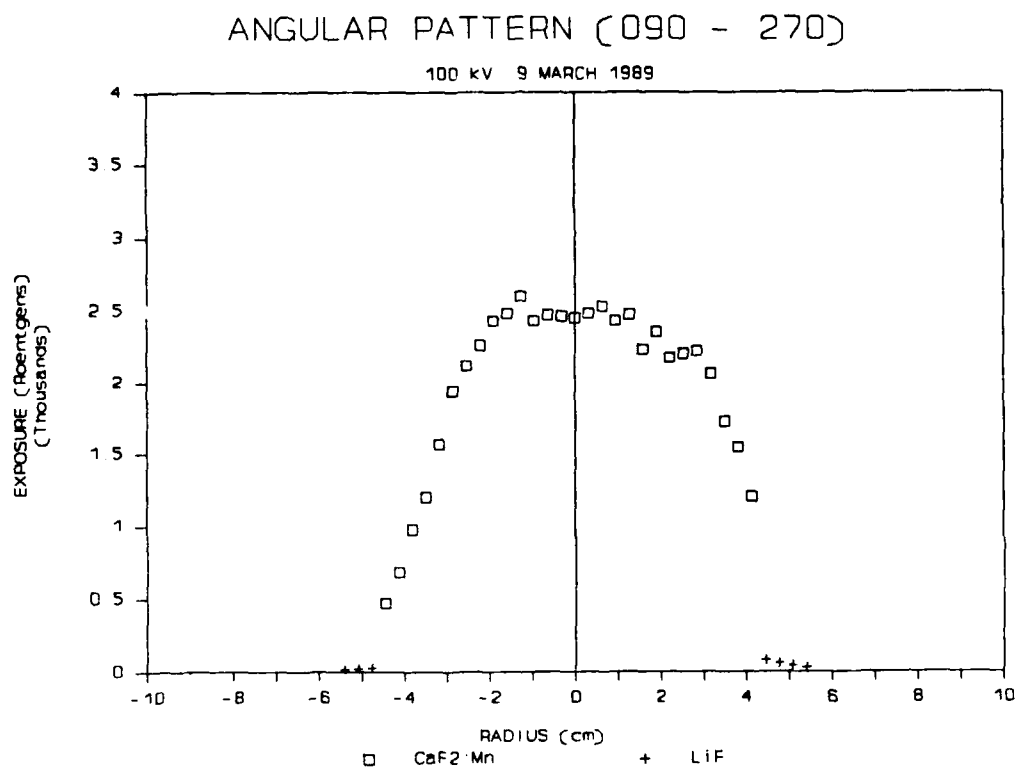


Figure 60: Pulserad 112A 100 kV Exposure Pattern Measured with CaF₂:Mn TLD's Orientated 090° - 270° with respect to the Vertical. Central "dip" is much Less Pronounced.

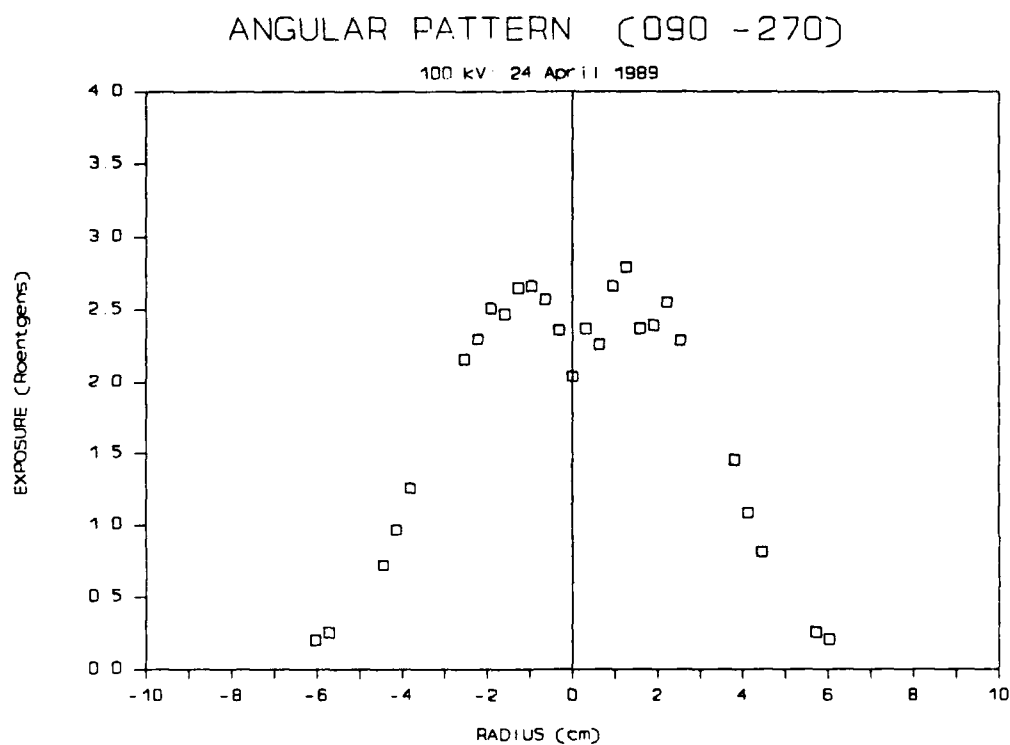


Figure 61: Pulserad 112A 100 kV Exposure Pattern Measured with $\text{CaF}_2:\text{Mn}$ TLD's Orientated 090° - 270° with respect to Vertical. Taken After Re-orientation of the Anode-cathode System; Note the Prominent Central "dip".

A photograph of the tantalum target taken prior to the 100 kV Series is shown in Figure 62. Of significance is the lack of symmetry of the anode damage with respect to the geometric center.



Figure 62: Tantalum Target in Pulserad 112A Anode Assembly. Note the Lack of Symmetry of the Anode Damage with Respect to the Geometric Center. (Orientation of target not noted upon disassembly.)

These results indicate that one of the primary factors in determining the intensity and pattern of the radiation field is the orientation and/or condition of the cathode. This latter effect is dramatically seen in Figures 63 and 64 below. Each represents the exposure recorded with $\text{CaF}_2:\text{Mn}$ TLD's orientated 090 - 270 with respect to the vertical, of single 75 kV shots made with two different "new" cathodes. The two cathodes were identically machined and polished, and made to the specifications of the original cathode. Yet, there was a factor of two difference in the exposure measured

from them. Additionally, the exposure of each was significantly less than the mean value of 600 R measured for the original cathode.

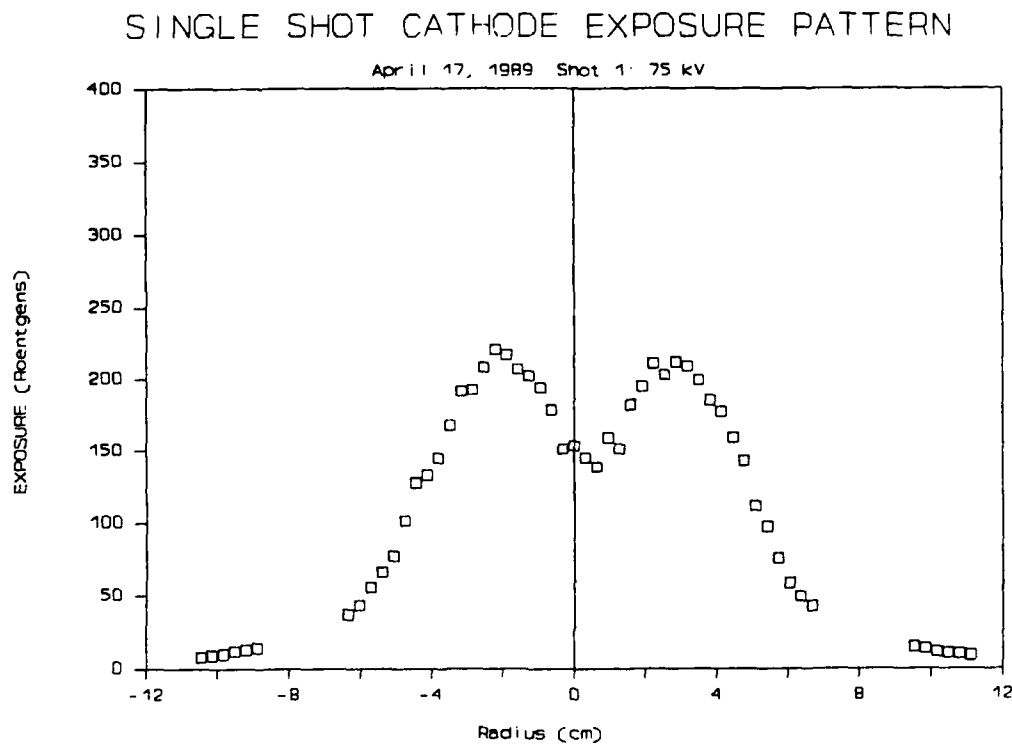


Figure 63: 75 kV Exposure Pattern of "New Cathode" Measured with $\text{CaF}_2:\text{Mn}$ TLD's Orientated $090^\circ - 270^\circ$ with respect to Vertical. Note the definite "dip" and Relatively Low Exposure.

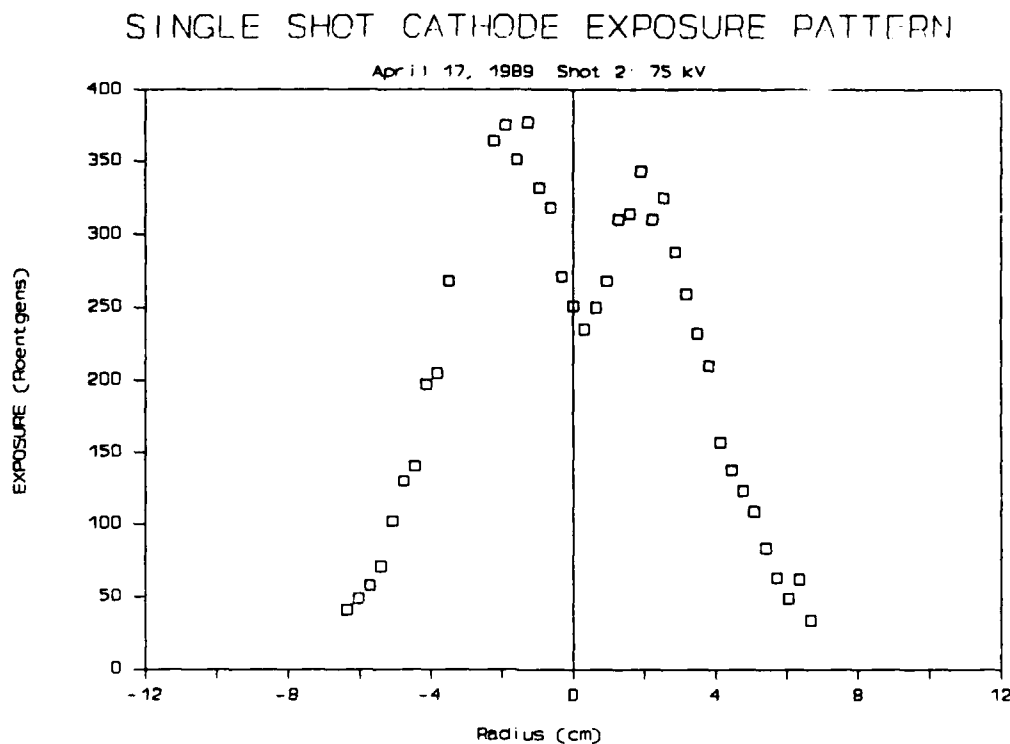


Figure 64: 75 kV Exposure Pattern of "New Cathode" Measured with $\text{CaF}_2\text{:Mn}$ TLD's Orientated $090^\circ - 270^\circ$ with respect to Vertical. Note: Definite "dip" in Pattern And Magnitude Nearly Double that of Previous Shot. (Fig 63)

In conclusion, although the variation between shots taken with different cathodes or different orientations of the same cathode on different days varies greatly, the shot-to-shot variation between shots made under identical conditions is not so dramatic. Figure 65 shows the results of two sequential shots made under identical conditions. Here, a series of $\text{CaF}_2\text{:Mn}$ TLD's were exposed at a $090 - 270$ Orientation. After the first "shot" every other chip was replaced with an annealed TLD and the series exposed again in the same orientation. Both "shots" were made at 75 kV. The resulting patterns between the two shots varied very little. The double exposed TLD's had a similar pattern with twice the exposure, as expected.

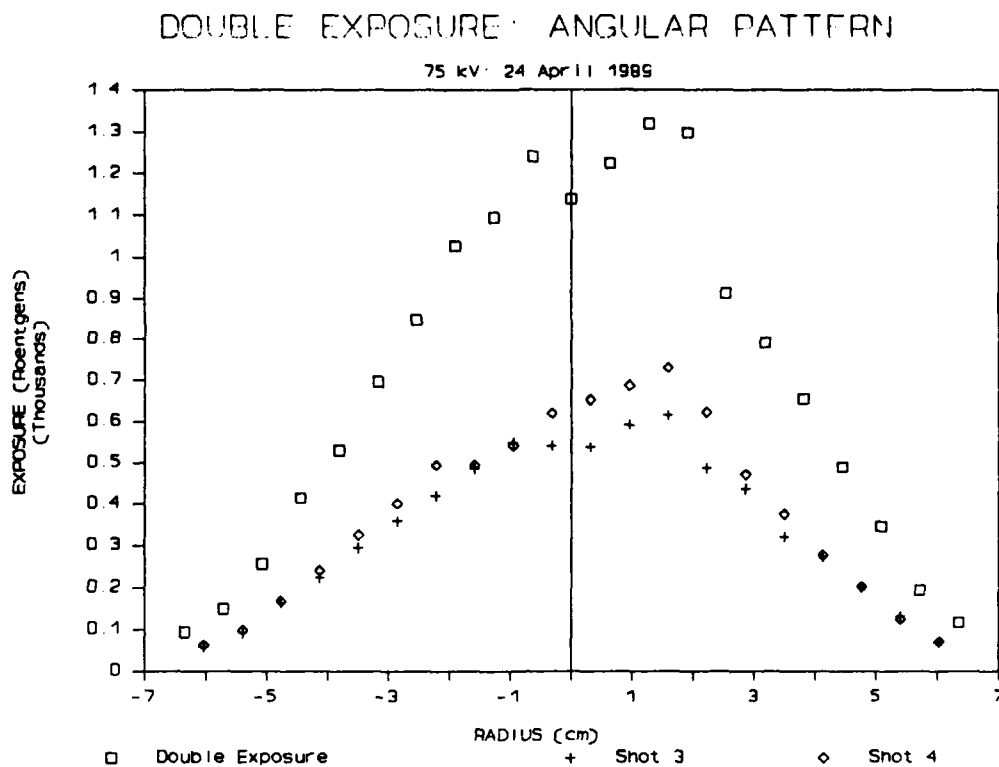


Figure 65: Exposure Pattern of Sequential 75 kV Shots Measured with $\text{CaF}_2:\text{Mn}$ TLD's Orientated at $090^\circ - 270^\circ$ with respect to Vertical. The Chips that were Irradiated Twice Measured Double the Dose of those Exposed only Once.

3. Attenuation of Radiation in Air

The purpose of this series of experiments was to determine how the radiation pattern varied as one moved axially outward from the faceplate of the anode assembly.

The following characteristics of the radiation field were noted:

- a. The characteristic center "dip" vanishes as the radiation field flattens out with increasing distance from the anode assembly.
- b. The on-axis exposure approximates a $1/R$ dependence, where R is the distance from the anode faceplate.

a. Procedure

CaF₂:Mn chip TLD's oriented at 090° - 270° with respect to vertical (Figure 41) were used to "map" the radiation field at various distances from the anode faceplate. The apparatus, shown in Figure 66, consisted of the TLD Holder (See Figure 40) mounted on an optical bench such that it's distance from the faceplate could be easily measured.

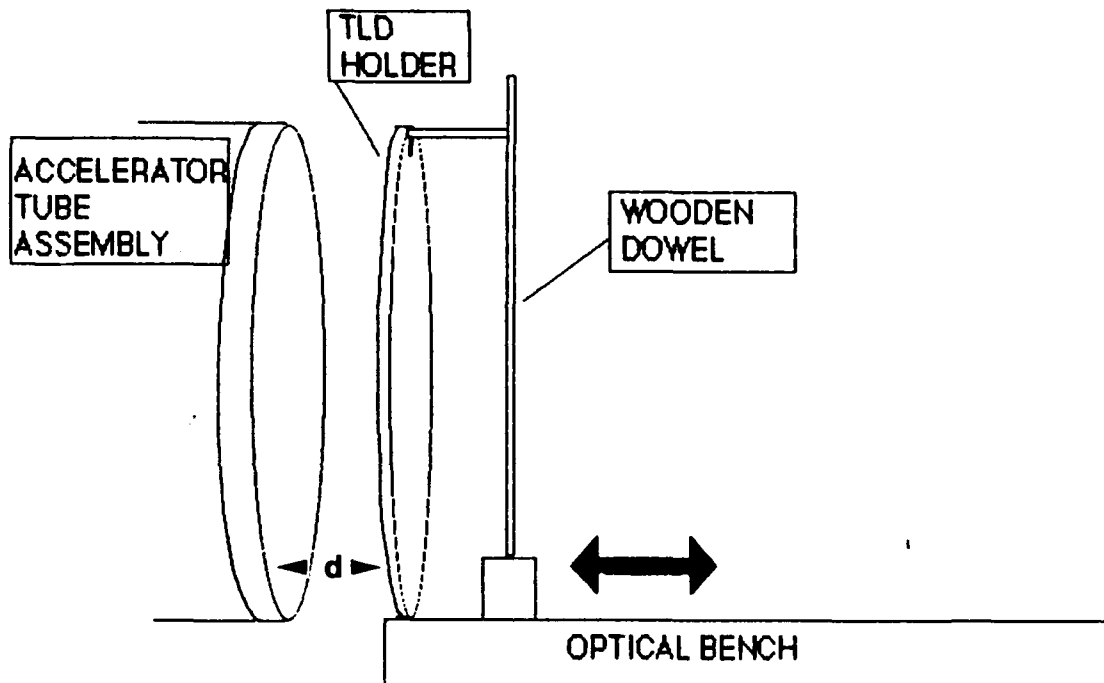


Figure 66: Experimental Set-up For Measurement of Pulserad 112A Exposure Patterns at Various Distances from Anode. Where d Denotes the Axial Distance from the Faceplate.

The chips were then exposed to the radiation field produced by the Marx Charge Voltage under investigation at various distances from the anode. This experiment was conducted for Marx Charge Voltages of 75 and 100 kV.

b. 75 kV

A series of seven 75 kV shots were taken at the following distances: 1.27 cm (1/2 in), 2.54 cm (1 in), 3.81 cm (1.5 in), 5.72 cm (2.25 in), 6.98 cm (2.75 in), 9.52 cm (3.75 in), and 12.06 cm (4.75 in). The data and resulting exposure patterns are shown in Appendix C. Even at a distance of 1.27 cm (1/2 in) the characteristic central "dip" is gone.

Figure 67 below shows a composite of four of the seven shots. Note how the exposure "flattens out" along the diameter as the distance away from the anode increases.

Prior to this experiment it was believed that the intensity would drop off as $1/R^2$, where R is the distance from the anode faceplate. This is not true for all directions. The On-Axis Exposures for various distances is tabulated below. (Table XIX) The actual dependence of the on-axis exposure is approximately $1/R$. (Figure 68). This is most likely due to the forward focus of the radiation source.

Linear Interpolation of the data in Appendix C was done to determine lines of "constant exposure dose". Figure 69 shows the results of this calculation for exposures of 50, 75, 100, 200, 300, and 400 R. (The "solid" symbols represent average values of exposure measured at a particular radial position on the faceplate.)

EXPOSURE VS RADIUS: VARIOUS DISTANCES

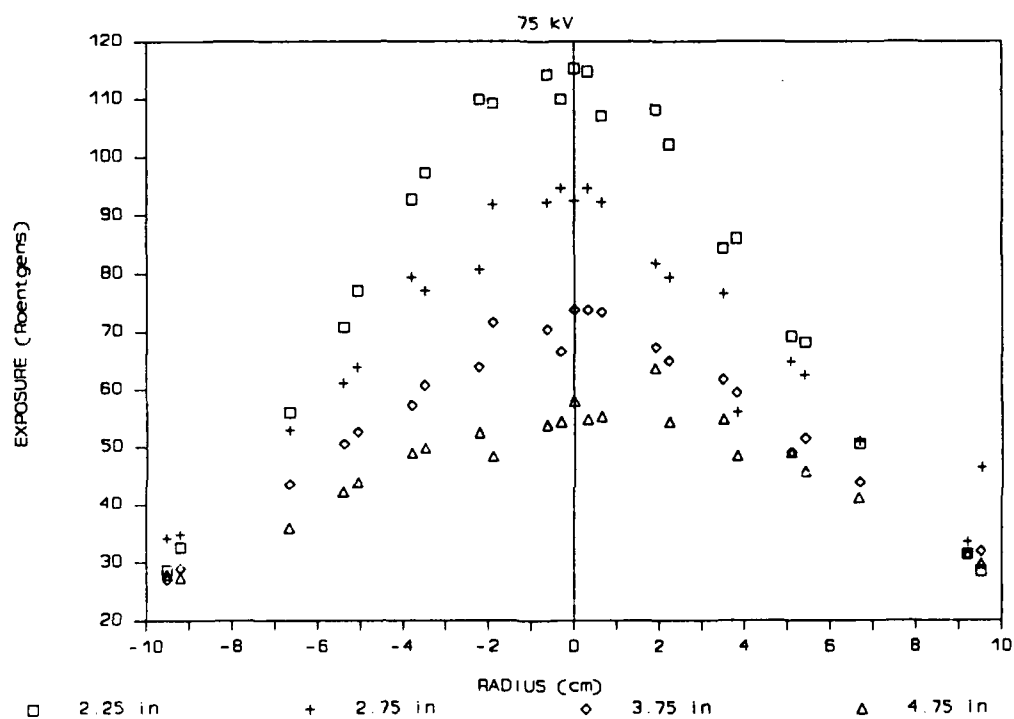


Figure 67: Pulserad 112A 75 kV Exposure Patterns at Various Distances from Anode (5.21 cm, 6.98 cm, 9.52 cm, 12.06 cm) Measured with $\text{CaF}_2:\text{Mn}$ TLD's Oriented at $090^\circ - 270^\circ$ with Respect to Vertical.

TABLE XIX: ON-AXIS EXPOSURE AT VARIOUS DISTANCES FROM THE ANODE FACEPLATE (75 kV)

Distance (cm)	Exposure (R)
1.27	403
2.54	276
3.81	141
5.72	115
6.98	92
9.52	77
12.06	58

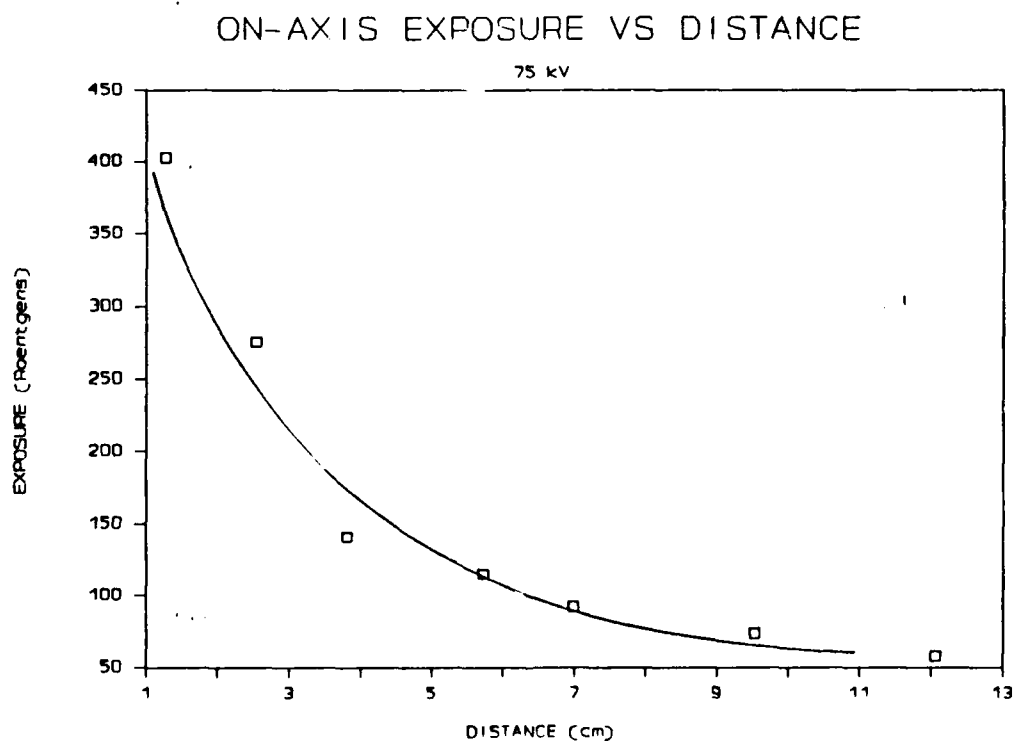


Figure 68: On-Axis Exposure for Various Distances Measured with $\text{CaF}_2:\text{Mn}$ TLD's. Marx Charge Voltage of 75 kV. Note: Intensity Decreases at approximately $1/\text{Distance}$, (Solid Line).

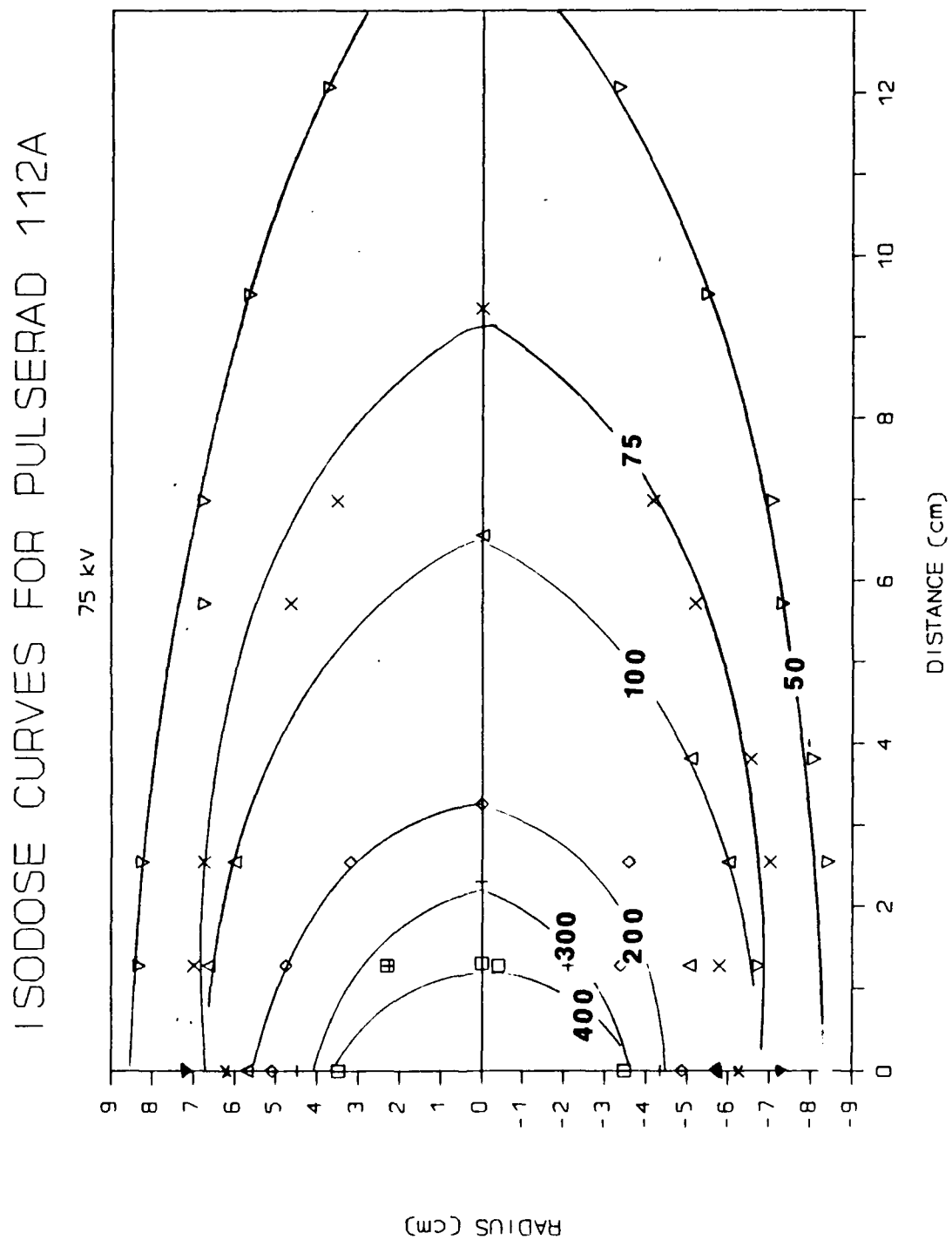


Figure 69: Pulserad 112A 75 kV Contours of Constant Exposure (R), as Measured with $\text{CaF}_2\text{:Mn}$ TLD's. The Symbols are Interpolated Values. (See Text)

The orientation of these contours with respect to the anode faceplate is a plane perpendicular to the anode faceplate orientated at 090 - 270 with respect to the vertical. This is shown in Figure 70 below.

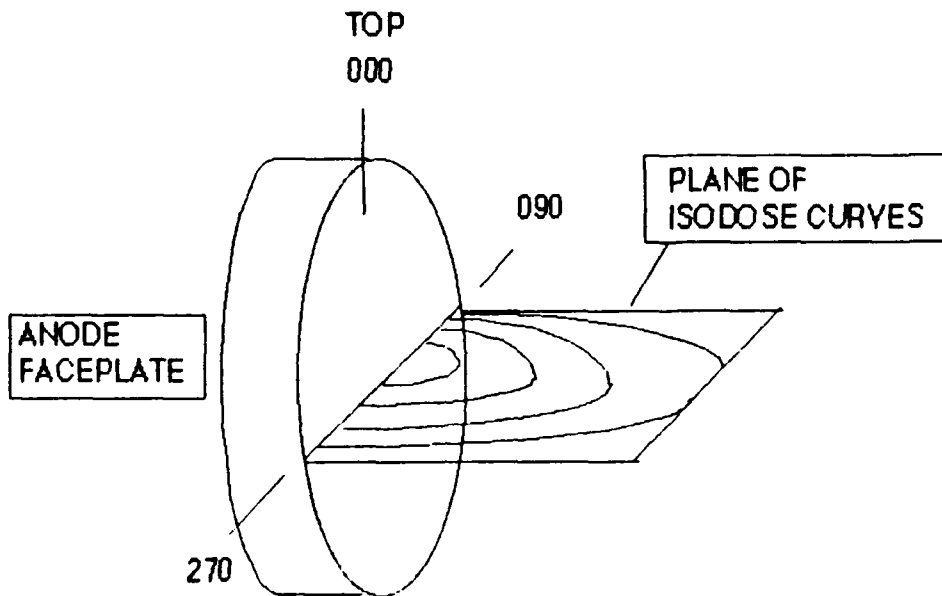


Figure 70: Orientation of Isodose Contour lines (Figure 69) with Respect to the anode Faceplate.

c. 100 kV

A series of seven 100 kV shots was taken at the following distances from the anode assembly: 0.64 cm (1/4 in), 1.27 cm (1/2 in), 1.9 cm (3/4 in), 2.54 cm (1 in), 5.08 cm (2 in), 10.16 cm (4 in), and 15.24 cm (6 in). The data and resulting radiation exposure patterns are summarized in Appendix D.

Figure 71 is a composite of three of the seven shots. Again, the pattern "flattens" considerably with increasing distance. The On-Axis Exposure at various distances is summarized in Table XX. Again, the dependence approximates $1/R$, where R is the distance from the anode. (See Figure 72)

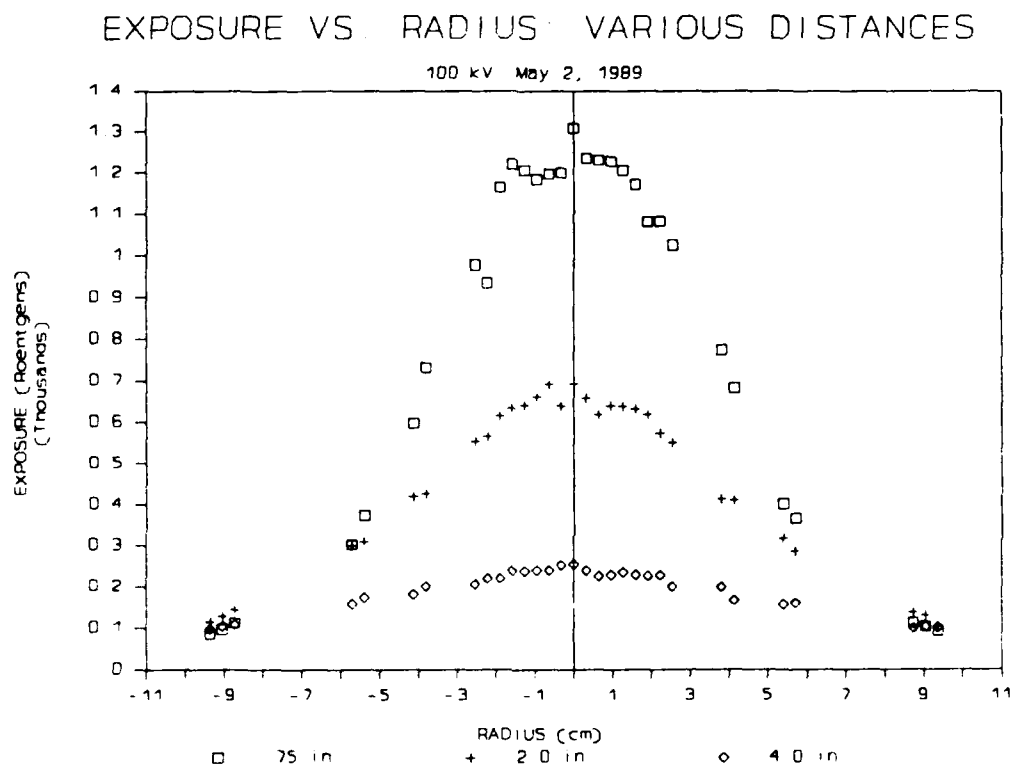


Figure 71: Pulserad 112A 100 kV Exposure Patterns at Various Distances from Anode (1.9 cm, 5.08 cm, 10.16 cm) Measured with $\text{CaF}_2\text{:Mn}$ TLD's Orientated at $090^\circ - 270^\circ$ with Respect to Vertical.

TABLE XX: ON-AXIS EXPOSURE AT VARIOUS DISTANCES FROM THE ANODE FACEPLATE (100 kV)

Distance (cm)	Exposure (R)
0.64	2290
1.27	2180
1.90	1309
2.54	1064
5.08	693
10.16	255
15.24	125

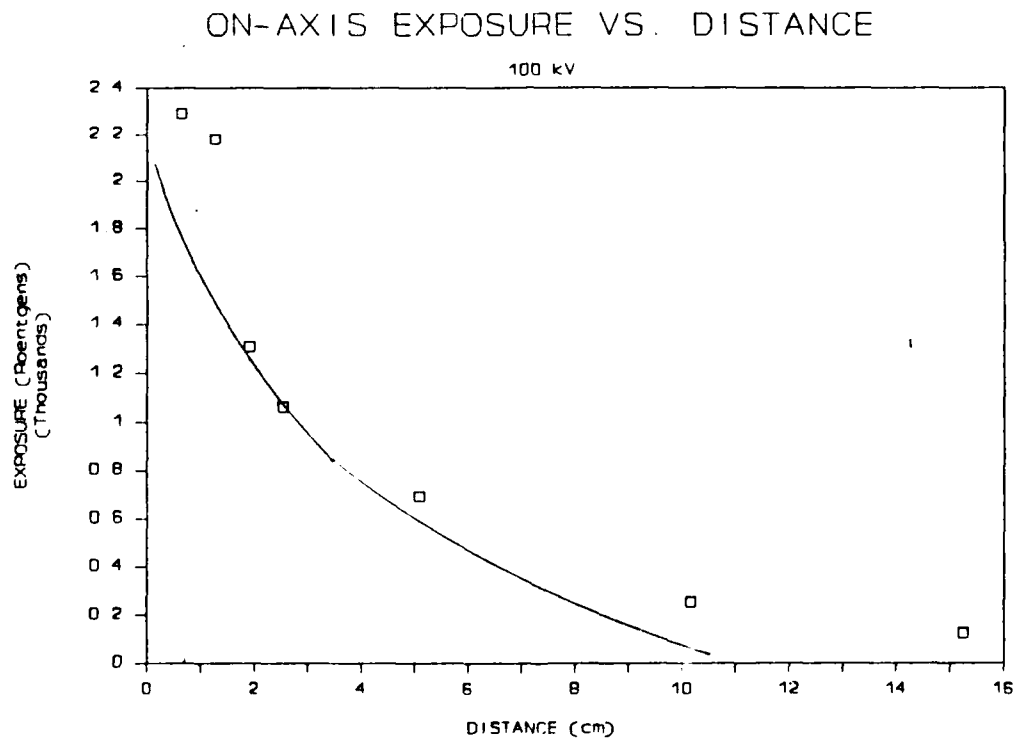


Figure 72: On-Axis Exposure for Various Distances Measured with $\text{CaF}_2\text{:Mn}$ TLD's. Marx Charge Voltage of 100 kV. Note: Intensity decreases at approximately $1/\text{Distance}$. (Solid Curve)

Linear interpolation of the 100 kV data in Appendix D was done to determine lines of "constant exposure dose". Figure 73 show the resulting "isodose curves" for exposures of 100, 250, 500, 1000, 1500, and 2000 Roentgens.

d. Discussion

The results reported in this section should be used with care. They are not corrected for variations between shots and are not meant as "definitions" of the exposure pattern. The isodose curves in Figures 69 and 73 should be used only as a guide for predicting the dose at some point relative to the faceplate.

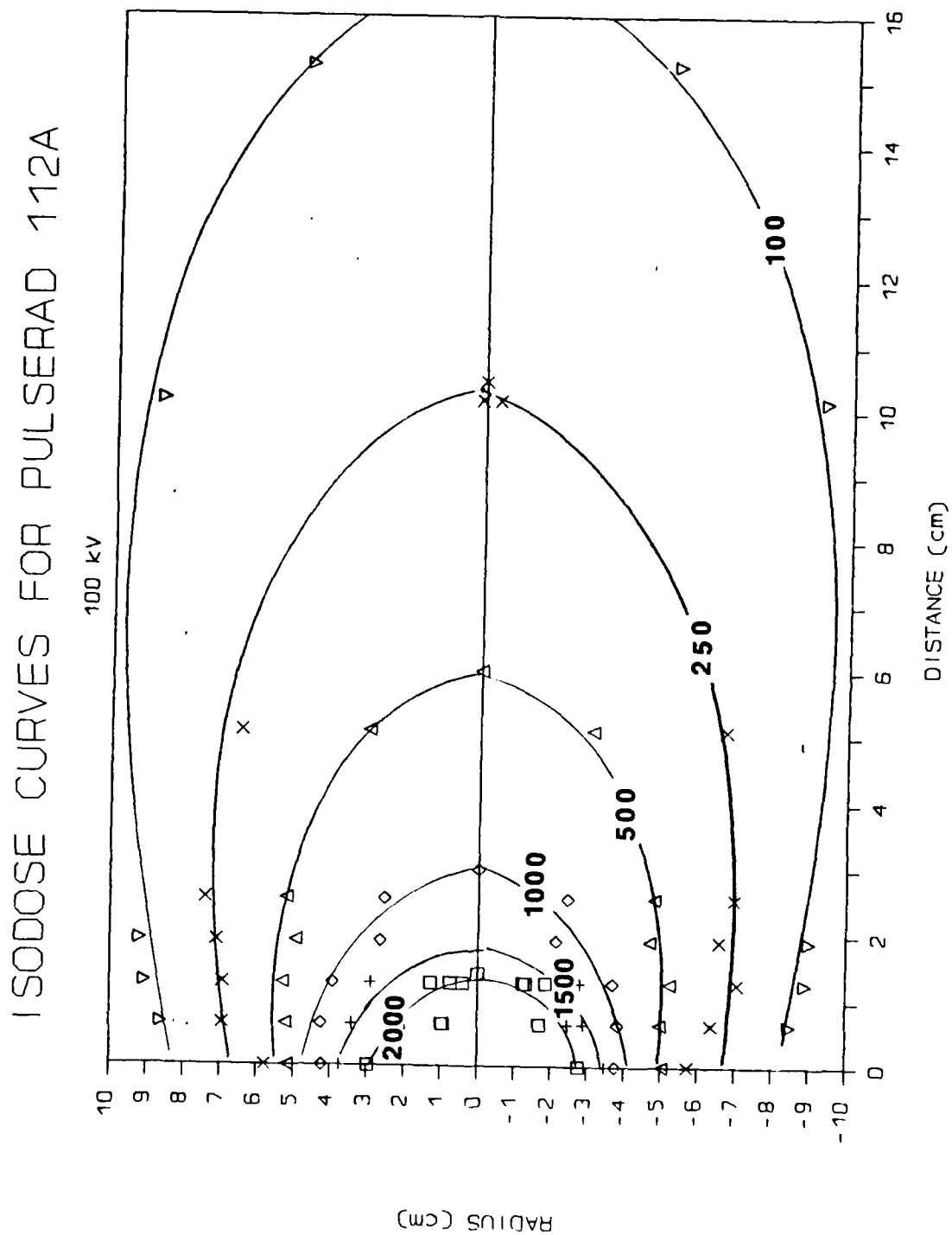


Figure 73: Pulserad 112A 100 kV Contours of Constant Exposure (R), as Measured with $\text{CaF}_2\text{:Mn}$ TLD's. The Symbols are Interpolated Values. (See Text)

VI. CONCLUSIONS AND RECOMMENDATIONS

The radiation field generated by the Pulserad Model 112A Pulsed X-Ray Generator is influenced by a variety of factors. One of the most noticeable in the initial radiation "mapping" experiments was the orientation and condition of the cathode. Additionally, it was found that accurate dosimetry information is dependent upon a thorough knowledge of the radiation source and response of the test material.

In practical radiation hardening experiments, precise measurement of dose is neither possible nor necessary. As a result, general knowledge of the photon energy spectrum coupled with an appropriately calibrated dosimetry system used under conditions of charged particle equilibrium, provide sufficient information for most applications. To this end, to make effective and meaningful use of the Pulserad Model 112A Pulsed X-Ray Generator at the Naval Postgraduate School the following areas are recommended for continued research.

1. Determination of the anode-cathode spacing that produces a "matched impedance" between the Blumlein and the diode, thereby maximizing the current and output radiation.
2. Determination of the effect of cathode and anode damage on the resulting radiation field. (Research on cathode damage is currently underway.)
3. Calculation of the photon energy spectrum using the Integrated TIGER Series of Coupled Electron/Photon Monte Carlo Code System (ITS). (Initial investigation at NPS indicates the characteristic "dip" may be a function of the geometry of the beam-anode intersection. [Ref. 18])
4. Establishment of standard procedures for calibration of TLD's and TLD Readers used in Fluorescence Measurement at NPS.

APPENDIX A

ANALYSIS OF BLUMLEIN "RESONANCE" CHARGE CIRCUIT

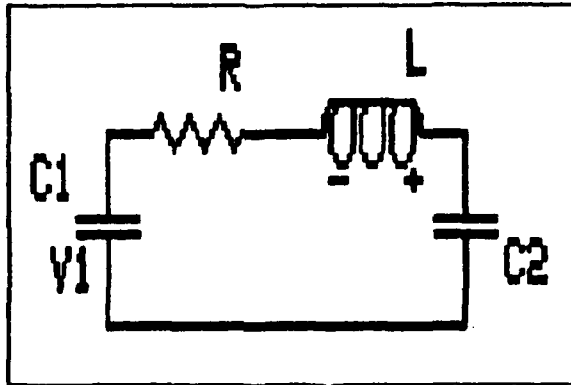


Figure A-1. Schematic Diagram of Blumlein "Resonance" Charge Circuit.

Applying Kirchoff's Law around the loop:

$$V_1 - \frac{Q_1}{C_1} - IR - L \frac{di}{dt} - \frac{Q_2}{C_2} = 0$$

Differentiating with respect to time:

$$\frac{1}{C_1} + \frac{dQ_1}{dt} + R \frac{di}{dt} + L \frac{d^2 i}{dt^2} + \frac{1}{C_2} \frac{dQ_2}{dt} = 0$$

But

$$\frac{dQ_1}{dt} = i_1$$

And

$$\frac{dQ_2}{dt} = i_2$$

Since i is constant around the loop, $i_1 = i_2$ and

$$\frac{1}{C} i + R \frac{di}{dt} + L \frac{d^2 i}{dt^2} = 0$$

where

$$C = \frac{C_1 C_2}{C_1 + C_2}$$

Rearranging terms:

$$\frac{d^2 i}{dt^2} + \frac{R}{L} \frac{di}{dt} + \frac{1}{LC} i = 0$$

The characteristic equation of this differential equation is:

$$s^2 + \frac{R}{L} s + \frac{1}{LC} = 0$$

with the following roots:

$$s = -\frac{R}{2L} \pm \sqrt{\left(\frac{R}{2L}\right)^2 - \frac{1}{LC}}$$
$$= -\alpha \pm \sqrt{\alpha^2 - \omega^2}$$

Since $\left(\frac{R}{2L}\right)^2 < \frac{1}{LC}$ (See Table III) this has solutions of the form:

$$i(t) = A_1 e^{-\alpha t} \sin \beta t + A_2 e^{-\alpha t} \cos \beta t$$

where

$$\beta = \sqrt{\omega^2 - \alpha^2}$$

Applying initial conditions:

$$1. \quad i(0) = 0$$
$$A_2 = 0$$

So

$$i(t) = A_1 e^{-\alpha t} \sin \beta t$$

2. At $t = 0$ all voltage is dropped across the inductor; i.e.

$$L \frac{di(0)}{dt} = V_1$$

$$\frac{di}{dt} = -\alpha A_1 e^{-\alpha t} \sin \beta t + \beta A_1 e^{-\alpha t} \cos \beta t$$

$$\frac{di(0)}{dt} = \frac{V_1}{L} = \beta A_1$$

$$A_1 = \frac{V_1}{\beta L}$$

therefore

$$i(t) = \frac{V_1}{\beta L} e^{-\alpha t} \sin \beta t$$

To calculate the voltage across the load (C_2)

$$\begin{aligned} v_{C_2}(t) &= \frac{1}{C_2} \int i(t) dt \\ &= \frac{1}{C_2} \frac{V_1}{\beta L} \int e^{-\alpha t} \sin \beta t dt \\ &= \frac{1}{C_2} \frac{V_1}{\beta L} \left[\frac{e^{-\alpha t}}{\alpha^2 + \beta^2} (-\alpha \sin \beta t - \beta \cos \beta t) \right] + K \end{aligned}$$

At $t = 0$ the voltage across C_2 is zero.

$$v_{C_2}(0) = 0 = \frac{1}{C_2} \cdot \frac{V_1}{\beta L} \frac{1}{\alpha^2 + \omega^2} (-\beta) + K$$

$$K = \frac{1}{LC_2} \frac{V_1}{\alpha^2 + \beta^2}$$

Therefore,

$$v_{C_2}(t) = \frac{V_1}{\alpha^2 + \omega^2} \left[-\frac{e^{-\alpha t}(\alpha \sin \beta t + \beta \cos \beta t)}{\beta} + 1 \right]$$

But

$$\alpha^2 + \beta^2 = \frac{1}{LC}$$

and

$$C = \frac{C_1 C_2}{C_1 + C_2}$$

therefore,

$$v_{C_2}(t) = \frac{V_1}{C_1 + C_2} \left[1 - e^{-\alpha t} \left(\frac{\alpha \sin \beta t + \beta \cos \beta t}{\beta} \right) \right]$$

If

$$\left(\frac{R^2}{2L} \right) \ll \frac{C_1 + C_2}{LC_1 C_2}$$

then

$$\begin{aligned} \beta &= \sqrt{\frac{1}{LC} - \left(\frac{R}{2L} \right)^2} \\ &\approx \sqrt{\frac{1}{LC}} = \omega \end{aligned}$$

and $\frac{\alpha}{\beta}$ is small.

Therefore,

$$v_{C_2}(t) \approx \frac{V_1 C_1}{C_1 + C_2} [1 - e^{-\alpha t} \cos \omega t]$$

APPENDIX B

CHARACTERISTICS OF SULFUR HEXAFLUORIDE AND COPPER SULFATE

A. SULFUR HEXAFLUORIDE

Sulfur Hexafluoride (SF_6) is the pressurizing gas used in the spark gap switches. The characteristics of SF_6 as listed in the Matheson Gas Products Data Sheet [Ref. 19] is summarized below.

PHYSICAL DATA

Molecular Weight: 146.054

Sublimation Point at 1 atm: -63.7°C

Vapor Pressure at 21.1°C : 2,210 kPa (gauge)

Specific Volume at 1 atm, 21.1°C : $0.156 \text{ m}^3/\text{kg}$

Relative Density, (Air = 1): 5.114 at 1 atm, 20°C

Solubility in Water at 1 atm, 25°C : $5.4 \text{ cm}^3/\text{kg}$ water

Description: At room temperature and atmospheric pressure sulfur hexafluoride is a colorless, odorless, nontoxic gas. It is shipped as a liquified gas under its own vapor pressure.

HAZARD DATA

Fire Hazard: Non-flammable

Health Hazard:

Permissible Exposure Limits:

OSHA TWA: 1,000 ppm

ACGIH TWA: 1,000 ppm

ACGIH STEL: 1,250 ppm

Acute Effects of Overexposure: Sulfur Hexafluoride is considered to be nontoxic. It can act as a simple asphyxiant by displacing air. Symptoms of asphyxia include rapid respiration, dizziness and fatigue. Contact may cause frostbite.

FIRST AID INFORMATION

Inhalation: Move victim to fresh air. If not breathing, give artificial respiration. If breathing is difficult, give oxygen. Call a physician.

B. COPPER SULFATE

Copper Sulfate (CuSO_4) is combined with distilled water to make the liquid resistors used in the Pulserad 112A. PVC tubing is cut to the required length and filled with the solution. Concentration is adjusted until the desired resistance is obtained.

The following is a summary of the characteristics of Copper Sulfate. [Ref. 20]

PHYSICAL DATA

Molecular Weight: 249.7

Specific Gravity: 2.29 at 15°C

Physical State at 15°C, 1 atm: solid

Color: Blue

HAZARD DATA

Fire Hazard: Non-flammable

Health Hazard:

Personal Protective Equipment: Filtering masks to minimize inhalation of dust.

Effects of Ingestion: Nausea, vomiting, or loss of consciousness.

Solid Irritant Characteristics: Causes smarting of the skin and first degree burns on short exposure; may cause second degree burns on long exposure.

FIRST AID INFORMATION

Ingestion:

Victim Conscious: Drink water or milk; induce vomiting

Victim Unconscious or Having Convulsions: Keep warm

Treatment for Exposure to Skin and Eyes: Wash with water.

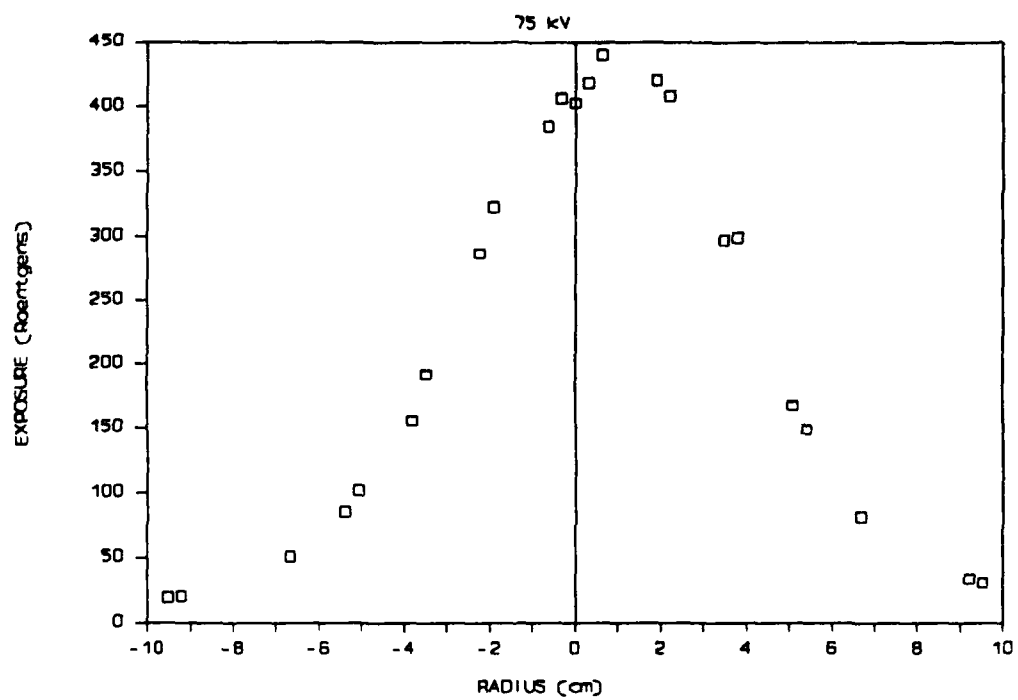
APPENDIX C

RADIATION EXPOSURE IN AIR AS A FUNCTION OF AXIAL DISTANCE FROM FACEPLATE (See Figure 66) DATA FOR 75 kV SERIES

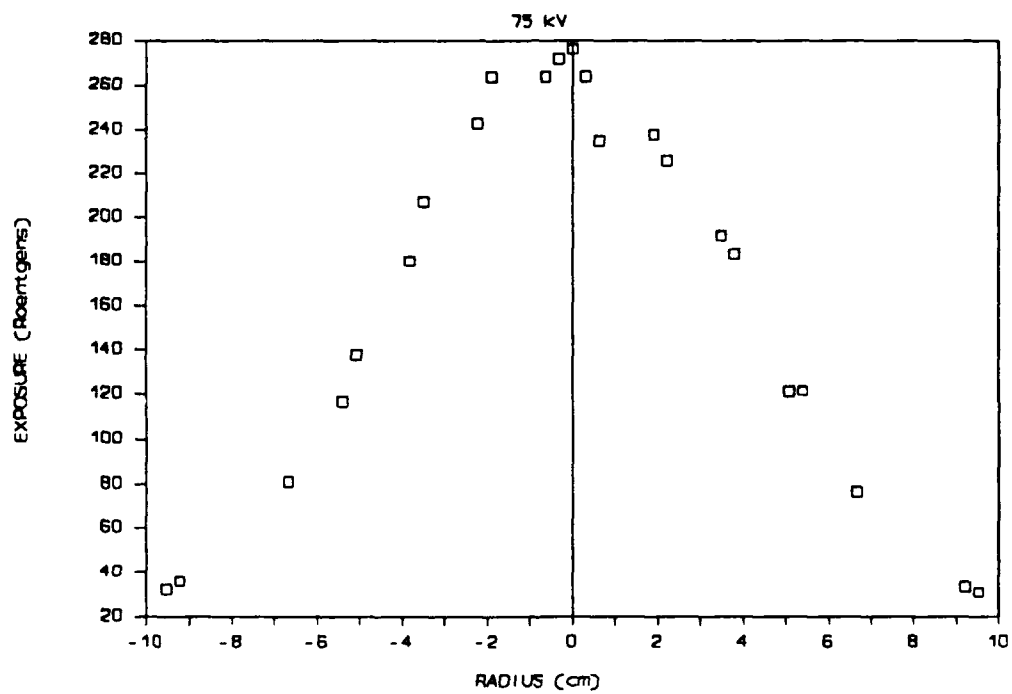
RADIUS (cm)	EXPOSURE (R) .5 in	EXPOSURE (R) 1.0 in	EXPOSURE (R) 1.5 in	EXPOSURE (R) 2.25 in	EXPOSURE (R) 2.75 in	EXPOSURE (R) 3.75 in	EXPOSURE (R) 4.75 in
-9.53	19.2	32.1	32.2	28.6	34.2	27.1	27.9
-9.21	20.3	36.1	31.2	32.6	34.8	29	27.4
-6.67	51.1	81	73.1	56	52.9	43.5	35.9
-5.40	85.4	117	92.2	70.8	61.2	50.5	42.2
-5.08	101.8	137.9	100.2	77.1	63.9	52.6	43.8
-3.81	155.4	180.1	128.4	92.7	79.4	57.2	48.9
-3.49	191.6	207	142.2	97.2	77.1	60.7	49.7
-2.22	287	243	163.9	109.9	80.7	63.8	52.4
-1.91	323	264	165.2	109.2	91.8	71.6	48.3
-0.64	385	264	168.2	114.2	92.2	70.4	53.8
-0.32	406	272	175.5	110	94.6	66.5	54.4
0.00	403	276	141.1	115.3	92.4	73.7	58
0.32	418	264	186.9	114.7	94.6	73.7	54.7
0.64	440	235	189.4	107	92.2	73.3	55.2
1.91	420	238	162.4	108.1	81.8	67.2	63.6
2.22	408	226	163	102.2	79.4	64.9	54.3
3.49	297	191.9	150.5	84.3	76.5	61.7	54.8
3.81	299	183.2	134.8	86	56	59.4	48.4
5.08	167.2	121.4	107	69.1	64.8	49	49
5.40	148.4	121.6		68.1	62.5	51.4	45.7
6.67	81.1	76.4		50.5	51	43.8	41.1
9.21	33.5	33.4		31.4	33.5	31.3	31.4
9.53	30.7	30.8		28.5	46.4	31.9	29.8

(Note: Negative radii refers to 270° with respect to top of anode assembly. See Fig. 41.)

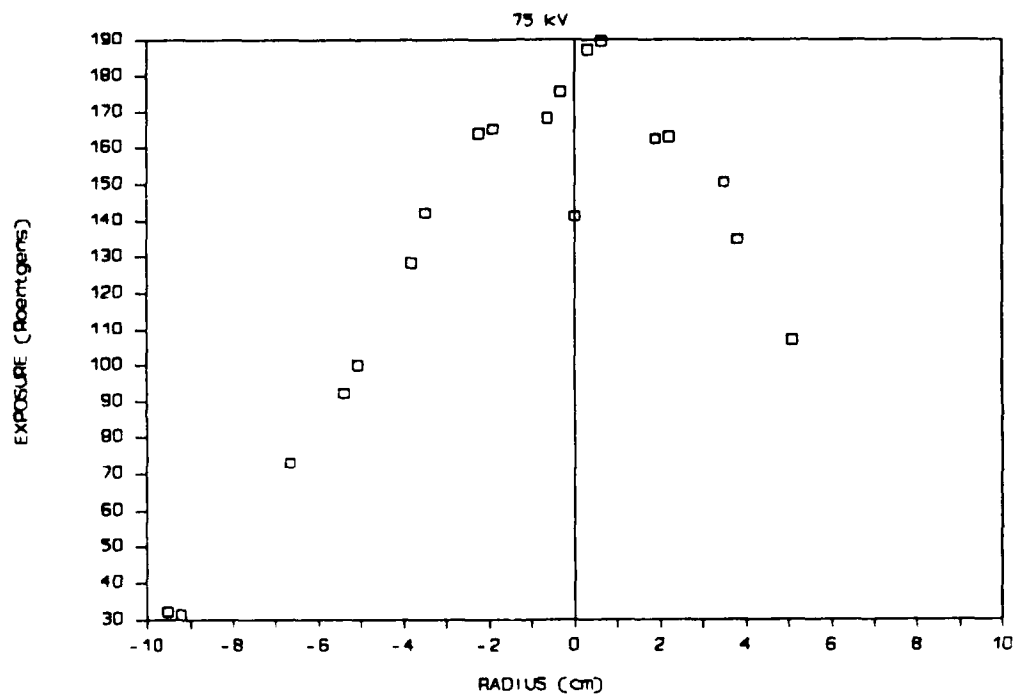
EXPOSURE VS RADIUS AT DISTANCE .5 IN



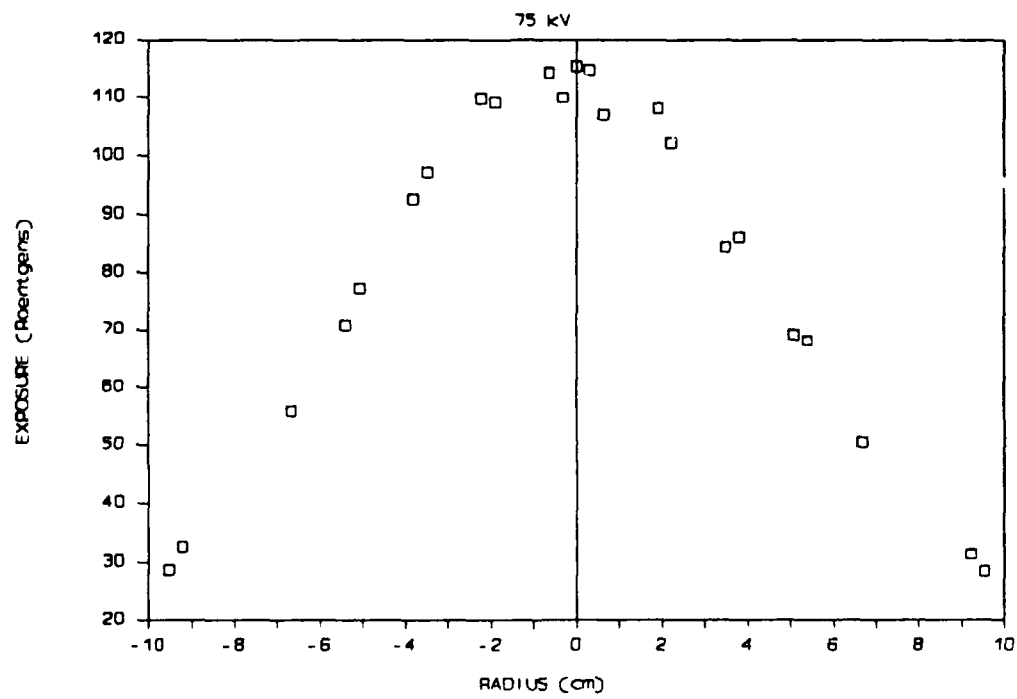
EXPOSURE VS RADIUS AT DISTANCE 1.0 IN



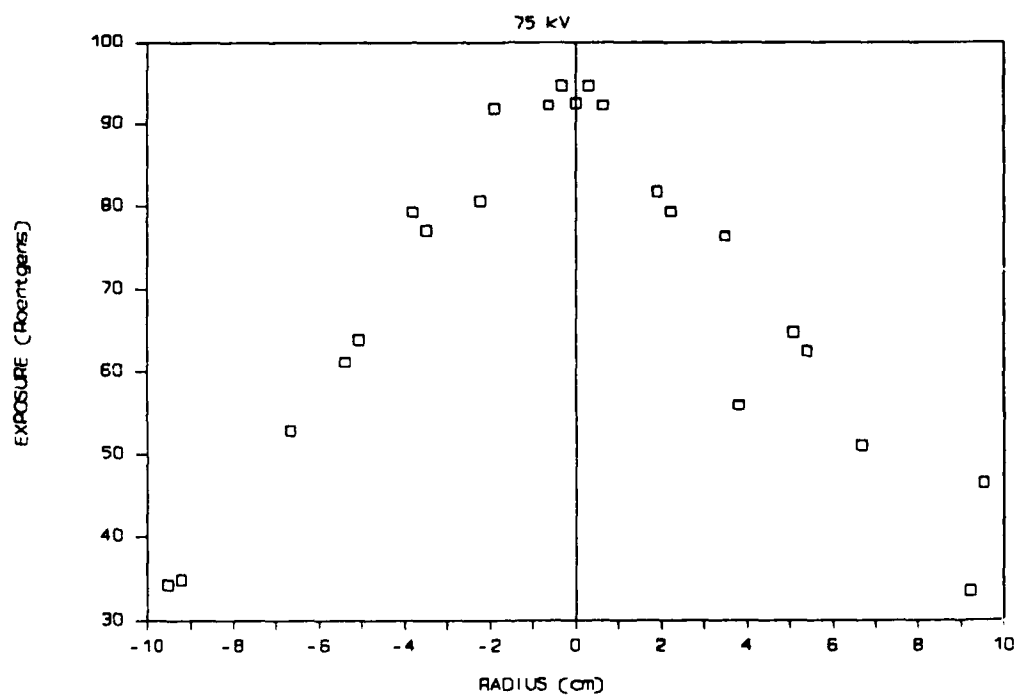
EXPOSURE VS RADIUS AT DISTANCE 1.5 IN



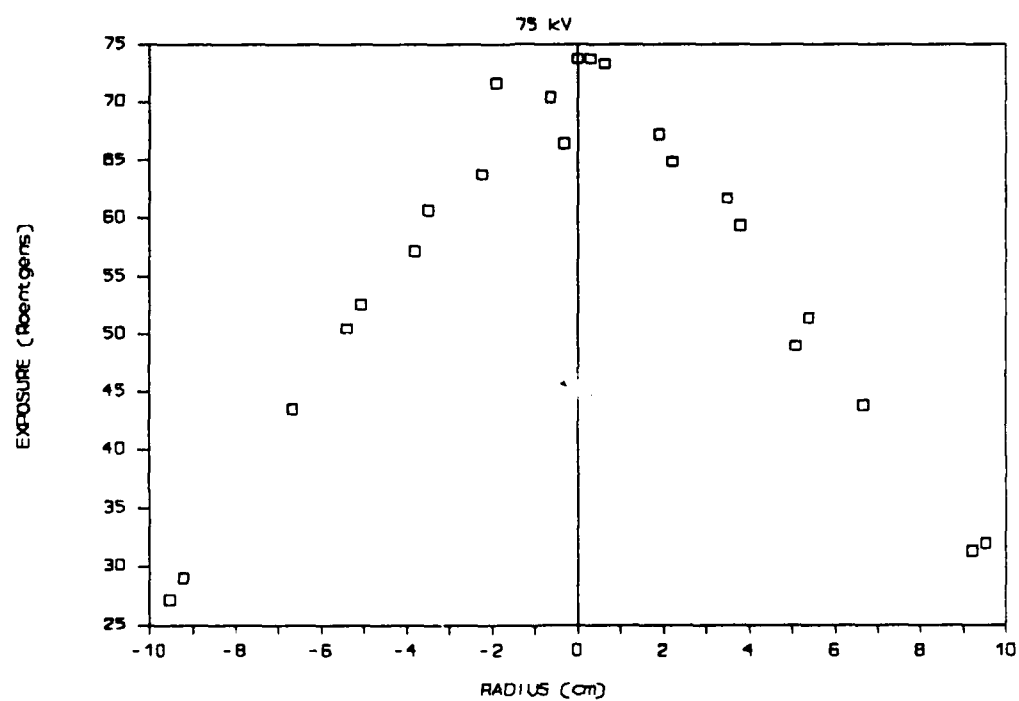
EXPOSURE VS RADIUS AT DISTANCE 2.25 IN



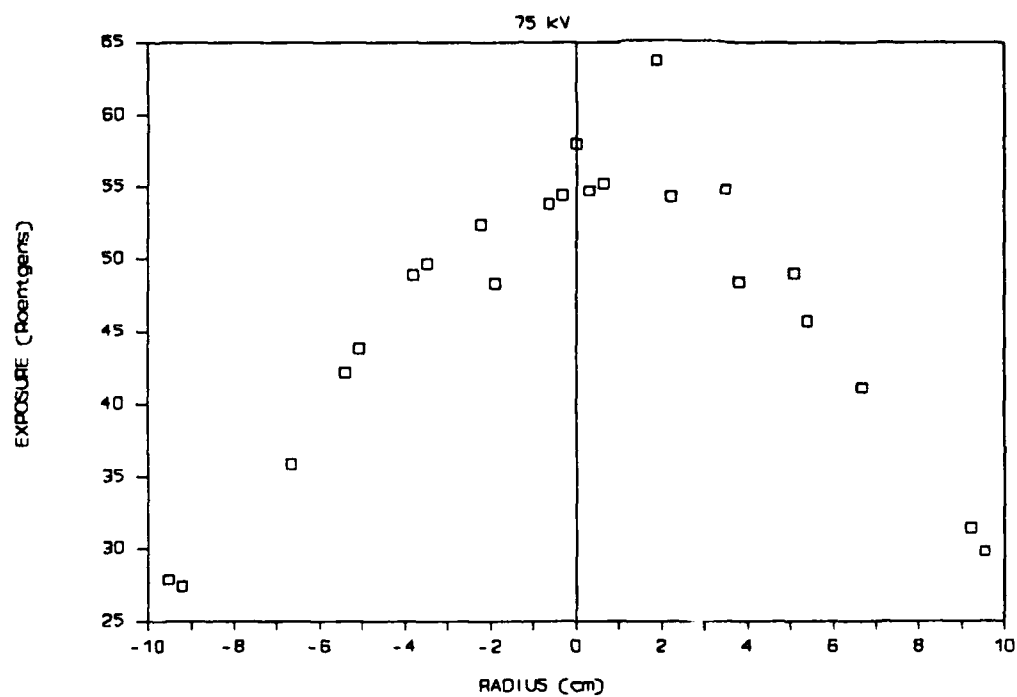
EXPOSURE VS RADIUS AT DISTANCE 2.75 IN



EXPOSURE VS RADIUS AT DISTANCE 3.75 IN



EXPOSURE VS RADIUS AT DISTANCE 4.75 IN



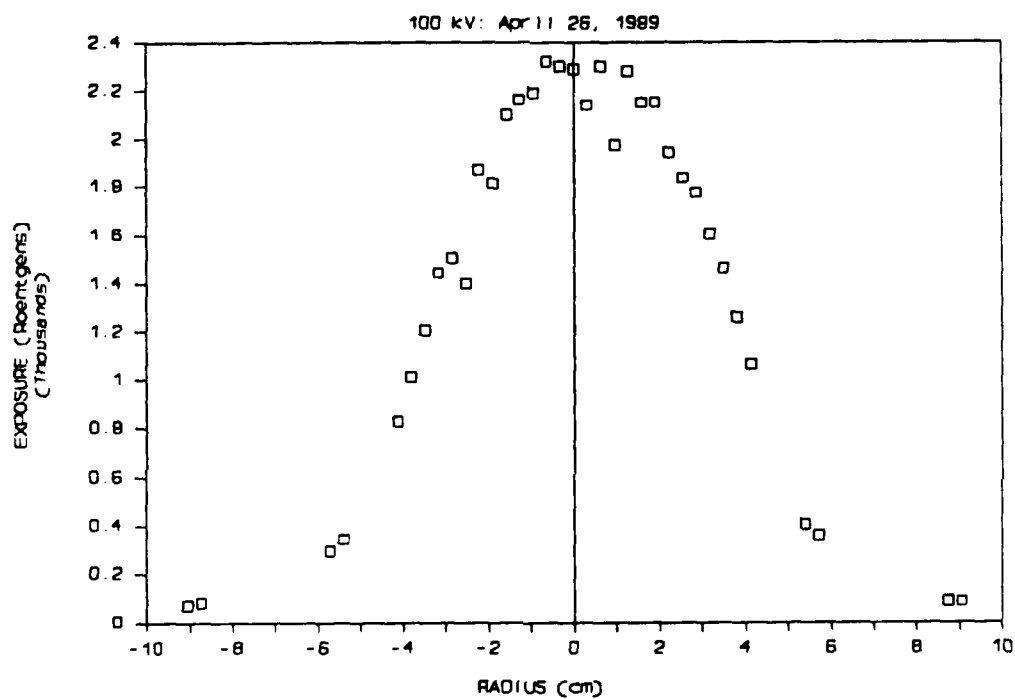
APPENDIX D

RADIATION EXPOSURE IN AIR AS A FUNCTION OF AXIAL DISTANCE FROM FACEPLATE (See Figure 66) DATA FOR 100 kV SERIES

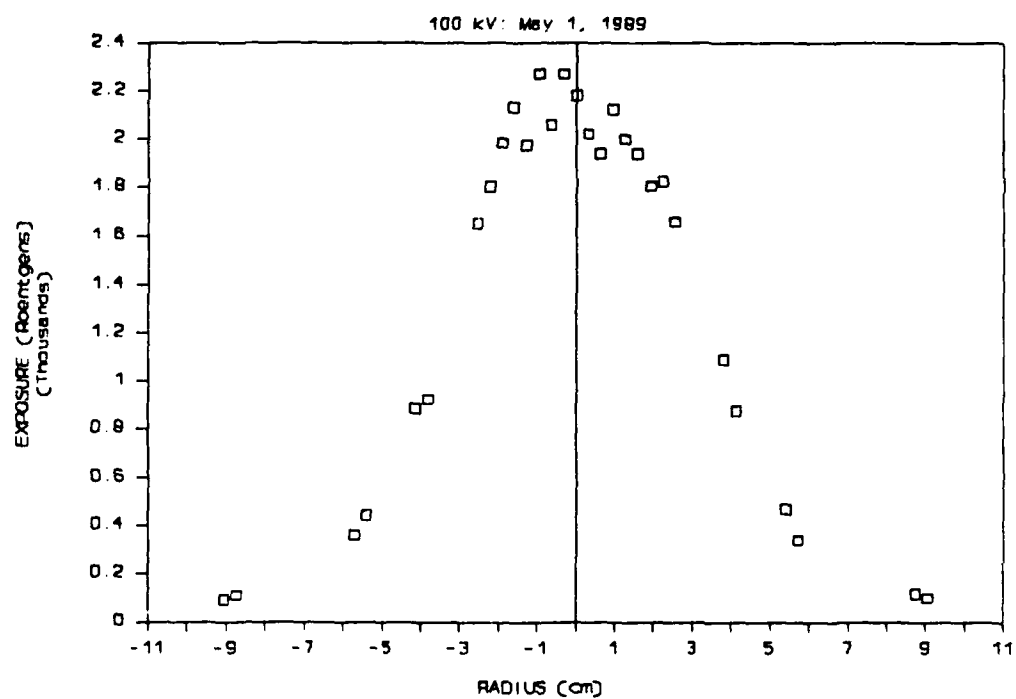
RADIUS (cm)	EXPOSURE (R) .25 in	EXPOSURE (R) .5 in	EXPOSURE (R) .75 in	EXPOSURE (R) 1 in	EXPOSURE (R) 2 in	EXPOSURE (R) 4 in	EXPOSURE (R) 6 in
-10.32							61.9
-10.00							66.6
-9.68							69.5
-9.37			86.4		116.5	98.5	70.5
-9.05	71.6	91.9	97.6	110.6	129.9	104.8	75.7
-8.73	82.1	110.4	114.4	125.5	144.7	109	75.7
-5.72	296	362	303	337	301	159.2	96.3
-5.40	345	443	374	389	311	173.7	97.7
-4.13	829	886	598	618	420	181.5	110.2
-3.81	1012	926	732	621	428	201	109.8
-2.54	1398	1649	979	974	554	206	108.5
-2.22	1872	1803	937	1045	566	220	114.6
-1.91	1811	1982	1165	1051	615	220	103.4
-1.59	2100	2130	1221	1142	633	239	118.2
-1.27	2160	1977	1206	1198	641	238	122.8
-0.95	2190	2270	1184	1188	661	240	122.7
-0.64	2320	2060	1197	1145	691	240	117.3
-0.32	2300	2270	1200	1282	640	253	120.6
0.00	2290	2180	1309	1064	693	255	124.7
0.32	2140	2020	1235	1278	658	240	119.9
0.64	2300	1939	1231	1262	619	226	113.4
0.95	1974	2120	1228	1249	640	229	115.8
1.27	2280	1998	1206	1184	638	235	120.6
1.59	2150	1938	1172	1123	632	229	108.6
1.91	2150	1806	1081	1140	618	226	114.3
2.22	1942	1822	1082	1120	574	228	117.6
2.54	1837	1658	1025	1003	551	199.9	110
3.81	1259	1092	775	820	414	198.9	107.2
4.13	1064	877	683	679	411	166.5	109.8
5.40	405	468	402	472	318	157.2	92.2
5.72	360	340	367	386	287	161.5	95.5
8.73	87.6	116.1	113.8	147.5	138.6	99.7	73.8
9.05	83.6	100.1	105	131.8	131.3	102.9	71.1
9.37			93.7		104.7	102.1	67.5
9.68							65.1
10.00							61
10.32							64.6

(Note: Negative radii refer to 270° with respect to top of anode assembly. See Fig. 41)

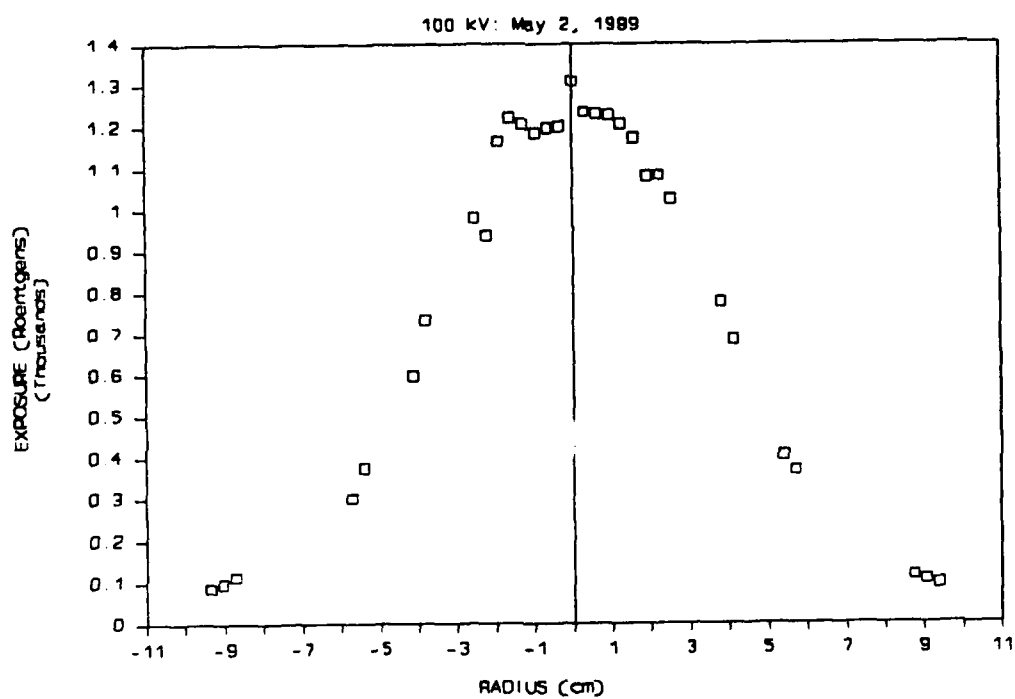
EXPOSURE VS RADIUS AT DISTANCE .25 IN



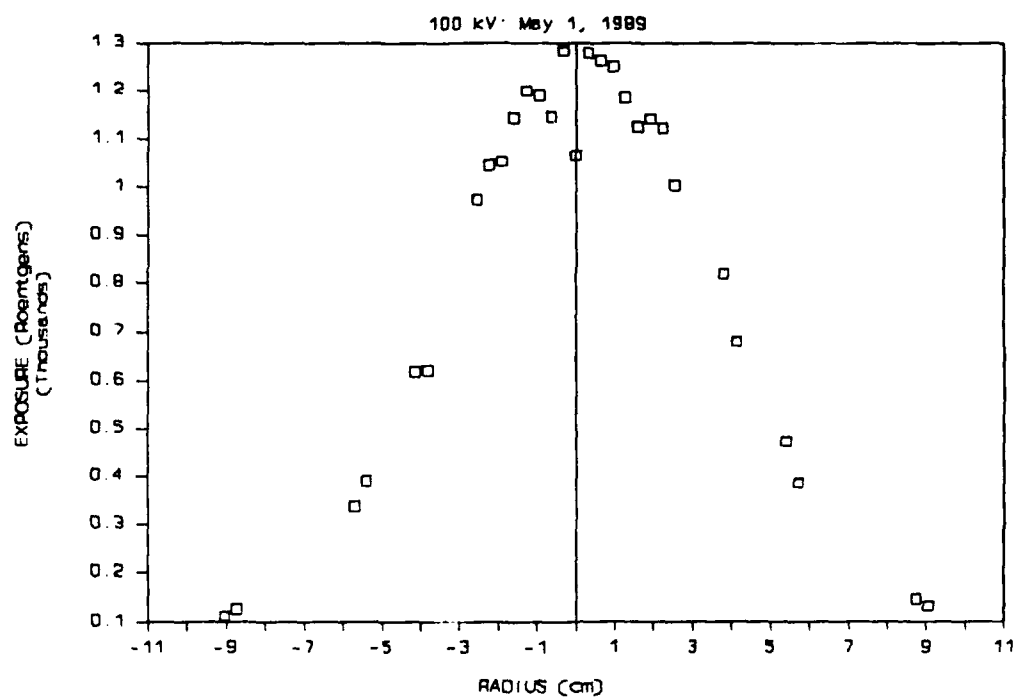
EXPOSURE VS. RADIUS AT DISTANCE .5 IN



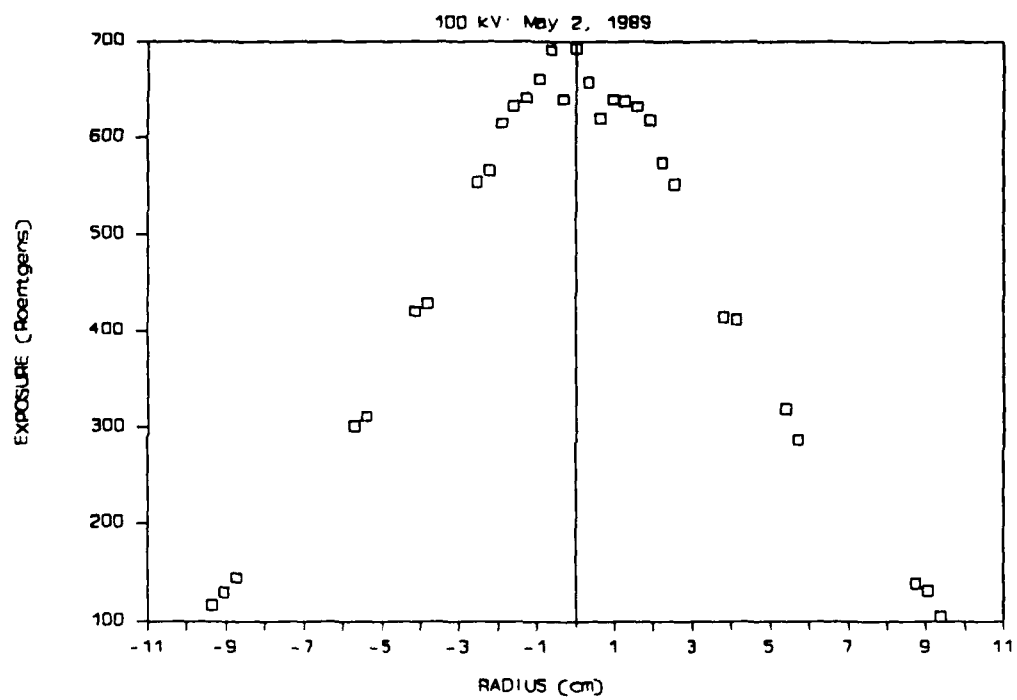
EXPOSURE VS. RADIUS AT DISTANCE .75 IN



EXPOSURE VS. RADIUS AT DISTANCE 1.0 IN

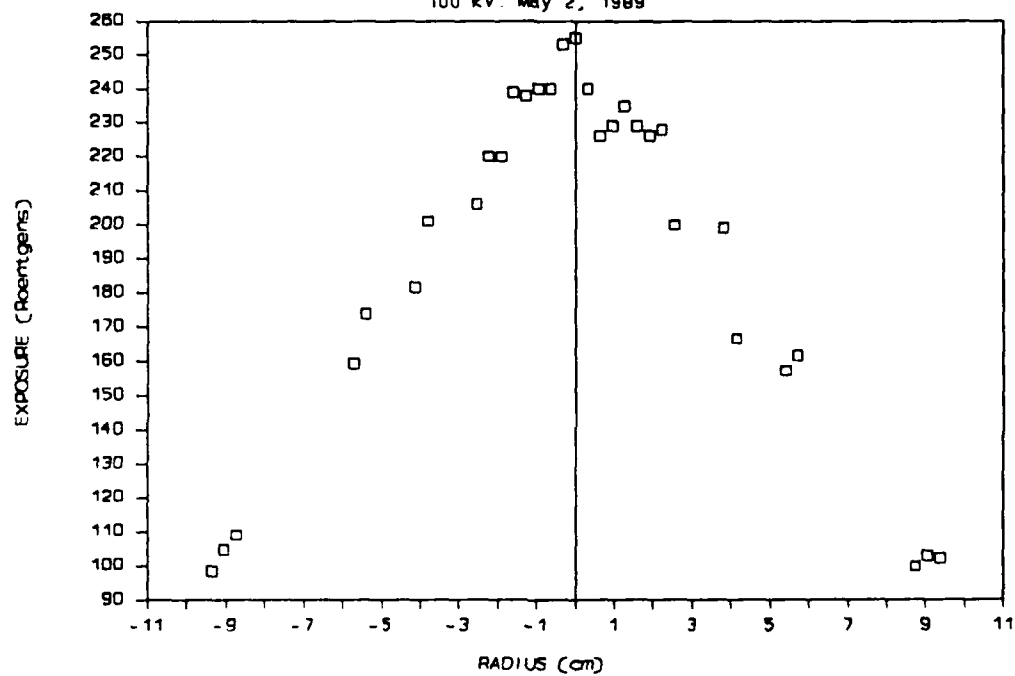


EXPOSURE VS. RADIUS AT DISTANCE 2.0 IN

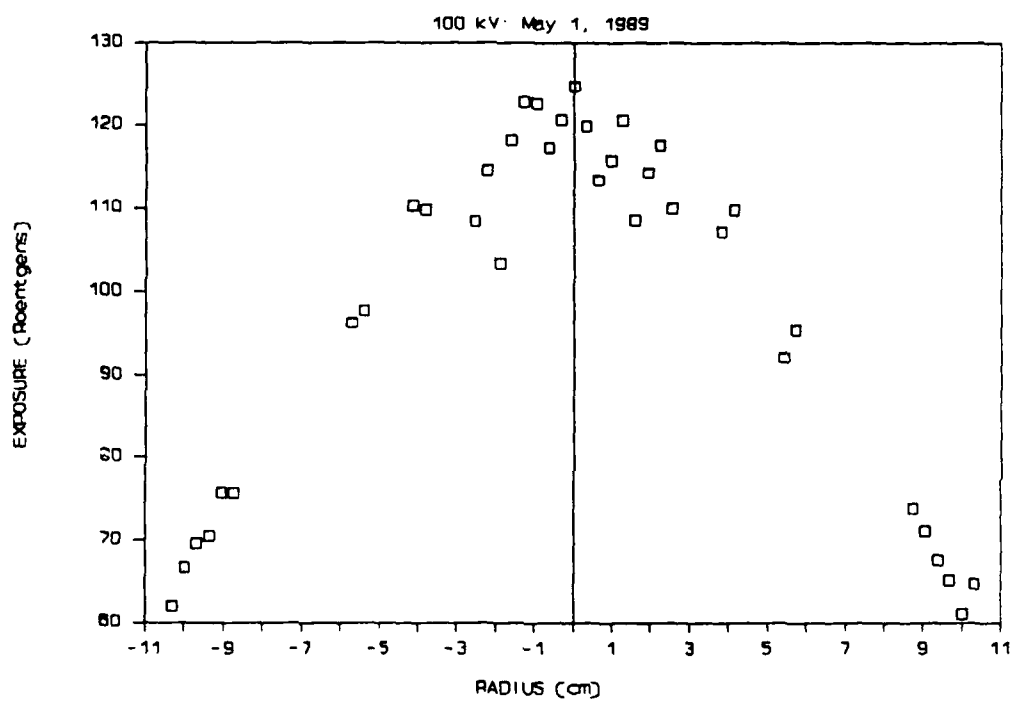


EXPOSURE VS. RADIUS AT DISTANCE 4.0 IN

100 kV: May 2, 1989



EXPOSURE VS. RADIUS AT DISTANCE 6.0 IN



ACKNOWLEDGEMENT

It is with pleasure that I gratefully acknowledge the assistance of my advisor, Dr. X. K. Maruyama. His unbounded enthusiasm and energy made this project a most rewarding experience. The previous work of Lcdr. E. C. Zurey [Ref. 21] was instrumental in laying the groundwork for the Flash X-Ray Facility, and the efforts of Mr. Richard Mendosa of Physics International were invaluable in the initial installation and operation of the Model 112A Pulserad Pulsed X-Ray Generator. Special thanks are also due to Mr. Don Snyder and Mr. Harold Rietdyk of the Naval Postgraduate School, without whose help and technical assistance this project would not have been possible.

LIST OF REFERENCES

1. Nation, J. A., "High-Power Electron and Ion Beam Generation," Particle Accelerators, v. 10, pp. 1-29, 1979.
2. Miller, R. B., An Introduction to the Physics of Intense Charged Particle Beams, Plenum Press, 1982.
3. Physics International Company, Model 112A Pulserad pulsed X-Ray Generator Operations and Maintenance Manual, January 1986.
4. Physics International Company, Model 112B pulserad Pulsed X-Ray Generator Operations and Maintenance Manual, February 1987.
5. Eisberg, R., and Resnick, R., Quantum Physics of Atoms, Molecules, Solids, Nuclei, and Particles, 2d ed., pp. 40-42, John Wiley & Sons, Inc., 1985.
6. Attix, F. H., Introduction to Radiological Physics and Radiation Dosimetry, John Wiley & Sons, Inc., 1986.
7. U. S. Army Laboratory Command Report HDL-TR-2107, The Theory and Practice of Radiation Dosimetry in the Radiation Hardness Testing of Electronic Devices and Systems, by K. G. Kerris, April 1987.
8. U. S. Department of Commerce, National Bureau of Standards, Report of the International Commission on Radiological Units and Measurements (ICRU), pp. 1-7, Government Printing Office, Washington, DC, 10 April 1957.
9. American Society for Testing and Materials Standard E170-84b, Standard Terminology Relating to Radiation Measurement and Dosimetry, 1988 Annual Book of ASTM Standards, v. 12.02, pp. 8-13, American Society for Testing and Materials, 1988.
10. American Society for Testing and Materials Standard E668-78, Standard Practice for the Application of Thermoluminescence-Dosimetry (TLD) Systems for Determining Absorbed Dose in Radiation-Hardness Testing of Electronic Devices, 1988 Annual Book of ASTM Standards, v. 12.02, pp. 249-263, American Society for Testing and Materials, 1988.
11. Whyte, G. N., Principles of Radiation Dosimetry, John Wiley & Sons, Inc., 1959.
12. American Society for Testing and Materials Standard E666-78, Standard Practice for Calculating Absorbed Dose from Gamma or X Radiation, 1988 Annual Book of ASTM Standards, v. 12.02, pp. 243-248, American Society for Testing and Materials, 1988.

13. Cracknell, A. P., and others, "The Determination of the Photon Energy Spectrum of a Flash X-Ray Tube", Radiation Effects, v. 2, pp. 233-242, March 1970.
14. Cameron, J. R., "Radiophotoluminescent and Thermoluminescent Dosimetry", in Manual on Radiation Dosimetry, Holm, N. W. and Zagorski, Z. P. ed., pp. 118-120, Marcel Dekker, Inc., 1970.
15. Knoll, G. F., Radiation Detection and Measurement, p. 758, John Wiley & Sons, Inc., 1979.
16. Victoreen Inc., Instruction Manual for Model 2800 Thermoluminescence Dosimeter Reader, September 1986.
17. Victoreen Inc., Preliminary Instruction Manual for Thermoluminescence Dosimetry (TLD) Reader Model 2800M, September 1988.
18. Conversation between Major J. R. Kim, Korean Army, Master's Thesis Student, Naval Postgraduate School, Monterey, Ca., and the author, May 1989.
19. Matheson Gas Products, Material Safety Data Sheet 081: Sulfur Hexafluoride, October 1985.
20. Department of Defense Hazardous Materials Information System DOD 6050.5-LR, Copper (II) Sulfate Pentahydrate, 1 August 1988.
21. Zurey, E. C., Facilities Requirements for a Flash X-Ray Machine, Master's Thesis, Naval Postgraduate School, Monterey, California, June 1985.

INITIAL DISTRIBUTION LIST

	No. Copies
1. Defense Technical Information Center Cameron Station Alexandria, Virginia 22304-6145	2
2. Library, Code 0142 Naval Postgraduate School Monterey, California 93943- 5002	2
3. Dr. K. E. Woehler, Code 61Wh Department of Physics Naval Postgraduate School Monterey, California 93943-5100	1
4. Dr. X. K. Maruyama, Code 61Mx Department of Physics Naval Postgraduate School Monterey, California 93943-5100	10
5. Dr. F. R. Buskirk, Code 61Bs Department of Physics Naval Postgraduate School Monterey, California 93943-5100	2
6. Dr. J. R. Neighbors, Code 61Nb Department of Physics Naval Postgraduate School Monterey, California 93943-5100	2
7. Mr. Donald Snyder, Code 61 Accelerator Laboratory Department of Physics Naval Postgraduate School Monterey, California 93943-5100	1
8. Mr. Harold Rietdyk, Code 61 Accelerator Laboratory Department of Physics Naval Postgraduate School Monterey, California 93943-5100	1

- | | | |
|-----|---|---|
| 10. | Physics Library, Code 61
Department of Physics
Naval Postgraduate School
Monterey, California 93943-5100 | 2 |
| 11. | Lt. R. B. Pietruszka, USN
502 Groom Street
Perth Amboy, New Jersey 08861 | 2 |
| 12. | Dr. Thomas Peacock
H23
Naval Surface Warfare Center
White Oak Laboratory
10901 New Hampshire Ave.
Silver Spring, Maryland 20903-5000 | 1 |
| 13. | Lt. Scott Stapp
WL/NTCTR
Kirtland Air Force Base
Albuquerque, New Mexico 87117-6008 | 1 |
| 14. | Dr. William Stapor
Code 4610
Naval Research Laboratory
Washington, D.C. 20375 | 1 |
| 15. | Dr. Nicholas Colella
L278
Lawrence Livermore National Laboratory
P.O. Box 808
Livermore, California 94550 | 1 |
| 16. | Dr. Joseph Kimbrough
L278
Lawrence Livermore National Laboratory
P.O. Box 808
Livermore, California 94550 | 1 |
| 17. | SP-2340
Strategic System Program
Washington D.C. 20376
Attn. Captain W. Bassett
Lcdr. P. Cromar | 2 |

- | | | |
|-----|---|---|
| 18. | Lcdr. E. C. Zurey
Department of Physics
U.S. Naval Academy
Annapolis, Maryland 21402-5026 | 1 |
| 19. | Mr. Richard Mendosa
Physics International Company
P.O. Box 1538
San Leandro, California 94577 | 1 |
| 20. | Major J. R. Kim, Korean Army
Naval Postgraduate School SMC 1659
Monterey, California 93943 | 1 |
| 21. | Lt. S. Minnick, USN
Naval Postgraduate School SMC 2883
Monterey, California 93943 | 1 |
| 22. | Mr. Dale Galowicz, Code 61
Department of Physics
Naval Postgraduate School
Monterey, California 93943-5100 | 1 |
| 23. | Mr. Richard A. Smith
ATR
14900 Sweitzer Lane
Suite 104
Laurel, Maryland 20707 | 1 |